FINAL REPORT

Key Fate and Transport Processes Impacting the Mass Discharge, Attenuation, and Treatment of PFAS and Comingled Chlorinated Solvents or Aromatic Hydrocarbons

SERDP Project ER-2720

JULY 2021

Christopher Higgins, Ph.D.
Colorado School of Mines

Lisa Alvarez-Cohen, Ph.D.
University of California, Berkeley

Jennifer Field, Ph.D.
Oregon State University

Charles Schaefer, Ph.D.
CDM Smith

SERDP
DOD ▪ EPA ▪ DOE

REPORT DOCUMENTATION PAGE

Form Approved
OMB No. 0704-0188

1. REPORT DATE *(DD-MM-YYYY)*	**2. REPORT TYPE**	**3. DATES COVERED** *(From - To)*
15/07/2021	SERDP Final Report	7/20/2017 - 7/20/2021

4. TITLE AND SUBTITLE

Key Fate and Transport Processes Impacting the Mass Discharge, Attenuation, and Treatment of PFAS and Comingled Chlorinated Solvents or Aromatic Hydrocarbons

5a. CONTRACT NUMBER
17-C-0043

5b. GRANT NUMBER

5c. PROGRAM ELEMENT NUMBER

6. AUTHOR(S)
Christopher Higgins, Ph.D., Colorado School of Mines
Lisa Alvarez-Cohen, Ph.D., University of California, Berkeley
Jennifer Field, Ph.D., Oregon State University
Charles Schaefer, Ph.D., CDM Smith

5d. PROJECT NUMBER
ER-2720

5e. TASK NUMBER

5f. WORK UNIT NUMBER

7. PERFORMING ORGANIZATION NAME(S) AND ADDRESS(ES)
Colorado School of Mines
1500 Illinois Street
Golden, CO 80401

8. PERFORMING ORGANIZATION REPORT NUMBER
ER-2720

9. SPONSORING/MONITORING AGENCY NAME(S) AND ADDRESS(ES)
Strategic Environmental Research and Development Program (SERDP)
4800 Mark Center Drive, Suite 16F16
Alexandria, VA 22350-3605

10. SPONSOR/MONITOR'S ACRONYM(S)
SERDP

11. SPONSOR/MONITOR'S REPORT NUMBER(S)
ER-2720

12. DISTRIBUTION/AVAILABILITY STATEMENT
DISTRIBUTION STATEMENT A. Approved for public release: distribution unlimited.

13. SUPPLEMENTARY NOTES

14. ABSTRACT
The overall goal of this project was to attain improved insight into the fundamental fate and transport processes that control per- and polyfluoroalkyl substance (PFAS) fate and transport as well as comingled chlorinated solvents and/or fuel hydrocarbons in groundwater at aqueous film forming foam (AFFF)-impacted sites. We focused on the release and transformation of polyfluorinated substances to perfluoroalkyl acids (PFAAs) in source zones as well as the impact of commonly employed remediation technologies for co-contaminants on PFAS fate.

15. SUBJECT TERMS
Mass Discharge, Attenuation, and Treatment of Poly- and Perfluoroalkyl Substances, PFAS, Comingled Chlorinated Solvents, Aromatic Hydrocarbons

16. SECURITY CLASSIFICATION OF:			**17. LIMITATION OF ABSTRACT**	**18. NUMBER OF PAGES**	**19a. NAME OF RESPONSIBLE PERSON**
a. REPORT	**b. ABSTRACT**	**c. THIS PAGE**			Christopher Higgins
UNCLASS	UNCLASS	UNCLASS	UNCLASS	107	**19b. TELEPHONE NUMBER** *(Include area code)* 720-984-2116

Table of Contents

List of Tables

List of Figures

List of Acronyms

AFB	air force base
AFFF	aqueous film-forming foam
AmPr-FASA	N-dimethyl ammonio propyl perfluoroalkane sulfonamide
AmPr-FASA-PrA	N-dimethyl ammonio propyl perfluoroalkane sulfonamido propanoic acid
AmPr-FHxSA	N-dimethyl ammonio propyl perfluorohexane sulfonamide
AmPr-FHxSA-PrA	N-dimethyl ammonio propyl perfluorohexane sulfonamido propanoic acid
AmPr-FPeSA-PrA	N-dimethyl ammonio propyl perfluoropentane sulfonamido propanoic acid
AmPr-FPrSA-PrA	N-dimethyl ammonio propyl perfluoropropane sulfonamido propanoic acid
BTEX	benzene, toluene, ethylbenzene, and xylene
Cl-PFAS	chloro-perfluoroalkanesulfonate
CMC	critical micelle concentration
CMeAmPr-FASA	N-carboxymethyldimethylammoniopropyl-perfluoroalkanesulfonamide
COC	contaminants of concern
DGBE	diethyl glycol monobutyl ether
ESI	electrospray ionization
EtFHxSA	N-ethylperfluoro-1-hexane sulfonamide
EtFOSA	N-ethylperfluoro-1-octane sulfonamide
EtFOSAA	N-ethylperfluorooctane sulfonamido acetic acid
FHxSA	perfluorohexane sulfonamide
FHxSA-PrA	perfluorohexanesulfonamide propanoic acid
FOSA	perfluorooctanesulfonamide
FOSA-PrA	perfluorooctanesulfonamide propanoic acid
FTS	fluorotelomer sulfonate
FTSA-PrB	fluorotelomer sulfonamido betaine
H-PFAS	hydrido-perfluoroalkane sulfonate
HRMS	high-resolution mass spectrometry
ISCO	*in-situ* chemical oxidation
K-PFASs	deto-perfluoroalkanesulfonate
LC	liquid chromatography
LNAPL	light non-aqueous phase liquid
MeFOSA	N-methyl perfluoro-1-octane sulfonamide
MeFOSAA	N-methyl perfluorooctane sulfonamido acetic acid
MS	mass spectrometry
NAPL	non-aqueous phase liquid
NAS	naval air station
O-PFASs	oxa-perfluoroalkanesulfonate
OSU	Oregon State University
PFAA	perfluoroalkyl acid
PFAS	per- and polyfluoroalkyl substance
PFASi	perfluoroalkane sulfinate
PFBS	perfluorobutane sulfonate
PFCA	perfluoro-n-alkanoic acid
PFDoS	perfluorododecane sulfonate
PFDS	perfluorodecane sulfonate

PFHpS	perfluoroheptane sulfonate
AmPr-FHxSA	perfluorohexane sulfonamido amine
PFNA	perfluoro-n-nonanoic acid
PFOA	perfluoro-n-octanoic acid
PFOS	perfluorooctane sulfonate
PFPeA	perfluoro-n-pentanoic acid
PFSA	Perfluoroalkane sulfonate
PFUdA	perfluoro-n-undecanoic acid
QTOF	quadrupole time-of-flight
SPE	solid phase extraction
SPrAmPr-FASA	N-sulfo propyl dimethyl ammonio propyl perfluoroalkanesulfonamide
TCE	trichloroethene
TOC	total organic carbon
TOF	total organofluorine
TOP	total oxidizable precursor
UCB	University of California, Berkeley
UFTCA	unsaturated fluorotelomer carboxylic acid
UPFOS	unsaturated perfluorooctane sulfonate
USDA	United States Department of Agriculture
XIC	extracted ion chromatogram

Acknowledgements

We would like to thank the following for their assistance in method development, data collection, and the production of this report: Raymmah Garcia from OSU, Christopher Olivares and Katerina Tsou from UCB, Dina Dreenan, Paul Ho, and Dani Tran from CDM Smith, and Kayleen Chee, Megan Coney, Kevin To, Mary Mass, Daisy Fuchs, Andrew Maizel, and Anastasia Nickerson from Mines.

Executive Summary

The overall goal of this project was to attain improved insight into the fundamental fate and transport processes that control per- and polyfluoroalkyl substance (PFAS) fate and transport as well as comingled chlorinated solvents and/or fuel hydrocarbons in groundwater at aqueous film forming foam (AFFF)-impacted sites. We focused on the release and transformation of polyfluorinated substances to perfluoroalkyl acids (PFAAs) in source zones as well as the impact of commonly employed remediation technologies for co-contaminants on PFAS fate.

Specific objectives included:

Task 1) Investigation of the fundamental mechanisms controlling the release of PFASs from complex source-zone phases;
Task 2) Examination of the coupled diffusion and potential abiotic reactions of PFASs and comingled contaminants in low permeability materials;
Task 3) Assessment of the biotic transformation of the wide range of PFASs and co-contaminants (chlorinated solvents and BTEX) present in the dissolved plume and the impacts of PFASs on co-contaminant bioremediation; and
Task 4) Quantification of the impacts of remedial activities targeting co-contaminants (i.e., BTEX, chlorinated solvents) on the PFAS plume.

The ultimate goal of improved insight into the fundamental fate and transport processes in these mixed contaminant systems should help facilitate the development and optimization of treatment strategies for management of PFAS sites comingled with co-contaminants.

The results from Task 1 indicate that at least for the two field-collected soils examined, PFAS elution clearly varied in relation to both the head group as well as perfluorinated chain length when the soils were flushed with artificial groundwater Indeed, several PFASs were only very slow to elute (>100 pore volumes before significant elution was observed). This has important implications for site monitoring and remediation, as some classes, including potential PFAA-precursors did not appear in the effluent until after the highly oxidized PFAAs were largely eluted. Elution of some slowly eluting PFASs such as FOSA was significantly impacted by porewater pH, suggest that soil buffering capacity is highly relevant to PFAS transport and that remedial actions that produce large groundwater pH shifts may cause rapid release of PFASs that are typically less mobile.

Task 1 also revealed that PFAA partitioning into bulk Jet Fuel A was not observed for PFAAs below eight carbons, though interfacial sorption coefficients (K_{nw}) for PFASs ranged from 0.06 – 0.26 cm. Perfluorocarboxylates (PFCAs) with 11 – 14 carbons showed greater accumulation at the interface than shorter-chained compounds. Further, experiments to determine the critical micelle concentrations (CMCs) for specific AFFF formulations indicated that the CMC was below the 3% AFFF application rate, indicating that micelles are present when AFFFs are applied to fires. Reduced surface and interfacial tensions of AFFF-impacted waters after application can potentially increase soil wetting and infiltration. The presence of micelles also increases potential for NAPL and other co-contaminant transport.

Under Task 2, experimentally determined aqueous diffusivities were in good agreement with previously performed experiments that measured PFAA uptake into activated carbon. The Wilke-Chang model was not able to accurately predict the values nor describe the trend for the range of PFAAs used in this study. The non-uniform trend in the PFAA diffusivities with respect to the molar volumes likely is reflective of unique molecular interactions associated with highly fluorinated compounds. In the clay soil tube diffusion experiments, comparison of the results to numeric models showed that neglecting surface diffusion resulted in a severe underprediction (>10x for PFOS) of predicted aqueous concentrations. For the PFAAs and clay soil examined herein, surface diffusion contributions became important (>10% of the overall diffusion) at K_d values greater than approximately 0.5 L kg^{-1}. Abiotic reactions with reactive iron, however, appear unlikely to be important with respect to reductive transformation of polyfluorinated PFAA precursors in AFFF. Ferrous iron minerals, however, may play a small role in precursor transformation under oxic conditions due to generation of hydroxyl radicals.

Under the third objective, a 3M AFFF formulation and a National Foam AFFF formulation had different responses to aerobic transformation of non-fluorinated and fluorinated components of AFFF. While there were initial decreases in a specific sulfonamide precursor observed in 3M AFFF, AmPr-FHxSA, in the live treatments, National Foam AFFF did not show a decoupling of the fluorotelomer compound 6:2 FTSA-PrB between the live treatment and autoclaved control. However, the non-fluorinated carbon (measured as total organic carbon; TOC) in the National Foam AFFF microcosms was apparently degraded, whereas the TOC in 3M stayed constant in the live treatment. More importantly, 3M AFFF completely inhibited BTEX biodegradation, though no inhibition was seen with AmPr-FHxSA alone. However, differences in extracellular and total metabolite abundances between AmPr-FHxSA, FHxSA, and PFHxS treatments compared to the PFAS-free control suggested AmPr-FHxSA (and perhaps other zwitterionic PFAS) may cause cell membrane leakage. Nevertheless, experiments with AmPr-FHxSA indicated that over the course of 70 days, it was transformed into FHxSA, and to a lesser extent PFHxS. Anaerobic microorganisms (TCE coculture, anaerobic BTEX biodegradation) appear to be more tolerant of AFFF than aerobic systems. Treatments with spiked AmPr-FHxSA had slowed TCE dehalogenation rates with no lag phase, suggesting that microorganisms did not recover from the inhibition. Addition of DGBE individually or via AFFF resulted in stimulation of TCE dehalogenation, presumably because of glycol fermentation.

Results from the final objective revealed that when aerobic microorganisms were specifically stimulated to mimic biosparging, transformation of multiple ECF-sulfonamide precursors was suspected based on mass balance, despite the surface soil being exposed to air and water for years prior to collection: source zone soils likely still have potential for PFAS transformation years after AFFF release. Both O_2-sparged and N_2-sparged columns released more fractional mass of ECF-sulfonamides than unaltered, non-biologically active columns (i.e., in comparison to Task 1). After 200+ pore volumes of flushing, detectable concentrations of many PFASs, particularly long chain PFSAs and zwitterionic compounds, remained on the column soils. In contrast, the in situ chemical oxidation (ISCO) simulation experiments, PFHxA, PFOA, and PFHxS increased in both the permanganate and persulfate-treated columns. All three example PFASs increased more rapidly and to higher concentrations in the permanganate-treated columns than the persulfate-treated columns but it remains unclear whether this difference is attributed to the chemical oxidants themselves or the different concentrations of each oxidant.

In summary, this project confirmed that there are significant reservoirs of polyfluorinated substances still remaining on AFFF-impacted soils which can be very slowly released to groundwater. The release of these PFASs is dependent on both the perfluorinated tail length and the head group. Some of these PFASs (particularly those present in 3M AFFF) also inhibit microbial activity, with anaerobic communities appearing to be more tolerant to AFFF than aerobic microbial communities. Some ECF-derived polyfluorinated substances do appear to transform, albeit slowly, to PFAAs such as PFHxS, though perfluoroalkyl sulfonamide such as FHxSA may be semi-stable intermediates. Natural abiotic subsurface reactions with polyfluorinated substances are likely not significant with respect to PFAS transformations. Finally, data collected under this project indicate that alterations in subsurface biogeochemistry, whether through alterations in soil porewater pH or changing redox conditions due to biosparging or ISCO, can significantly impact the time and magnitude of the release of PFAS mass from AFFF-impacted soils.

Objectives

This project was proposed in response to the SERDP Statement of Need ERSON-17-01 identifying the need to improve our ability to treat mixed contaminants of concern (COCs) in groundwater. This includes better understanding contaminant fate in low mobility zones when present in mixtures, identifying potential synergies among treatment technologies, and developing useful guidance for addressing mixed contaminant plumes. In this project, mixtures of PFASs with chlorinated solvents and hydrocarbons were specifically targeted. In response to the Statement of Need, this project was carried out as a collaborative effort among scientists and engineers at the Colorado School of Mines (Mines), CDM Smith, Oregon State University (OSU), and the University of California – Berkeley (UCB).

This project focused on the fundamental fate and transport processes controlling the mass discharge, attenuation, and ultimately treatment of PFASs and comingled chlorinated solvents and/or fuel hydrocarbons (i.e., BTEX) in groundwater impacted with AFFF. Rather than proposing new treatment technologies, this project examined the extent to which existing remediation technologies can be used synergistically to address mixed contaminant systems. Without insight into the fundamental processes occurring in these systems, any new treatment strategies are likely to be ineffective or inefficient, and may not benefit from the coupling of intrinsic natural attenuation processes with active remedial approaches. We were careful to focus on the PFASs of regulatory concern as well as those that occur at high frequency and concentration (μg/L and greater) at Department of Defense (DoD) facilities. We employed field-collected groundwater and soil/aquifer samples to serve as the primary source of these constituent compounds, thereby ensuring that the full suite of PFASs and other COCs that may be present in these mixed contaminant systems were appropriately assessed.

The presence of comingled priority pollutants has resulted in the application of treatment technologies, such as air biosparging for BTEX, microbially enhanced reductive dechlorination for chlorinated ethenes, and/or *in situ* chemical oxidation (ISCO) for treatment of BTEX or chlorinated solvents, that have unresolved potential impacts on PFAS transformation and release rates. Of equal importance are the unresolved potential impacts of PFASs on chlorinated solvent and aromatic hydrocarbon (i.e., BTEX) transformation and transport. The importance of understanding these impacts and processes is established by the fact that cost effective *in situ* treatment for PFASs has yet to be demonstrated. Proper assessment and quantification of impacts of treatment approaches on both priority COCs as well as PFASs will result in defensible justification to either forgo active treatment or to develop cost-effective strategies (e.g., targeted treatment, treatment trains) for mitigating risks associated with priority pollutants and PFASs.

We hypothesized that the complex nature of PFASs present in AFFF results in complex and long-term release from both primary sources (which may contain non-aqueous phase liquids (NAPLs)) and low permeability zones. Prior SERDP work by members of the project team indicated that there are many PFASs present at AFFF-impacted sites that have the potential to form the more problematic PFAAs under oxidizing conditions and that PFAAs interact with NAPLs. The improved insights from this work into PFAS fate and transport processes within source areas and low permeability zones will facilitate improved management and treatment approaches.

We further hypothesized that coupled biotic and abiotic transformation of PFASs to the more problematic PFAAs in source and low permeability zones are impacted by site mineral and geochemical conditions as well as the application of conventional treatment technologies. Identification and quantification of transformation kinetics will be vital for proper assessment of site risk, remedial technology selection, and overall plume management. These hypotheses, and the focus of this research, are illustrated in the figure below.

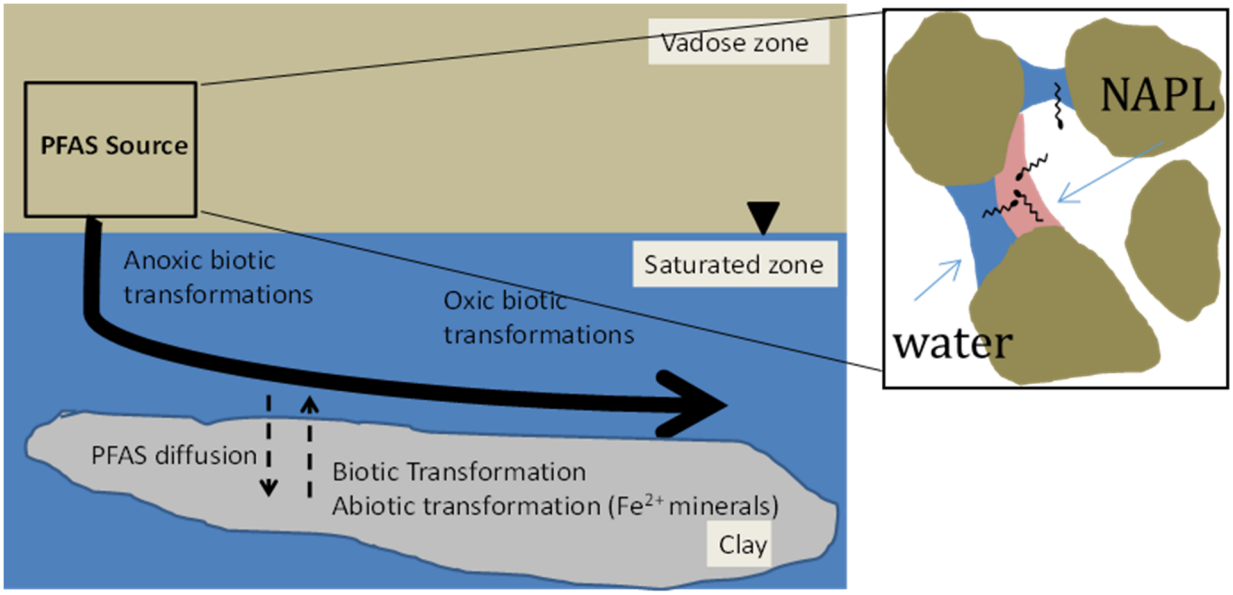

Conceptual model of PFAS release, diffusion, and migration through groundwater. PFAS behavior in the source area is complicated by their surfactant behavior, likely consisting of sorption at air-water, water-NAPL, and NAPL-air interfaces, and to a lesser extent partitioning into NAPL itself.

Key fundamental questions regarding these processes include the following:

- What is the nature of the PFAS source area, and how do mass discharge, PFAS and co-contaminant composition, and transformation process vary over time and as the source becomes depleted due to intrinsic or remediation-enhanced processes?
- What are the diffusional and reactive processes controlling PFAS behavior in low permeability zones, particularly in clayey materials containing ferrous minerals and in the presence of co-contaminants?
- How do PFASs impact chlorinated solvent/BTEX co-contaminants, and how do co-contaminants impact PFASs, with respect to biotic transformation under the wide range of biogeochemical conditions typically encountered at AFFF-impacted sites?
- How do remedial activities impact these mixed contaminant plumes, both in the source area and the more dilute downgradient plume?
- To what extent does improved insight into these fate and transport processes facilitate more effective site management and development of synergistic remedial approaches for groundwater impacted with PFASs and BTEX/chlorinated solvents?

The four main tasks of this project were:

TASK 1. SOURCE AREA RELEASES UNDER UNALTERED CONDITIONS. An investigation of the fundamental mechanisms controlling PFAS release from complex source zone phases. Efforts focused on assessing the nature of PFAS mass distribution among phases and at interfaces, determining how the composition and rate of mass discharge varies over time.

TASK 2. COUPLED DIFFUSION AND ABIOTIC REACTIONS WITHIN CLAYS. An examination of the coupled diffusion and potential abiotic reactions of PFASs and comingled contaminants in low permeability materials. As has been shown in many studies, chlorinated solvent and BTEX diffusive uptake and release in low permeability materials can have a large impact on plume longevity, treatment approach selection, and the nature of the contaminants (due to transformation).

TASK 3. BIOTIC TRANSFORMATION. An assessment of the biotic transformation of the wide range of PFASs and co-contaminants (chlorinated solvents and BTEX) present in the dissolved plume. Efforts focused on both reductive and oxidative processes occurring over a wide range (aerobic to methanogenic) of geochemical conditions, identifying biotransformation products and interactions among contaminant mixtures. This information is needed to determine the extent to which natural transformation processes are impacting PFASs, and the extent to which PFASs are impacting the transformation of chlorinated solvents and aromatic hydrocarbons.

TASK 4. IMPACTS OF REMEDIAL ACTIVITY ON PFAS RELEASE. An evaluation of the impacts of co-contaminant remediation technologies, specifically biosparging for BTEX as well as ISCO and biostimulated reductive biostimulation for TCE, on PFAS release and co-contaminant treatment. Experiments used columns containing field-collected, AFFF-impacted soils.

The details of each task and the associated results are summarized below.

TASK 1. SOURCE AREA RELEASES UNDER UNALTERED CONDITIONS.

Task 1.1. ***Collection and Characterization of AFFF-impacted Soil and Groundwater***. As recent work has demonstrated that there is no simple way to simulate field conditions from pure-phase chemicals spiked into simulated or artificial media, this project employed field-collected materials including soils, groundwater, and NAPLs to the maximum extent possible. Wherever feasible, we leveraged other efforts of the project team and our collaborators to identify and collect suitable experimental materials. Previously collected soils from the fire-training grounds of from several U.S. Navy and Air Force sites were evaluated for column experiments in Tasks 1.2 and 1.4.

Potential soils for column experiments described in Tasks 1.2 and 1.4 were initially evaluated for the presence of water-extractable PFASs by Mines. Water-extractable PFASs were isolated by combing ~ 1 g of soil and 10 mL of deionized water in a 15 mL centrifuge tube, which was then vortexed for 60 seconds, placed on a shaker table for 60 minutes, and centrifuged at 4,000 rpm for 10 minutes. The resulting supernatant was decanted and analyzed for target and suspect PFASs by liquid chromatography time-of-flight mass spectrometry (LC-QTOF-MS) as described below. Soils from the fire-training grounds were selected for use in column experiments because they were found to contain a chemically diverse set of water-extractable PFASs in high concentrations. Subsamples of the selected soils were sent to Agvise Laboratories (Northwood, ND) for analysis of soil pH, anion exchange capacity, cation exchange capacity, soil particle size distribution (sand/silt/clay) and organic carbon content. The results are provided in **Table 1.1**. The soils were both classified as sandy loams and predominantly consist of sand (particles with diameter greater than 0.05 mm). They also have comparable bulk chemical properties with similar ion exchange capacities, carbon content, and pH when mixed 1:1 with deionized water.

Table 1.1. Bulk characterization of soils used in Task 1.2 and 1.4 column experiments.

	Soil A	**Soil B**
Size Distribution	79 % Sand, 10 % Silt, 11 % Clay	79% Sand, 6 % Silt, 15 % Clay
USDA Textural Class (hydrometer method)	Sandy Loam	Sandy Loam
Cation Exchange Capacity (meq / 100 g)	7.5	9.5
Anion Exchange Capacity @ pH 7	0.03	-0.04
% Carbonates	0.1	0.4
% Total Carbon	1.0	1.1
% Inorganic Carbon	0.0	0.0
% Organic Carbon	1.0	1.1
pH (Water)	6.5	6.7

Soil extracts from these soils were prepared as described below and were analyzed in quadruplicate at Mines for target and suspect PFASs. Further, in response to a question raised at the initial ER-2720 IPR, subsamples of the experimental soils from Tasks 1.2 and 1.4 were sent, in triplicate, to SGS Axys to confirm Mines-measured concentrations of PFAAs, fluorotelomer sulfonic acids (X:2 FTSs), and sulfonamide-based compounds.

PFAS Analysis by LC-QTOF-MS. "Target" and "suspect" PFAS analysis was performed simultaneously at Mines with a SCIEX 500R LC-QTOF-MS (Framingham, MA), coupled to an

adjustable polarity electrospray interface. Target PFAS analysis describes the quantitation of compounds by comparison against reference standards with stable isotope-enriched internal standards. Suspect screening describes the matching of identified mass spectral features against an extracted ion chromatogram (XIC) list, which contains PFASs that have been previously identified or were speculated to exist, but lack commercially available reference standards. The Mines XIC list employed for this work contained MS/MS spectra for >300 AFFF-associated PFASs and molecular formulas and neutral masses for >1,400 PFASs, including a wide variety of well-characterized PFASs, PFASs reported in literature, and theoretical homologs. Structures and chemical formulas can be found in Table S3 of the SI of Nickerson et al.[1]

For ESTCP ER-201633, Mines developed a procedure to quantitatively extract both anionic and cationic PFASs from AFFF-impacted soils. Approximately 0.2 g of soil was weighed out into 50 mL centrifuge tubes and spiked with a volume of internal standard solution such that the mass of each internal standard was within 10x of estimated mass of the highest concentration target analyte present in the soil. The soils were then twice extracted with basic methanol (1% (v/v) ammonium hydroxide in methanol) and twice extracted with acidic methanol (0.5 M hydrochloric acid). For each extraction, tubes were vortexed for 30 seconds, sonicated for 15 minutes at 30 °C, centrifuged at 3500 rpm for 20 minutes, and the supernatants were decanted. Basic and acidic extracts were separately passed through ENVI-Carb SPE tubes, and the pH of the acidic extracts was brought to 6 – 7 by neutralization with a 1:1 ammonium hydroxide:methanol solution. Each extract was then dried in a nitrogen evaporator at 30 °C. Finally, 1.5 mL of reconstitution solvent (1% (v/v) glacial acetic acid in methanol) was added to the dried basic extract, which was then vortexed. Next, the reconstitution solvent was transferred to the dried acidic extract, vortexed again and decanted into a microcentrifuge tube. Extracts were held at 0 °C overnight, then centrifuged at 17,000 g for 10 minutes. The final soil extract supernatants were combined with volumes of water, isopropanol, methanol, and 1:1 ammonium hydroxide:methanol such that the pH was between 6-8, the overall composition was identical to prepared aqueous samples, and no more than 20 ng of any single target PFAS was present. The prepared soil extracts were again centrifuged at 17,000 g for 10 minutes and then the supernatant was poured off and injected directly into the LC-QTOF-MS. Method blanks were created and analyzed with each analytical batch and approximately 10% of samples were prepared and analyzed in triplicate. Relative standard deviations were typically less than 10%.

For all LC-QTOF-MS analysis, a liquid chromatography protocol was utilized that separates branched and linear PFAS isomers to obtain insight into the nature of the perfluorocarboxylates (PFCAs) and other intermediates. In general, sample aliquots (1 mL) were injected into an LC system containing a Gemini C18 analytical column (3 mm x 100 mm x 5 µm; Phenomenex, Torrance, CA) preceded by one carbo C18 Guard Cartridge (4 mm x 2 mm I.D.; Phenomenex) and two Zorbax DIOL guard columns (4.6 mm x 12.5 mm x 6 µm; Agilent, Santa Clara, CA), held in a column oven set to 40 ºC. A Luna 5 µm 100 Ä LC column (30 x 3 mm I.D.; Phenomenex) was used as a delay column to prevent PFASs derived from LC mobile phases from co-eluting with PFASs present in samples. The aqueous mobile phase (A) was 20 mM ammonium acetate (Optima, Fisher Scientific) in water (Optima, Fisher Scientific) and the organic mobile phase (B) is 100% HPLC-grade methanol (Optima, Fisher Scientific). The eluent flow rate was held at 0.60 mL/min, and composition was ramped from 90% A to 50% A over the first 0.5 minutes, then to 1.0% A at 8 minutes and held until 13 minutes, then ramped to 90% A at 13.5 minutes and held to 20 minutes.

Target and suspect data acquisition were performed simultaneously with SWATH® Data-Independent Acquisition. Precursor ion data were collected for m/z 100-1200 over 1283 cycles with a total scan time of 842 ms and accumulation time of 20 ms. Ion spray voltage was set at -4500 V and temperature set to 550 ºC. The ion source, curtain, and collision gas were set to 60 psi, 35 psi, and 10 psi, respectively. The collision energy was set to -5 V and the declustering potential to -20 V, both with no spread. Product ion (MS/TOF-MS) scanning was conducted for m/z 50-1200 Da, across 10 SWATH windows. The accumulation time for each SWATH window was 50 ms and collision energy was -35 V with 30 V spread. As seen in **Figure 1.1**, the combination of liquid chromatography with SWATH acquisition provided the retention time, exact parent m/z, parent isotope ratio, and exact fragment m/z for each mass spectral feature. The instrument was mass calibrated every 5 injections using SCIEX ESI calibration solutions.

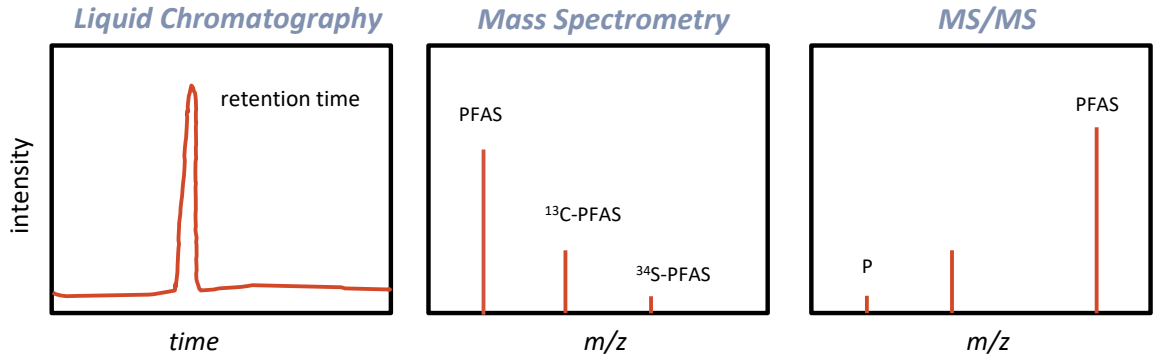

Figure 1.1. Data types obtained for combined target/suspect LC-QTOF-MS analysis.

Target data analysis and processing were performed with a combination of SCIEX OS, custom R scripts, and Microsoft Excel. Confirmation of targeted analytes with signal:noise ratio > 10:1 was based on LC retention time and accurate mass (XIC window 0.01 Da) compared to analytical standards. Expected retention times for each analyte were determined from a mid-range calibration point. Initial integration parameters included defining 90% of lowest-intensity peaks as noise, using a baseline-subtract window of 2 minutes, a minimum peak intensity of 100, and a peak width of 10 points. Some peaks with peak intensity below these thresholds were manually integrated if retention time, accurate mass, and isotope confidence were determined to be satisfactory. A list of target analytes and internal standards used for quantitation is provided in **Table 1.2**. Calibration range, limit of quantitation, and linear fit (r^2) of calibration curves for all analytes were recorded for each analytical run. Calibration ranges and quantitation limits were determined by the linear range of initial calibrations, which were evaluated with $1/x^2$–weighted linear regressions, where each calibration point must show recovery with 30 % of its nominal value and the overall r^2 must be over 0.97. For most analytes on most runs, calibration ranges span roughly 1 – 5000 pg injected. Minimum reporting limits were adjusted to be three times the highest concentration in the blanks.

Part of the way through this project, the DOD/DOE QSM requirements went into effect with regards to PFAS analysis. This affected our analyses by adding additional blanks, laboratory control samples, matrix spikes, and replicates.

Table 1.2. Target PFASs quantified by LC-QTOF-MS, with common abbreviation, molecular formula, and associated internal standard.

Chemical Name	Acronym	Neutral Molecular Formula	Internal Standard
Perfluoroalkanoic acids			
Perfluoro-n-butanoic acid	PFBA	C4HO2F7	13C4-PFBA
Perfluoro-n-pentanoic acid	PFPeA	C5HO2F9	13C5-PFPeA
Perfluoro-n-hexanoic acid	PFHxA	C6HO2F11	13C2-PFHxA
Perfluoro-n-heptanoic acid	PFHpA	C7HO2F13	13C4-PFHpA
Perfluoro-n-octanoic acid	PFOA	C8HO2F15	13C4-PFOA
Perfluoro-n-nonanoic acid	PFNA	C9HO2F17	13C5-PFNA
Perfluoro-n-decanoic acid	PFDA	C10HO2F19	13C2-PFDA
Perfluoro-n-undecanoic acid	PFUdA	C11HO2F21	13C2-PFUdA
Perfluoro-n-dodecanoic acid	PFDoA	C12HO2F23	13C2-PFDoA
Perfluoro-n-tridecanoic acid	PFTrDA	C13HO2F25	13C2-PFTeDA
Perfluoro-n-tetradecanoic acid	PFTeDA	C14HO2F27	13C2-PFTeDA
Perfluoro-n-hexadecanoic acid	PFHxDA	C16HO2F31	13C2-PFHxDA
Perfluoro-n-octadecanoic acid	PFODA	C18HO2F35	13C2-PFHxDA
Perfluoroalkane Sulfonates			
Perfluoropropane sulfonate	PFPrS	C3HO3SF7	13C3-PFBS
Perfluorobutane sulfonate	PFBS	C4HO3SF9	13C3-PFBS
Perfluoropentane sulfonate	PFPeS	C5HO3SF11	13C2-PFOS
Perfluorohexane sulfonate[i]	PFHxS	C6HO3SF13	18O2-PFHxS
Perfluoroheptane sulfonate	PFHpS	C7HO3SF15	18O2-PFHxS
Perfluorooctane sulfonate[i]	PFOS	C8HO3SF17	13C4-PFOS
Perfluorononane sulfonate	PFNS	C9HO3SF19	13C4-PFOS
Perfluorodecane sulfonate	PFDS	C10HO3SF21	13C4-PFOS
Perfluoroundecane sulfonate	PFUdS	C11HO3SF23	13C4-PFOS
Perfluorododecane sulfonate	PFDoS	C12HO3SF25	13C4-PFOS
Chlorinated perfluoroalkane sulfonates and ether sulfonates			
8-chloro-perfluorooctane sulfonate	Cl-PFOS	C8HO3SClF16	13C4-PFOS
9-chloro-3-oxa-perfluorononane sulfonate	Cl-O-PFNS	C8HO4SClF16	13C4-PFOS
11-chloro-3-oxa-perfluoroundecane sulfonate	Cl-O-PFUdS	C10HO4SClF20	13C4-PFOS
Perfluoroalkane sulfonamides			
Perfluorobutane sulfonamide*	FBSA	C4H2O2SNF9	13C8-FOSA
Perfluorohexane sulfonamide*	FHxSA	C6H2O2SNF13	13C8-FOSA
Perfluorooctane sulfonamide	FOSA	C8H2O2SNF17	13C8-FOSA
N-methylperfluoro-1-octane sulfonamide	MeFOSA	C9H4O2SNF17	d3-MeFOSA
N-ethylperfluoro-1-octane sulfonamide	EtFOSA	C10H6O2SNF17	d5-EtFOSA
Perfluoroalkane sulfonamido acetic acids			
Perfluorooctane sulfonamido acetic acid[ii]	FOSAA	C10H4O4SNF17	d3-MeFOSAA
N-methylperfluorooctane sulfonamido acetic acid[i, ii]	MeFOSAA	C11H6O4SNF17	d3-MeFOSAA
N-ethylperfluorooctane sulfonamido acetic acid[i, ii]	EtFOSAA	C12H8O4SNF17	d5-EtFOSAA
Fluorotelomer Sulfonates			
4:2 fluorotelomer sulfonate	4:2 FTS	C6H5O3SF9	13C2-4:2 FTS
6:2 fluorotelomer sulfonate	6:2 FTS	C8H5F13SO3	13C2-6:2 FTS
8:2 fluorotelomer sulfonate	8:2 FTS	C10H5O3SF17	13C2-8:2 FTS
10:2 fluorotelomer sulfonate	10:2 FTS	C12H5O3SF21	13C2-8:2 FTS
Fluorotelomer Alkanoic Acids			
6:2 fluorotelomer carboxylic acid[iii]	6:2 FTCA	C8H3O2F13	13C2-6:2 FTCA

8:2 fluorotelomer carboxylic acid[iii]	8:2 FTCA	C10H3O2F17	13C2-8:2 FTCA
10:2 fluorotelomer carboxylic acid[iii]	10:2 FTCA	C12H3O2F21	13C2-10:2 FTCA
3:3 fluorotelomer carboxylic acid	3:3 FTCA	C6H5F7O2	13C2-6:2 FTCA
5:3 fluorotelomer carboxylic acid	5:3 FTCA	C8H5F11O2	13C2-6:2 FTCA
7:3 fluorotelomer carboxylic acid	7:3 FTCA	C10H5F15O2	13C2-8:2 FTCA
2H-Perfluoro-2-octenoic acid (6:2)[iii]	6:2 UFTCA	C8H2O2F12	13C2-6:2 UFTCA
2H-Perfluoro-2-decenoic acid (8:2)[iii]	8:2 UFTCA	C10H2O2F16	13C2-8:2 UFTCA
2H-Perfluoro-2-dodecenoic acid (10:2)[iii]	10:2 UFTCA	C12H2O2F20	13C2-10:2 UFTCA
Other ESI- analytes			
3H-4,8-dioxa-perfluorononanoic acid*	ADONA	C7F12O4H2	C7F12O4H2
Perfluoro ethyl cyclohexane sulfonate*	PFEtCHxS	C8HF15O3S	18O2-PFHxS
ESI+ analytes			
N-dimethyl ammonio propyl perfluorohexane sulfonamide	AmPr-FHxSA	C11H13O2N2SF13	N/A
6:2 fluorotelomer sulfonamido propyl betaine	6:2 FTSA-PrB	C15H19O4N2SF13	N/A
N-trimethylammoniopropyl perfluorohexane sulfonamide*	TAmPr-FHxSA	C12H15O2SN2F13	N/A
5:3 fluorotelomer betaine*	5:3 FTB	C12H14O2NF11	N/A
6:2 hydrido-fluorotelomer betaine*	6:2 H-FTB	C12H13O2NF12	N/A

*These standards became available after the start of this project were therefore omitted from earlier analyses.

i. Exist in the standard as the linear and branched isomers.
ii. FOSAA, MeFOSAA, and EtFOSAA were excluded from high-level (>3.85 ng/mL) calibration standards to prevent instrument carryover.
iii. Stored in 100% Optima HPLC-grade isopropanol (IPA) to limit potential degradation. (All other compounds stored in 100% HPLC-grade methanol.)

Results of target PFAS and suspect analysis (described below) of the Task 1.2 and 1.4 soils are shown in **Figure 1.2**. Reporting limits were determined by calibration ranges and method blanks, and ranged from 0.00075 - 0.015 ng / g. All results were corrected from blank concentrations and error values reflect the standard deviation of quadruplicate measurements. PFAS concentrations were not corrected for water content, which was below 5% in both soils.

Overall, PFAS concentrations were dramatically higher in Soil B, in which PFOS is present at approximately 8.5 µg/g and 17 individual compounds were present at concentrations exceeding 10 ng/g. Broad cross-section of PFASs were identified both soils, including PFCAs, PFSAs, sulfonamide-based PFASs, X:2 fluorotelomer sulfonates, and, in Soil B, PFOS with a single Cl substitution (Cl-PFOS). Soil A contained a higher fraction of long-chain PFAS than Soil B, for example, compounds longer than PFOA account for 42 % of the PFCA mass in Soil A, and less than 1 % in Soil B. Additionally, multiple X:2 FTS compounds were detected in both soils with 6:2 FTS present in the second highest concentration of any target PFAS in Soil A. Since X:2 FTSs are typically not found in AFFFs, their presence in high concentrations may indicate the *in-situ* processing of compounds originally present in AFFF.[2] Finally, the presence of sulfonamide and fluorotelomer compounds in both soils may indicate that AFFFs from multiple sources were used at each site.

In response to a question raised at the 2018 IPR for ER-2720, the soils were sent to SGS Axys Analytical Services Ltd. for PFAS analysis to confirm the measurements made at Mines. Overall, 27 PFAS concentrations were evaluated at both laboratories, including eleven PFCAs (C4 – C14), eight PFSAs (C4 – C12), three X:2 FTSs (4:2, 6:2, 8:2), and five sulfonamide compounds (FOSA,

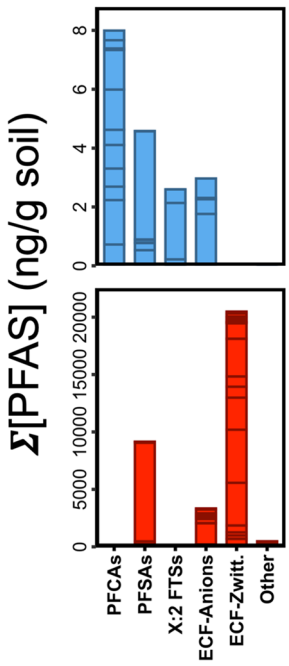

Figure 1.2. Concentrations of various PFAS classes in Soil A (top) and Soil B (bottom).

MeFOSA, EtFOSA, MeFOSAA, EtFOSAA). At Mines, soil extractions were performed with a protocol that combined acidic and basic extraction solutions, while at Axys only a basic extraction solution was used. Further, at Mines, quantitation was performed by LC-QTOF-MS, while LC-MS/MS was used at Axys. A comparison of the measured results is shown in **Figure 1.3**.

Overall, measurements made by the two laboratories corresponded well. Twenty compounds were quantitated in Soil A by both laboratories, with an average ratio of 1.06 ± 0.45, and sixteen compounds were quantitated in Soil B by both labs with an average ratio of 1.15 ± 0.49 (PFNS excluded). Long chain PFSAs (i.e., PFNS, PFDS, PFDoS) were consistently higher in measurements made at Mines, with Mines recording a PFNS concentration of 230 ± 64 ng /g vs. 2.9 ± 0.2 ng / g recorded by Axys. Additionally, while Axys reported non-detects for PFDS and PFDoS, Mines reported values of 11.3 ± 4.2 and 0.7 ± 0.3 ng / g, respectively. Also, two sulfonamidoacetic acids, MeFOSAA and EtFOSAA, were not reported in Soil B by Axys, while Mines recorded values of 10.5 ± 0.9 and 1.3 ± 0.3 ng/g, respectively. Later work revealed that these compounds may have mis-identified, and were actually newly discovered structural isomers. That the compounds for which large discrepancies were observed share chemical characteristics may indicate that that the Mines extraction protocol, which uses both acidic and basic extraction solvents, is more effective at extracting longer chain or sulfonamide-based PFASs from soils.

Suspect Analysis. The identification of suspect PFASs was based on accurate mass measurement for the parent molecular ion, isotopic pattern matching scores, and, for compounds present in the MS/MS library, the library purity score. Samples were screened by searching for the deprotonated molecular ion [M-H]- using an XIC window of 0.01 Da, a signal:noise threshold of 10:1, a minimum peak intensity 100, with baseline subtraction over 2 minutes. In cases where there were multiple possible hits for one peak, the largest peak found was reported unless other lines of evidence, such as retention times of homologous compounds, supported the identification of a smaller peak. The HRMS MS/MS library was screened for matches using a mass error threshold of 0.1 Da for the precursor ion and 0.4 Da for the product ion, and an intensity threshold of 5% of the

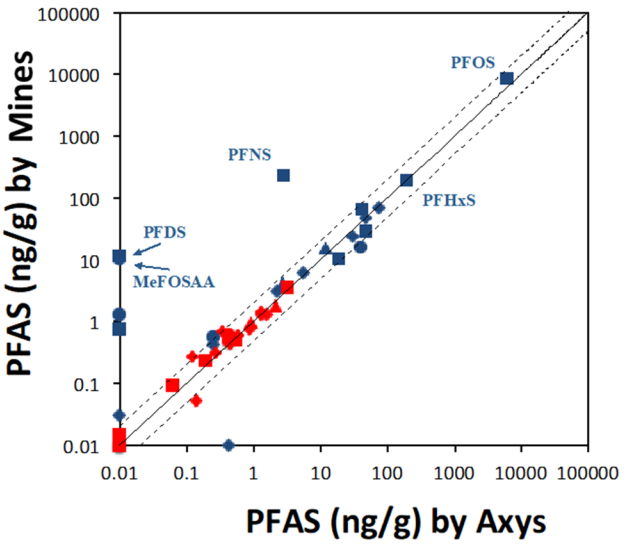

Figure 1.3. Target PFAS concentrations in Soil A (red) and Soil B (blue), measured at Mines (y-axis) and Axys Laboratories (x-axis). A 1:1 ratio is indicated by the solid line, 2:1 ratios by dotted lines. Non-detects are visualized as having a concentration of 0.1 ng / g.

highest peak in the MS/MS spectrum. Library purity score was calculated by an algorithm in SCIEX OS software based on the quality of match between the library and experimental MS/MS spectrum (both presence/absence of expected fragments and relative fragment abundance).

To confirm MS/MS library and XIC list matches, data were exported from SCIEX OS and parsed using a custom R script. An example output of this R script is shown in **Figure 1.4**. Peaks were considered to be XIC list matches when well-defined peaks with a consistent retention time were observed, with even spacing between homologous series members, mass errors predominantly < 5 % and isotope pattern errors predominantly < 10%. Features for which there was more than one possible identification, based on mass and isotope pattern, were flagged as isomers, unless MS/MS fragmentation allows compound differentiation.

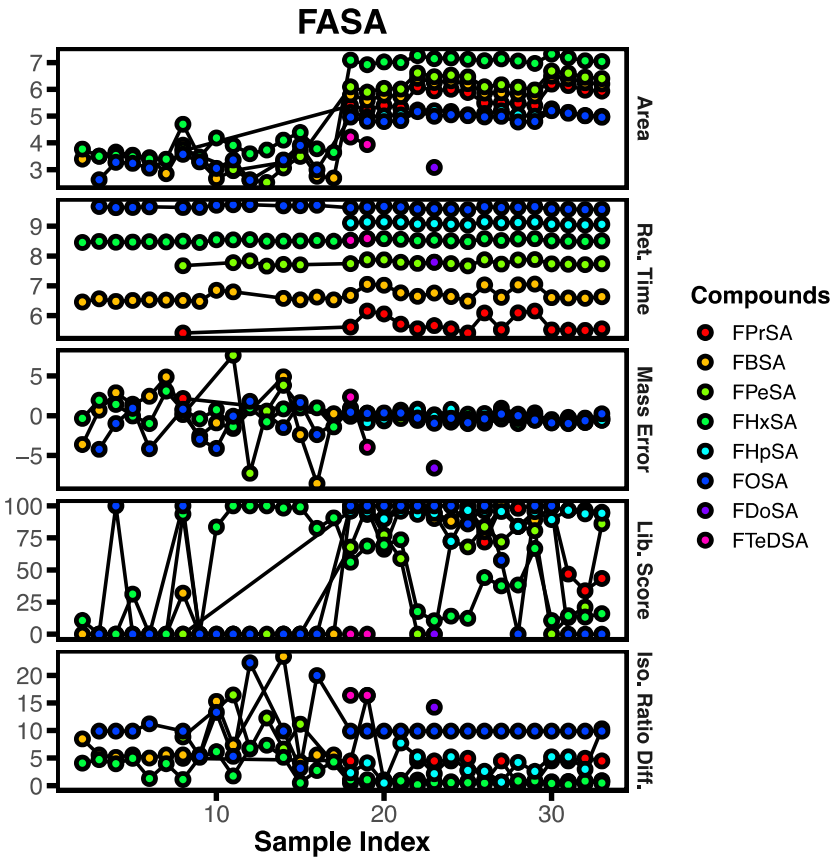

Figure 1.4. Example output of custom R script used to evaluate suspect screening hits at Mines. The top panel displays log(peak area), the second panel retention time (minutes), the third panel mass error (ppm), the forth panel Library Score, and the fifth panel Isotope Ratio Difference (%).

Suspect analysis results were reported in terms of peak area counts or in estimated concentrations by semi-quantitation. Suspect match semi-quantitation proceeds by an identical process as target compound quantitation, by associating each suspect compound with a calibrant and internal standard that agree closely in ionizable functional groups and perfluorinated chain length. The concentration of suspect matches was determined as a function of the response factor of the associated calibrant/internal standard pair, the molar mass of the calibrant, the molar mass of the suspect compound, the observed peak area of the suspect compound, the observed peak area of the internal standard, and the nominal mass of the internal standard as in **Equation 1.1**. All reported semi-quantification results specify the calibrant and internal standards used to estimate the concentration of suspect compounds.

$$"mass"_{suspect} = (response\ factor_{CAL-IS}) \times \frac{molar\ mass_{suspect}}{molar\ mass_{CAL}} \times \frac{area_{suspect}}{area_{IS}} \times nominal\ mass_{IS} \qquad \textbf{(Equation 1.1)}$$

Suspect PFAS Analysis Results. Based on the suspect screening protocol described above, three suspect compounds in three homologous series classes were identified in Soil A, while 76 suspect compounds in 18 homologous series classes were identified in Soil B. As with the target analysis, suspect screening identified a combination of sulfonamide and fluorotelomer compounds in Soil A, suggesting that both 3M and fluorotelomer-based AFFFs were used. In Soil A, the suspect PFASs identified in were all closely related to compounds identified by target PFAS analysis, with two differentiated from observed target compounds by a single substitution (i.e., 1OH-6:2 FTS vs. 6:2 FTS, UPFOS vs. PFOS). In Soil A EtFHxSA was semi-quantitated at 2.8 ± 2.6 ng / g, which was only exceeded by PFOS. Overall, suspect compounds were estimated to be contribute a total PFAS mass of 2.81 ng / g, well below the sum of target PFASs (15.8 ng / g) for the Soil A soil.

In Soil B, a diverse range of substituted PFSAs were identified by suspect screening, including H-PFASs, Cl-PFASs, O-PFASs, keto-PFASs (K-PFASs), unsaturated PFASs (U-PFAS), as well as F5S-PFASs and perfluorosulfinates (PFASi). Additionally, a variety of branched, sulfonamide-based compounds, including compounds that are expected to be zwitterionic at environmental pH, were identified. Many of the sulfonamide-based classes, including AmPr-FASA, AmPr-FASA-PrA, CMeAmPr-FASA, and SPrAmPr-FASA, were previously identified in 3M AFFFs.[3,4] The overall concentrations of suspect PFASs were much higher than those observed in Soil A, with five compounds semi-quantitated at concentrations over 500 ng /g and FHxSA semi-quantitated at almost 8000 ng / g. Suspect compounds were estimated to contribute a total PFAS mass of 37.3 µg / g, far in excess of the sum of target PFASs (9.2 µg / g). Additionally, over 98% of the semi-quantitated suspect compound mass is comprised of sulfonamide-based compounds that are likely PFSA precursors.

To provide further detail into the process of confirming suspect PFAS hits, results for the N-dimethyl ammonio propyl perfluoroalkane sulfonamido propanoic acid class (AmPr-FASA-PrA) are provided as an example in **Figure 1.5.** Members of this class with 3-8 perfluorinated carbons were previously identified in a 3M AFFF.[4] Four members of this class were identified in Soil B, and remained present following gamma irradiation. An example chromatogram of the four observed AmPr-FASA-PrA compounds in Soil B, with possible branching of the perfluorinated carbon chains indicated by the split peaks of AmPr-FPeSA-PrA and AmPr-FHxSA-PrA, is shown in **Figure 1.6**.

In addition to compound confirmation by matched accurate parent mass and isotope ratio distribution the MS/MS spectra of AmPr-FPrSA-PrA and AmPr-FHxSA-PrA were matched with reference MS/MS spectra. An example MS/MS spectrum for AmPr-FHxSA-PrA is shown in **Figure 1.7**, which demonstrates agreement between the observed spectrum for both parent mass as well as numerous fragment masses.

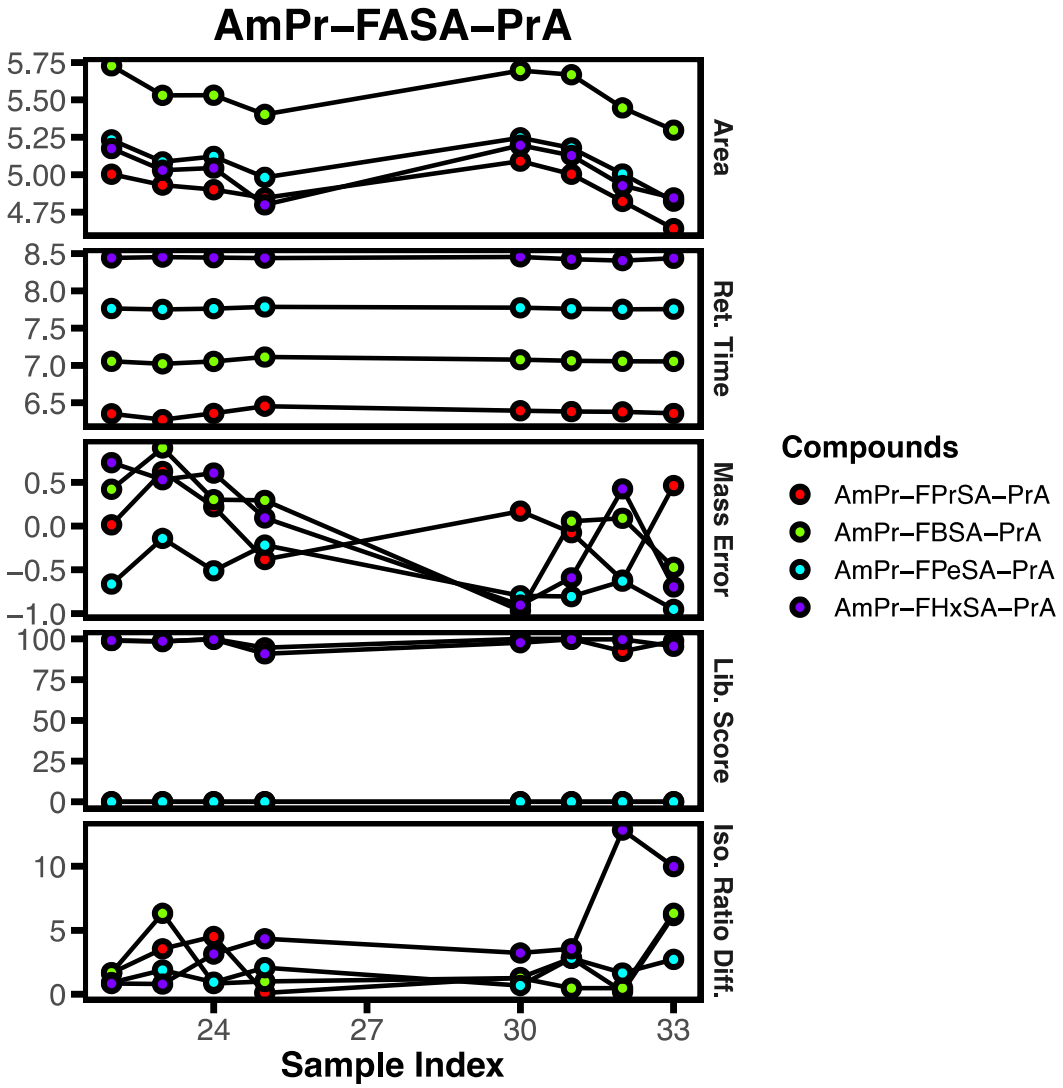

Figure 1.5. Suspect hit dashboard for the class AmPr-FASA-PrA in Soil B (sample index 30 – 34) and gamma-irradiated Soil B (sample index 22 – 25). Area is shown in logarithmic units, retention time is shown in minutes, mass error is shown in ppm, library score is shown in %, and isotopic ratio distribution is shown in %.

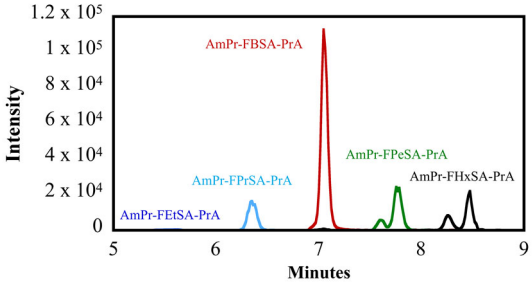

Figure 1.6. Chromatogram of AmPr-FASA-PrAs extracted from Soil B.

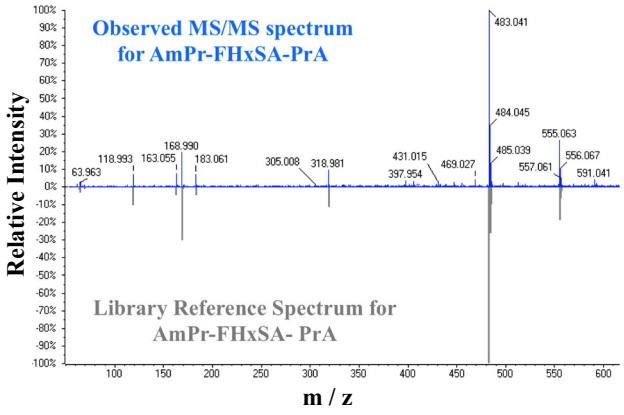

Figure 1.7. MS/MS spectrum of AmPr-FHxSA-PrA from an extract of Soil B against a library reference spectrum of the same compound.

Aqueous Sample Preparation. Sample preparation for aqueous samples in Tasks 1.2, 1.4, and Task 4.2 was conducted in 15 mL centrifuge tubes. A combination of sample and water (Optima, Fisher) was added to a centrifuge tube such that the total volume was 1780 µL and less than 20 ng of any single PFAS was present. Then, 470 µL methanol (Optima, Fisher), 260 µL isopropanol (Optima, Fisher), 90 µL of basic water (5 µL concentrated ammonium hydroxide in 50 mL Optima water), and 100 µL of a solution containing internal standards at 2 ng / mL in 80:20 methanol water, were added to the vial, which was vortexed for 30 seconds and centrifuged at 3,500 rpm for 15 minutes. The supernatant was poured off and injected directly into the LC-QTOF-MS. Method blanks were created and analyzed with each analytical batch and approximately 10% of samples were prepared and analyzed in triplicate. Relative standard deviations were typically less than 10%. Sample preparation for aqueous samples in Task 4.1 was similar to the above except samples were diluted directly into the autosampler vials with identical solvent composition. Isopropanol was omitted from vials prepared for ESI+ analysis due to causing peak broadening.

Suspect Screening for Hydrocarbon Surfactants in AFFF and AFFF-Contaminated groundwater. The role of hydrocarbon surfactants in AFFF remains largely unexplored in regards to key processes that impact PFAS mass discharge, attention, and treatment of groundwater contaminated by AFFFs. The first step to understanding how hydrocarbon surfactants impact key processes is to determine which hydrocarbon surfactants are in AFFFs and which are in AFFF-impacted groundwater. Hydrocarbon surfactants are added along with PFASs to create proprietary mixtures of AFFFs that are used to extinguish hydrocarbon-based fuel fires. More is known about the identity of PFASs that comprise only 0.9-1.5% (w/w) in AFFF, compared to hydrocarbon surfactants, which comprise 5-10% (w/w) of AFFFs.[5,6]

To remedy the lack of data on the classes and homolog distribution of hydrocarbon surfactants in AFFFs or AFFF-contaminated groundwater, we undertook a suspect screening study. The objective of this study was to use this semi-automated, homologous series detection method for elucidating suspect surfactants in eight AFFFs and 10 AFFF-contaminated groundwaters collected from fire-fighter training areas source zones on nine US military bases. The AFFFs included four 3M AFFFs and four fluorotelomer-based AFFFs including Buckeye, Ansul, ChemGuard, and National Foam. All samples were analyzed by LC-QTOF-MS. Suspect screening on AFFFs and AFFF-impacted groundwater was performed using a screening list of hydrocarbon surfactants from the Norman suspect list exchange database[7] and the enviMass workflow for data processing. The suspect list includes some degradation products, none of which were detected in AFFF or AFFF-contaminated groundwater. Non-target analysis to identify unknown surfactant series and degradation products was beyond the scope of this study. A schematic of the data analysis workflow used for surfactant identification is shown in **Figure 1.8**.

A total of nine hydrocarbon surfactant classes were identified with confidence level 2-3 in the eight AFFFs with seven common to both 3M and fluorotelomer AFFFs (**Table 1.3**). Homologous series of octylphenol polyethoxylates found in AFFFs is consistent with AFFF patents.[8] Similar ranges in EO units between stored AFFFs and patent literature indicates stability of the octylphenol polyethoxylates over the long period of AFFF storage, which ranged up to 20 years since the time of AFFF manufacture (1988-2012; **Table 1.3**). Nonylphenol polyethoxylates and its degradation products, mono- and diethoxycarboxylates were on the suspect list but were not detected in any AFFFs. Linear alcohol ethoxylates ($EO_{2\text{-}10}$) appear in 3M AFFFs and Buckeye. Linear alcohol

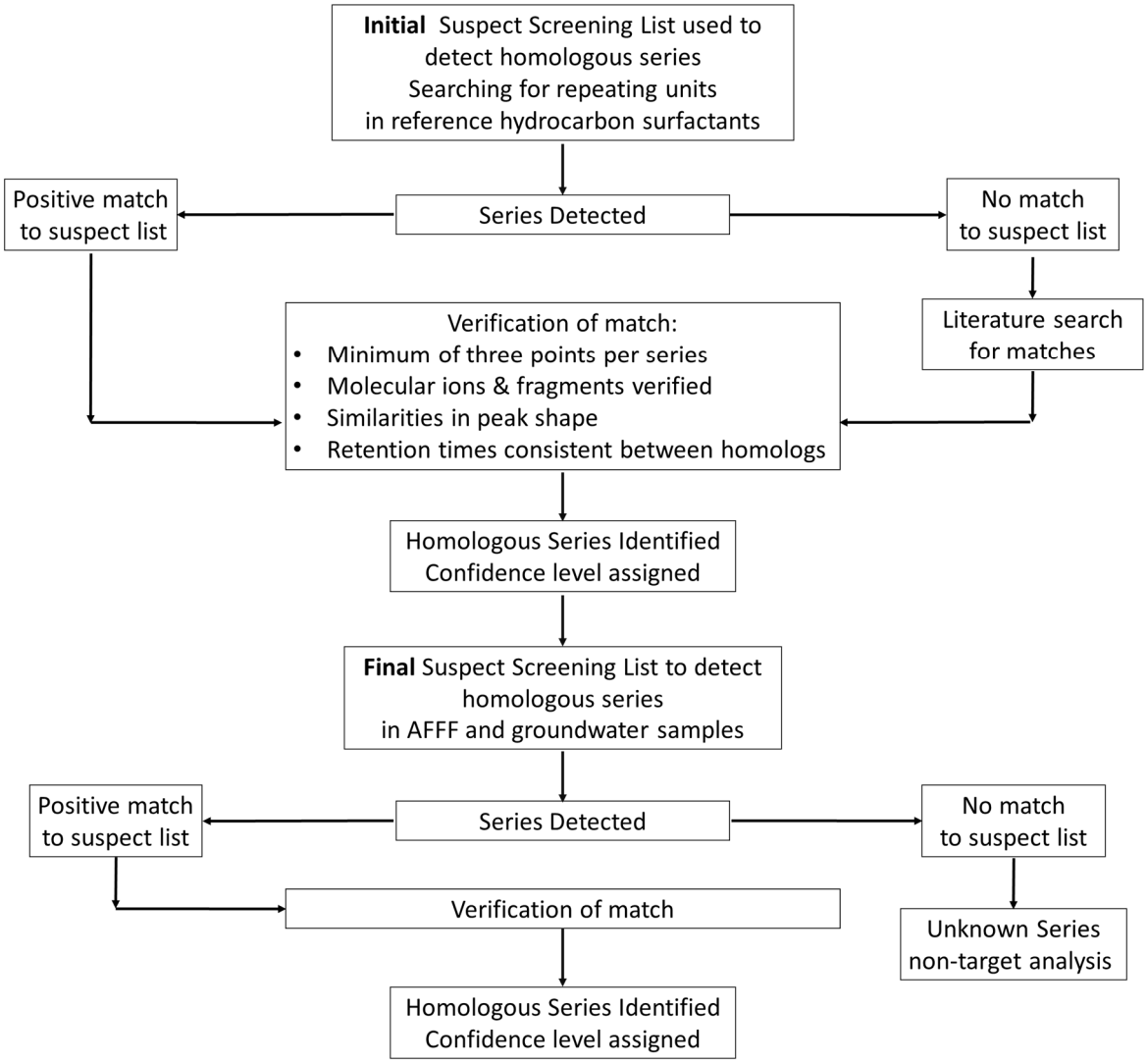

Figure 1.8. Workflow indicating steps to create final suspect list from database and Reference Materials and to detect homologous series of hydrocarbon surfactants in AFFF and AFFF-contaminated groundwater.

ethoxylates are added to AFFFs to reduce surface tension.[6] Ethoxylated cocoamines ($C_{14\text{-}17}EO_3$) were only detected in telomer-based AFFFs (Buckeye and National foam). Homologous series of alkyl ether sulfates, which are characterized as "foam boosters",[8] were found in seven out of eight AFFFs. Alkyl amido dipropionates were found in only Buckeye and Chemguard, which are telomer-based AFFF. Linear alkyl benzene sulfonates ($C_{10\text{-}13}$) were detected in six out of eight 3M and telomer-based AFFFs. Alkyl sulfonates and alkyl sulfates were detected in three and six out of eight 3M and telomer-based AFFFs. Polyethylene glycols were found in five out of eight AFFF with similar EO. Additional unknown series characterized by repeating alkyl, and ethoxylate units remain unidentified in the AFFFs, but identifying surfactants not in the suspect list (non-target analysis) was beyond the scope of the study. Importantly, many of these surfactants were also detected in AFFF-impacted groundwater (**Table 1.4**).

Although concentrations were not determined, it is important to know that hydrocarbon surfactants are present since they are likely to cause foaming once they enter surface water, exert a biological oxygen demand upon entering surface waters, compete with PFASs on treatment systems like

activated carbon, and consume oxidants during ISCO or the TOP assay. Hydrocarbon surfactants may also impart toxicity to aquatic organisms in surface water when in their parent chemical forms or upon biodegradation. For example, octylphenol polyethoxylates biodegrade to weakly estrogenic form octylphenol upon biodegradation.[9]

Table 1.3. Hydrocarbon surfactant classes classified by repeating units in 3M and fluorotelomer-based AFFFs (Buckeye, Ansul, Chemguard, National Foam). Multiple repeating units are separated by "/".

Class	3M 1993a	3M 1993b	3M 1988	3M 1989	Buckeye 2009	Ansul 2012	Chemguard 2010	National Foam 2003
Octylphenol polyethoxylate[a,b,c] EOn	ND	ND	3-16	ND	4-9	4-10	4-20	ND
linear alcohol ethoxylate[c] Cn / EOn	10/2-10	10/2-10	ND	ND	10/2 -7	ND	ND	ND
Ethoxylated Cocoamine[c] Cn / EOn	ND	ND	ND	ND	14,15,16/3	ND	ND	14,15,16,17/3
Alkyl ether sulfate[b] Cn / EOn	15,16,17/1 12/1-8	15,16,17/1 12/1-7	ND	15,16,17/1 12/1-6	14/1,2,3 12/1-7	15,16,17/1	14/1,2,3 12/1-10	15,16,17/1
Alkyl amido-dipropionates[b] Cn	ND	ND	ND	ND	12,13,14	ND	12,13,14	ND
linear alkyl benzene sulfonate [b] Cn	11,12,13	10,11,12,13	ND	10,11,12,13	10,11,13	10,11,12,13	ND	10,11,12,13
Alkyl sulfonates[b] Cn	8,9,10	ND	ND	9,10,12	ND	ND	ND	9,10,12
Alkyl sulfates[a,b,c] Cn	8,10,12	8,10,12	ND	8,10,12	8,9,10,11,12	ND	8,9,10,12	8,9,10,11,12
Polyethylene Glycol EOn	8-13	ND	8-13	8-13	8-13	10-13	ND	ND

ND= Non Detected, which means that no homologous series matched that of the suspect list. Reports of surfactants present in AFFF reported by a) Pabon et al.[5] b) Thomas Marin[6] c) U.S. Patent No. 6,015,838.

Table 1.4. Hydrocarbon surfactant classes classified by repeating units in groundwater. Multiple repeating units are separated by "/".

Class	A	B	C	D	E	F	G	H	I	J
Octylphenol polyethoxylate[a, b,c] EOn	4-11	4-11	4-9	ND	4-11	ND	7-11	5-10	5-9	3-11
linear alcohol ethoxylate[c] Cn / EOn	ND	ND	ND	ND	ND	ND	10/2-8	10/2-7	10/3-7	10/3-8
Ethoxylated cocoamine[c] Cn	ND	ND	ND	ND	ND	ND	ND	ND	ND	14-16

Alkyl ether sulfate[b] Cn / EOn	ND	ND	ND	ND	ND	ND	ND	ND	15/1-6	16/8-12
Diethanolamide Cn	ND	7, 9, 11, 13	7, 9, 11, 13	7, 9, 11, 13	11, 13,15	7, 9, 11, 13	ND	7,11, 13, 15	9,11,13	ND
Alkyl amido betaine[b] Cn	ND	ND	ND	ND	ND	4,5,6,7	ND	4,5,6	ND	4,5,6
Alkyl amido dipropionate[b] Cn	ND	ND	ND	ND	ND	8,10,12	ND	ND	ND	6,8,10
Linear alkyl benzene sulfonate[b] Cn	ND	ND	ND	11,12, 13,14	ND	ND	ND	ND	10,11, 13,14	ND

ND= Non Detected, which means that no homologous series matched that of the suspect list. Reports of surfactants present in AFFF reported by a) Pabon et al.[5] b) Thomas Marin[6] c) U.S. Patent No. 6,015,838

Task 1.2 ***Release of PFASs in the Absence of NAPL.*** This subtask investigated the release of anionic, cationic, and zwitterionic PFASs from field-collected AFFF-contaminated soils. To that end, experiments were conducted in which AFFF-impacted soils, collected at the fire-training grounds of two Air Force Bases (Soil A and Soil B), were packed into glass columns through which artificial groundwater (AGW) was pumped and the effluents collected.

Soil Column Experiments under Unaltered Conditions. Soil A and Soil B were sifted through 2 mm sieves and analyzed for water content. To identify the role of biological processes, an aliquot of each soil was sent to the School of Nuclear Science and Engineering at Oregon State University, where they were sterilized by exposure to gamma rays at a dose of 2.5 x 10^6 Rad. Kimble Chase Kontes Chromaflex glass columns (48 x 150 mm) were selected to allow experimental flow rates that provided sufficient effluent volume for the analysis of PFASs, anions, cations, pH, and optical properties. Each soil was packed into duplicate glass columns by repeatedly pouring out ~ 1 cm of soil, then vortexing and mechanically compressing the columns until filled. Duplicate columns were similarly prepared with the gamma-irradiated soils. Each column was weighed prior to and following packing, as well as following saturation with synthetic groundwater in order to determine the mass of soil added as well as the column pore volume. A schematic of the experimental apparatus is shown in **Figure 1.9** and an image of the experimental apparatus and fraction collector is shown in **Figure 1.10.**

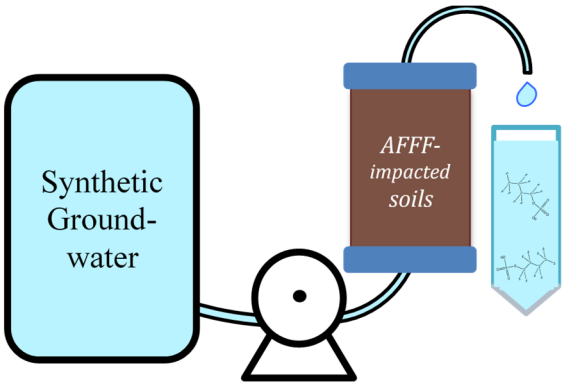

Figure 1.9. Schematic of experimental apparatus used in Task 1.2 and 1.4 column experiments.

Synthetic groundwater was prepared as in **Table 1.5**. Packed columns were found to have pore volumes of approximately 0.1 L, so the synthetic groundwater was pumped through columns at a flow rate of approximately 0.2 L / day, resulting in a hydraulic residence time of approximately ½

day. Effluent samples were collected using a custom-built fraction collector at intervals of ~4 samples / pore volume for the first 5 pore volumes, ~1 sample / pore volume to 20 pore volumes, ~1 sample / 4 pore volumes to 50 pore volumes, and ~1 sample / 10 pore volumes to 150 pore volumes. After each column was run for approximately 100 pore volumes, NaCl in the synthetic groundwater was replaced with an equimolar amount of NaBr for 5 pore volumes to determine column dispersivity.

Column effluent samples were analyzed for pH, UV-vis absorbance, dissolved organic carbon concentration, anion concentrations by ion chromatography, cation concentrations by inductively coupled plasma atomic emission spectroscopy, and target and suspect PFASs by LC-QTOF-MS.

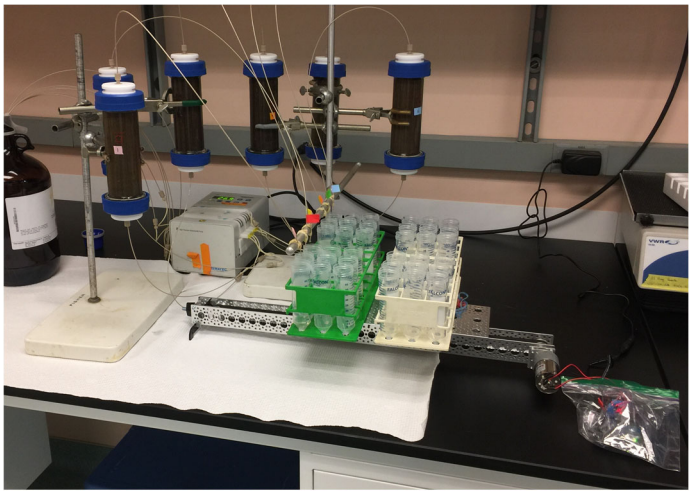

Figure 1.10. Fraction collector used to collect effluents from Task 1.2 and 1.4 columns.

Flow interruption experiments. A follow-up experiment was conducted after the original columns in Task 1.2 were complete to elucidate the processes driving the observed PFAS elution profiles. Chemical or physical nonequilibrium processes, such as rate-limited desorption or the presence of an immobile water phase with limited exchange with the bulk water phase, were thought to potentially be responsible for the observed PFAS effluent profiles. To evaluate the contribution of nonequilibrium processes, a column experiment was performed identically as to the Task 1.2 column experiments except that upon filling the column with AGW, flow into the column was paused for 89 days, during which the column was sealed and stored in the dark at 3°C. It was then brought to room temperature and flow was resumed for 23 days, interrupted for an additional 7 days, and finally resumed for 14 days.

Table 1.5. Components of artificial groundwater used in Task 1.2 column experiments.

Component	Concentration in Synthetic GW
$MnSO_4$ * H2O	1 mg / L
Na_2SO_4	180 mg / L
NaCl	113 mg / L
$NaHCO_3$	40 mg / L
Concentrated HCl	As needed to adjust pH to 7

Results. Each soil column was prepared in duplicate and approximately 150 pore volumes of AGW were pumped through each column. Column effluents were collected in 50 mL centrifuge tubes with a custom fraction collector to monitor PFAS release from the soils. PFAS concentrations were measured in the effluents by LC-QTOF-MS. To estimate the total PFAS mass released from the soil columns, effluent samples were taken continuously for roughly the first five pore volumes, and from then on PFAS concentrations in effluent were either directly measured or interpolated from adjacent samples. The release of target and suspect PFASs from columns packed with Soil A and Soil B is summarized in **Figure 1.11**. The cumulative mass of individual PFASs released from the packed soil columns varied depending on the compound observed. For example, on average 168% of the nominal mass of PFPeA was recovered in the effluent of the Soil A columns,

compared with only 8% of the mass of PFUdA. However, in effluent from Soil B-packed columns, $C_3 - C_{10}$ PFSA cumulative recoveries were 82 ± 41 % of the nominal PFSA mass initially present. More importantly, many of the precursors observed in Soil B were not completely eluted from the columns (**Figure 1.11**).

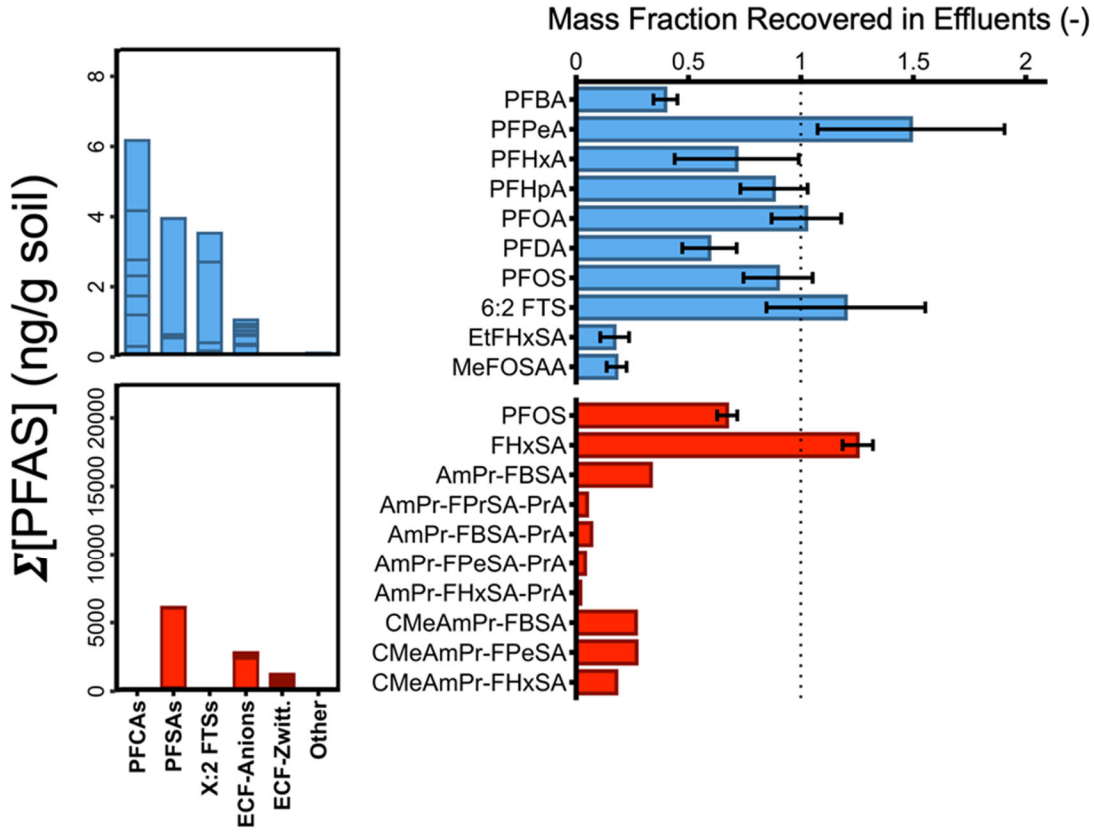

Figure 1.11. Total PFAS mass recovered in the Soil A column effluents (top left), divided into PFCAs, PFSAs, X:2 FtSs, anionic ECF-derived precursors (ECF-Anions), zwitterionic ECF-derived precursors (ECF-Zwitt.) and others, as well as fractional mass recovery (top right) in the Soil A column effluents of the ten highest concentration PFASs in Soil A. The analogous data for Soil B are provided in the bottom two panels.

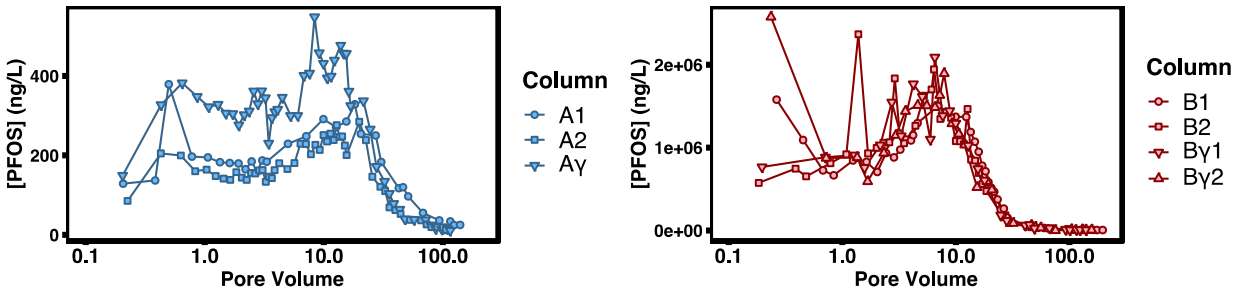

Figure 1.12. Example elution profile showing PFOS elution from replicate Soil A columns (left) and replicate Soil B columns (right).

Peak PFAS concentrations observed in the effluent from the Soil A columns were similar between the replicate columns (**Figure 1.12**). For example, the peak effluent concentrations of C_4-C_{11} PFCAs in column 7 was 74 ± 28 % of the peak concentrations in column 1. Similarly, there was good agreement in the total mass eluted, with the mass of C_4-C_{11} PFCAs eluted in column 7 was 78 ± 22 % of column 1. Similarly, there was good agreement between the total mass of C_4-C_{11} PFCAs eluted by the γ-irradiated Soil A column, which were 106 ± 31 % of the average mass eluted from the non-irradiated columns. Peak PFAS concentrations observed in the effluent from Soil B columns were also similar between replicate columns, with peak C_3 – C_{10} PFSA concentrations in column 4 being 118 ± 30 % of the peak concentrations in column 3. As with the Soil A soil columns there was good agreement in the total PFAS mass eluted between the replicate columns filled with Soil B, as well as between the columns filled with irradiated and non-irradiated soil. For example, the mass of C_4-C_8 PFCAs eluted in column 4 was 117 ± 47 % of the mass of the same compounds eluted from column 3. Further, the average cumulative mass of C_4 – C_9 PFSA from the columns with gamma-irradiated Soil B was 91 ± 11 % of the non-irradiated columns.

However, concentration profiles varied dramatically both within homologous series (**Figure 1.13**) and between compounds with the same perfluoroalkyl chain length and or the same head group (**Figure 1.14**). The data presented in **Figure 1.13** (top and bottom) as well as **Figure 1.14** (left panel) clearly show that compounds with the shortest perfluorinated carbon chains elute earlier (in the case of PFBA, typically within the first pore volume; **Figure 1.13**). In contrast, longer PFCAs show an initial increase in concentration followed by a steep decrease, with the period of initially increasing concentrations correlating with perfluorinated carbon chain length. A similar trend can be seen in the concentration profile of PFSAs in the effluent of a Soil B column (**Figure 1.13**, bottom). However, the elution profile of PFSAs is more complex than the PFCAs, as some show two maxima. One maxima is unrelated to perfluorinated chain length and occurs within the first pore volume, while longer chain PFSAs show a second maxima that occurs increasingly later for longer chain PFSAs.

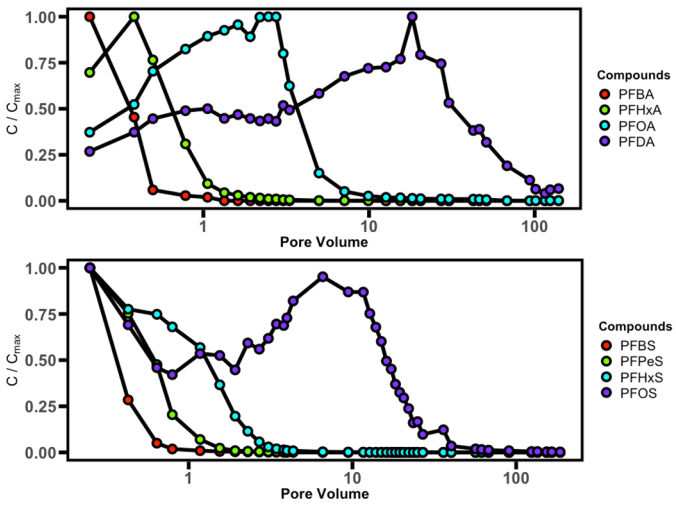

Figure 1.13. Effluent concentration profile of PFBA, PFHxA, PFOA, and PFDA in effluent from a column packed with Soil A (top). Effluent concentration profile of PFBS, PFPeS, PFHxS, and PFOS from a Soil B column (bottom).

The role of functional group in determining elution profile is apparent in **Figure 1.14** (right panel), which compares the elution profile of five compounds with six perfluorinated carbons. These later-eluting compounds are polyfluorinated precursors to compounds such as PFHxS. In other words, at later pore volumes, compounds that were slower eluted make up an increasing fraction of the effluent PFAS mass balance and the effluent make up moves away from highly oxidized PFAAs to potential PFAA precursors, such as sulfonamide-based compounds. As is clear in from the cumulative mass eluted profiles presented in **Figure 1.15**, some compounds only begin to elute

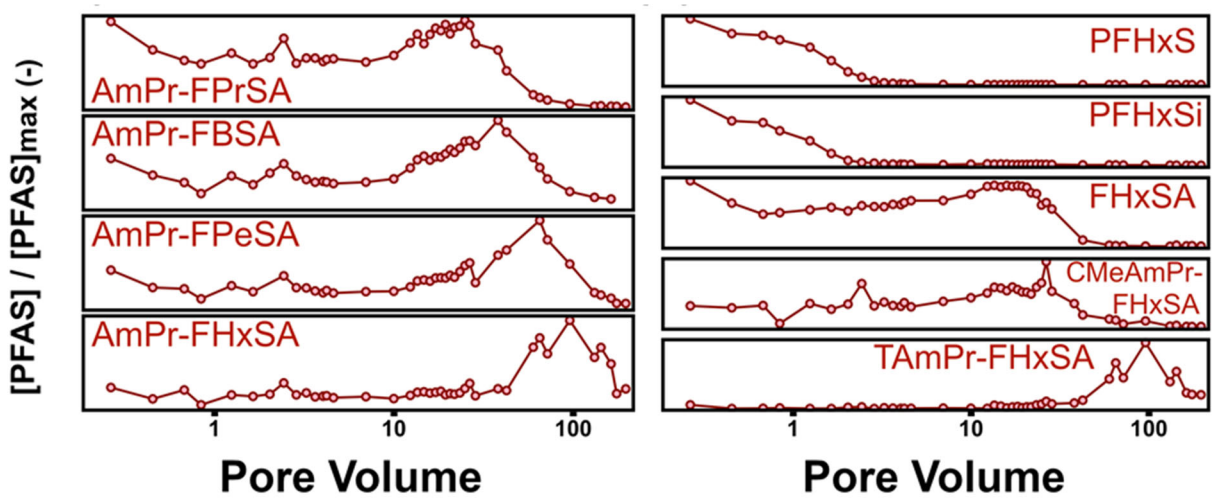

Figure 1.14. Maximum value normalized concentrations with eluted pore volumes of artificial groundwater of selected N-dimethyl ammonio propyl perfluoroalkane sulfonamides (left) and various six perfluorinated carbon PFASs (right) in the Column B1 effluents.

from the soil columns after other compounds have completely eluted even if these compounds share the same head group (**Figure 1.15**, top). As is also clear from **Figure 1.15**, the fractional mass eluted can be very different for compounds with the same perfluorinated chain length (**Figure 1.15**, bottom).

Stop flow experiments. The two month pause in flow was anticipated to allow PFASs present in the soil to come to equilibrium with the introduced groundwater phase and cause PFAS concentrations in the column effluent to steadily decline. The observed effluent concentration profiles were initially similar to the Task 1.2 experiments in that PFASs showed initially increasing PFAS effluent concentrations in all experiments (**Figure 1.16**).

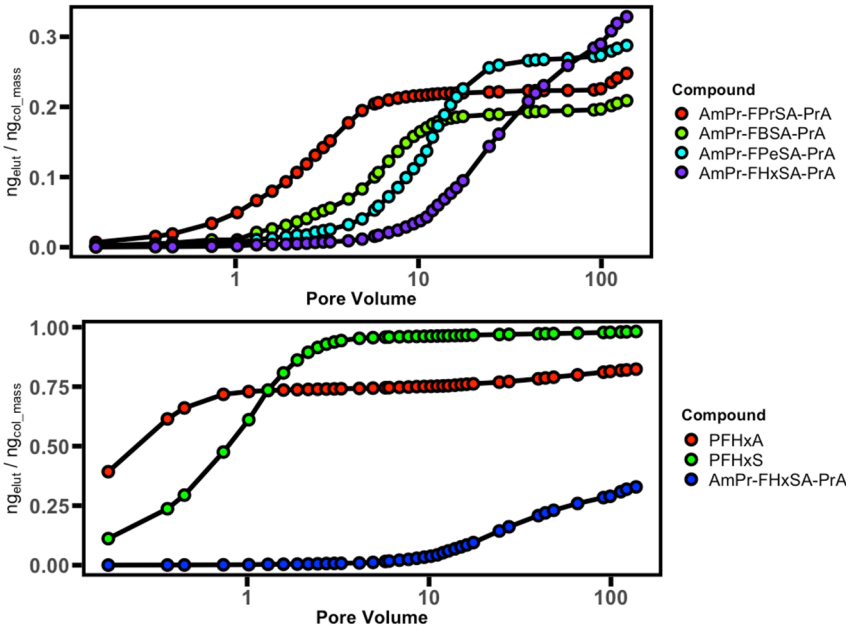

Figure 1.15. Fractional mass of AmPr-FPrSA-PrA, AmPr-FBSA-PrA, AmPr-FPeSA-PrA, and AmPr-FHxSA-PrA eluted in the Soil B column effluent (top), as well as fractional mass eluted of PFHxA, PFHxS, and AmPr-FHxSA-PrA eluted in the effluent of a column packed with Soil B (bottom).

However, a series of effluent concentration perturbations were observed when flow was resumed after the second interruption, indicating the influence of nonequilibrium processes (**Figure 1.17**). Effluent concentrations of shorter chain PFASs (e.g., PFBS, FBSA) increased by up to 12-fold upon flow

resumption and then fell with the continued passage of AGW. The increase in concentrations of shorter chain PFASs indicates that desorption was outpacing adsorption during the flow interruption, causing these PFASs to accumulate in the aqueous phase. Conversely, effluent concentrations of longer chain PFASs decreased after flow resumed, then climbed to transient maxima that were higher than the concentrations observed prior to the interruption. Similar effluent concentration perturbations have been observed for long chain PFAAs in spiked soil and sand columns.[10]

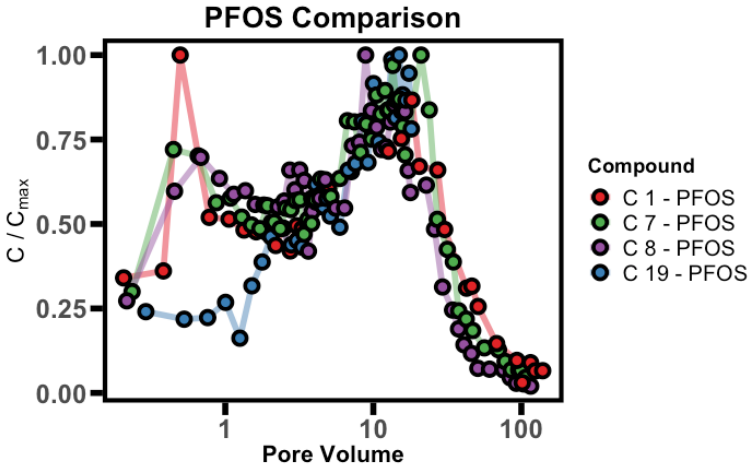

Figure 1.16. Normalized PFOS concentration in the effluents of packed soil columns filled with Soil A. that had been sterilized by γ-irradiation. Artificial groundwater flow was paused for over two months prior to the start of the experiment.

The immediate decrease in effluent concentrations of long chain PFASs upon flow resumption suggests adsorption was outpacing desorption near the effluent end of the column. However, the subsequent effluent concentration rebounds could indicate that desorption was outpacing adsorption farther upstream, creating pulses of elevated PFAS concentration that subsequently eluted. Together, these concentration perturbations arising from flow interruption demonstrate that PFAS release was not governed by equilibrium processes even at the low boundary fluxes used here (~ 0.12 m / day). Similar trends in effluent concentration profiles were seen at the start of flow through previously dry columns as well as after each of the flow interruptions, indicating that sudden increases in flow through either dry or wet soils may lead to transient PFAS pulse releases from AFFF-impacted soils.

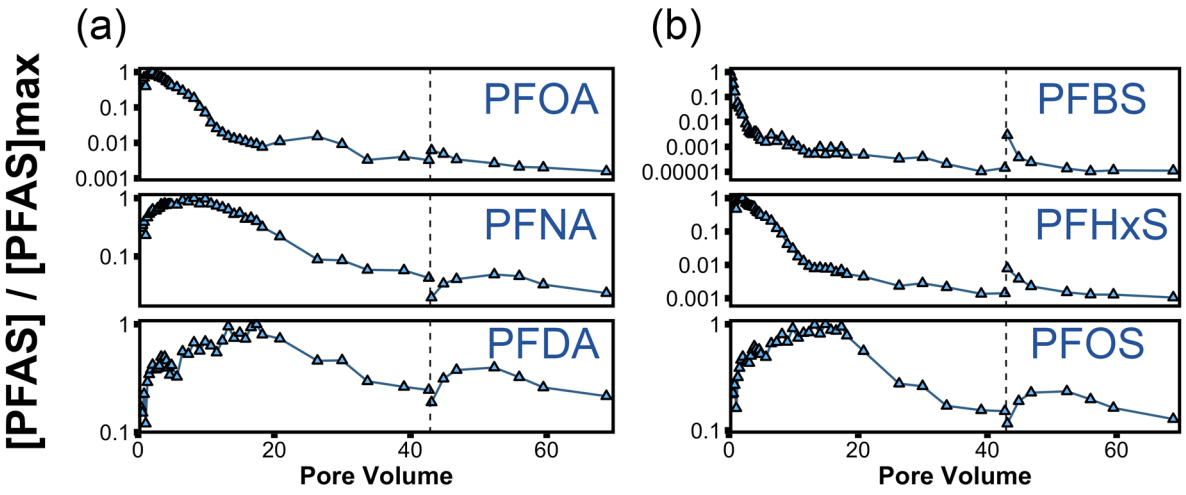

Figure 1.17. Maximum value normalized concentrations with eluted pore volumes of artificial groundwater of (a) selected PFCAS and (b) selected PFSAs in the Soil A effluents. The dashed line indicates a 7-day flow interruption.

Task 1.3. ***Assess PFAS Interactions with NAPL.***

Column Experiments: Sorption to the Air-Water Interface (no NAPL). Oregon State and CDM Smith conducted column experiments to establish water saturation curves in the absences of PFASs and NAPL. The first steps were to validate that PFASs could be quantitatively recovered from sand and that sorption of PFOS to sand was minimal.

Sand extraction validation. Validation of the extraction method was needed to measure PFAS concentrations in the individual column 'slices'. Validation consisted of a series of PFAS spike and recovery experiments performed to determine the accuracy and precision of the extraction/analytical process. In addition, blank slices containing the plastic ring and baked sand were also extracted. For extraction, 5 mL methanol was used to extract the sand slices in triplicate. After shaking, 1,452 μL solvent was used for PFAS analysis by LC-MS/MS.

Sand adsorption experiments (n=4) were performed by combining 6.2 g baked sand (similar mass in one slice) and 8 mL PFOS solution. The bottles were mixed for 24 h and the PFOS concentrations before and after shaking were used to determine the replicate single-point sorption coefficients.

Two-phase column experiments. A series of baked sand columns were constructed using 1 cm long rings according to the methods of Schaefer et al.[11] Columns containing baked sand were assembled, saturated, and allow to partially drain (**Figure 1.18**). Water saturation curves were determined by mass balance for each ring, thereby obtaining water saturation data in 1 cm increments along the length of the column, and the data were plotted as a function of saturation.

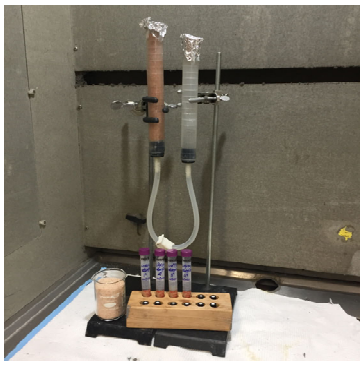

Figure 1.18 Unsaturated sand columns used in Task 1.3.

For the column experiments (with or without PFOS), polycarbonate rings and shrink tubing were used to make up the column. Each ring was 1cm high with 3.8 cm^2 cross-sectional area. The special tubing shrank and held the stacked rings together after being heated. A rubber stopper with a hole in the middle was used to plug the bottom of the column, and a tube with a valve was used to connect the sand column to the water reservoir. A metal screen was placed above the stopper to hold the sand but allow for water drainage in the sand column. During the experiment, the water reservoir was used to control the level of the water in the sand column. Silica sand with diameter in range of 0.1 to 0.2mm was baked at 500°C to remove any organics before being used to fill up the column. Deionized water amended with different concentrations of PFOS aqueous solution (250 - 1100 ng/L) were used in the experiments.

Several column experiments were conducted including a) water saturation tests, b) two-phase experiments to determine interfacial sorption coefficient (K_i) for PFOS, and c) initial three-phase (e.g., NAPL-water) experiments.

In the **water saturation experiments**, column experiments were conducted by first obtaining a saturated sand pack. Water was first poured into the column, followed by the sand, during which

the water level was kept higher than the top of sand bed to saturate the initial bed pore volume. The water reservoir was slowly lowered to lower the water saturation in the sand column until there was just 1 cm above the bottom of the sand column. In the lower section of the column the water saturation was equal to 1. Columns were deconstructed by separating the sand slices. Columns were equilibrated for 6-21 d.

Two-phase column: equilibration time and PFOS concentration. For the interfacial sorption coefficient, K_i, measurements for PFOS, column experiments were carried out in a manner similar to that of the water saturation experiments. With the system validated, a series of experiments were carried out to experimentally select the equilibration period for PFOS from at 1,100 ng/L using a 6, 12, and 21 equilibrium period. Once a final equilibration period was selected, additional two-phase column experiments were performed for 6:2 FTS, 8:2 FTS, PFNA, and FOSA. These PFASs, except for 6:2 FTS share a common eight-carbon fluorinated tail. In addition, duplicate column experiments were performed with groundwater from an AFFF-impacted site. The groundwater was overspiked to obtain data for PFASs including PFCA (C4-C9), PFSA (C4-C9), 6:2 FtS, 8:2 FtS, FHxSA, FOSA, and N-MeFOSAA.

The air-water interfacial partition coefficient (K_i) was calculated using the Gibbs adsorption equation, which expresses the relationship between the amount of surfactant sorbed at an interface per unit area and the related concentration:

$$\Gamma = -\frac{\mathrm{MW}}{\mathrm{RT}} \times \frac{\partial \gamma}{\partial C} = Ki \times C \qquad \textbf{(Equation 1.2)}$$

Where Γ is the surface excess (kg/m^2), γ presents the surface tension (mN/m), C is the PFAS concentration (kg/m^3), R is the gas constant (mJ/ mol K), MW is the molecular weight of surfactant (kg/mol), and Ki is the air-water interfacial partition coefficient (m). The surface excess Γ is related to the total mass of surfactant M_{total}.

$$M_{total} = M_w + M_{a\text{-}w} + M_{s\text{-}w} = CV + \Gamma \times a_{a\text{-}w} + M_{s\text{-}w} \qquad \textbf{(Equation 1.3)}$$

Where M_w is the mass of PFASs in water bulk (excluding the surfactant at the interface), $M_{a\text{-}w}$ is the mass of PFASs accumulated at the air-water interface, $M_{s\text{-}w}$ is the mass of PFASs sorbed by sand, and V presents the volume of water in each sectioned slice measured by weight difference (in the absence of NAPL).

Three-phase experiments. For three-phase experiments, octanol was used as NAPL phase for further 3-phase (air, water, and oil) columns. Octanol has a positive spreading coefficient, thus any PFOS surface excess measured in the columns is attributable to octanol-water interfacial sorption.

Results

Sand extraction method. The recovery and precision of 11 PFCAs (C4-C14), 7 PFSAs (C4-C10), 3 X:2 FTSs (4:2, 6:2, and 8:2), and two mass labelled internal standards (M2 PFOS and M2 PFOA) from sand ranged from 87 ± 8.8 (PFNS) to 110 ±9.9 (PFOS). The recovery experiments were performed using isopropanol as the extraction solvent; similar accuracy and precision results were

obtained, which indicates that either methanol or isopropanol can be used to extract PFASs from sand slices. Isopropanol was used to recover water and NAPL from the sand slices. The data generated by OSU on PFAS recovery verified that a single extraction protocol was appropriate for use in recovering all the species necessary to conduct the interfacial sorption experiments for Task 1.3.

PFOS sorption to sand. The sand sorption experiments for PFOS produced low K_{ds} (0.41 – 0.78 cm^3/g, as expected (**Table 1.6**), which corresponded to a sand concentration of 0.21 ng PFOS/g sand.

Table 1.6 Data for single-point K_d estimates of PFOS to sand sorption coefficient (no NAPL or air phase present). The final estimate is 0.2 ng PFOS/g sand.

Replicate	$C_w^{initial}$ (ng/L)	C_w^{final} (ng/L)	C_s^{equil} (ng/g)	C_w^{equil} (ng/L)	K_d (cm^3/g)
Bottle 1	447	391	0.16	391	0.41
Bottle 2	429	331	0.20	331	0.61
Bottle 3	571	402	0.31	402	0.78
Bottle 4	496	358	0.26	357	0.73

Water saturation. Water saturation experiments indicate that saturation profiles were reproducible (**Figure 1.19**) with values near one in the bottom slices and lower values in the upper (unsaturated) slices.

Two- phase column experiments with synthetic water. When the saturation was close to 1, the PFOS concentration was equal to the initial concentration (1,100 ng/L; **Table 1.7**). At low saturations, which have elevated air-water interfacial areas, the apparent PFOS concentration increased up to approximately 4,600 ng/L due to accumulation of PFOS at the air-water interface (apparent aqueous PFOS concentration = true aqueous concentration + PFOS sorbed at the air-water interface). At a lower (300 ng/L) PFOS concentration (**Table 1.8**) and low saturations, the apparent PFOS concentration increased up to approximately 600 ng/L due to accumulation of PFOS at the air-water interface.

Table 1.7 Water saturation versus apparent PFOS concentrations in unsaturated sand slices with initial PFOS concentrations of 1100 ng/L.

Water Saturation	PFOS Concentration (ng/L)
0.14	4520
0.16	4800
0.20	4680
0.46	2140
0.66	808
0.87	796
0.82	1190
0.94	1390
0.94	1260
0.94	832
0.87	1130
0.87	1130
0.94	1170

Table 1.8 Water saturation versus PFOS concentrations for lower (300 ng/L) initial PFOS concentrations in unsaturated sand columns.

Water saturation	PFOS concentration (ng/L)
0.29	637
0.60	234
0.65	456
0.64	515
0.93	269
0.93	329
0.92	353
0.92	495
0.94	388
0.92	450
0.94	347
0.94	551
0.97	348

Equilibration time. The time needed for equilibration was confirmed as 12 d by analyzing the column for different periods, 6 – 21 d (**Table 1.9**). The Ki at 12 and 21 d were similar but greater than that for 6 d. Thus, an 12 d equilibration period was selected for subsequent experiments. Examples of the water saturation curves for 6 and 13 d are depicted in **Figure 1.19**.

Table 1.9 PFOS Ki values for two-phase column experiments at 1,000 ng/L for 6, 12, and 21 d equilibration periods.

Equilibration Time, d	K (cm)i	No. replicates
6	0.011	1
12	0.024	3
21	0.021	2

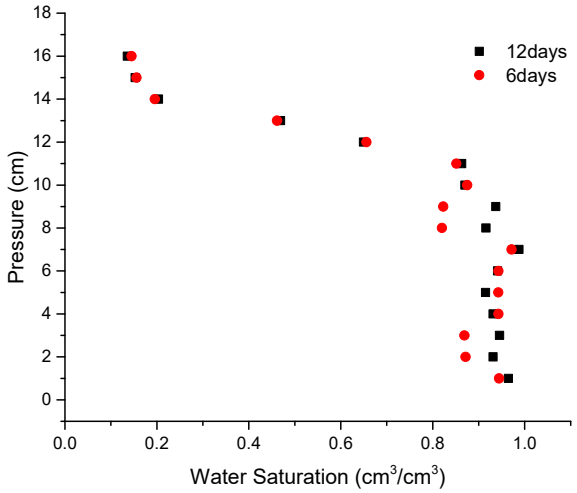

Figure 1.19 Water saturation patterns in the presence of 1,100 ng/L PFOS for 6 and 12 d equilibration periods. The water saturations are nearly identical to those obtained in the absence of PFOS (**Figure 1.20**). The data also indicate that the water saturation profile has equilibrated by 6 d.

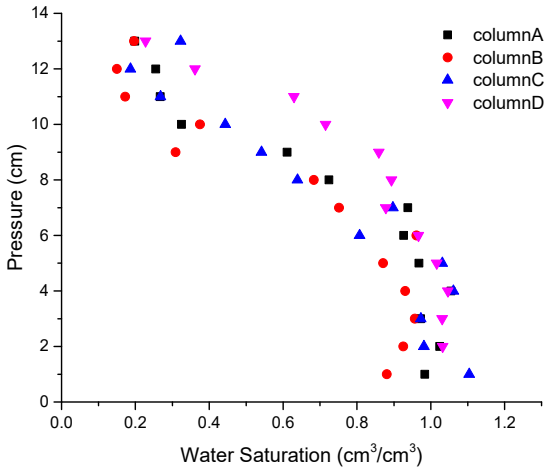

Figure 1.20 Pressure vs. water saturation curves for water-only (no PFOS) columns equilibrated for 6 days. Results show that the water saturation profiles in the sand columns were generally repeatable.

Table 1.10 Ki values for PFAS at 1,000 ng/L over a 12 d equilibration period.

PFAS	Ki (cm)	No. replicates
6:2 FTS	0.013	2
PFOS	0.024	3
8:2 FTS	0.026	1
PFNA	0.015	2
FOSA	0.027	1

Table 1.11 K_i (cm) values for PFASs spiked into AFFF-impacted groundwater.

PFAS	**Rep 1 Ki**	**Rep 2 Ki**	**From single compound experiment (Table above)**	**Brusseau Water Res (modeled) 2019**[12]	**Silva et al. Contam Hydrol (measured 1 mg/L) 2019**[13]
PFHxA	0.003	0.014		0.00002	0.000147
PFHpA	0.018	0.008		0.00006	0.000659
PFOA	0.010	0.013		0.00023	0.00405
PFNA	0.021	0.024	0.015	0.00093	0.03686

PFBS	0.001	0.001		0.00002	NA
PFPeS	0.003	0.003		NA	NA
PFHxS	0.008	0.009		0.00010	NA
PFHpS	0.027	0.021		0.00051	NA
PFOS	0.025	0.033	0.024	0.00230	NA
PFNS	0.020	0.043		0.03700	NA
FHxSA	0.010	0.020		NA	NA
FOSA	NA	0.028	0.027	NA	NA
MeFOSAA	0.026	0.023		NA	NA
6:2 FTS	0.011	0.014	0.013	NA	NA
8:2 FTS	0.027	0.030	0.026	NA	NA

To the best of our knowledge, these are the first experimentally measured K_i values for PFASs other than PFCAs and PFSAs in an AFFF-contaminated groundwater for PFAS concentrations lower than 1 mg/L, which are representative of conditions that currently exist at AFFF-contaminated sites. The measured K_i values give a reasonable trend with increasing K_i with number of fluorinated carbons (**Figure 1.21**). The change in K_i with each additional fluorinated carbon is 0.007 cm (e.g., slope of the curve).

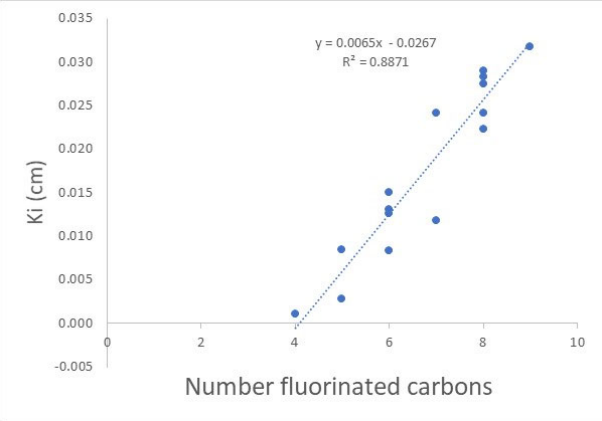

Figure 1.21. Trend in Ki with perfluorocarbon number.

The experimentally determined values are considerable larger than those experimentally determined at 1 mg/L by interfacial tension measurements[13] or by modeling.[12] The experimental system is much more complex, with multiple construction, deconstruction, and analytical steps compared to the interfacial tension measurement system (or modeling approach). Thus, there may be handling errors that lead to high estimates of K_i. While there appears to be reasonable agreement between PFNA and PFNS, the discrepancies are such that additional significant investments in time and energy would be needed to determine the source of the significant difference.

NAPL Experiments.

In late 2019, a new media source was required as the original supply had been exhausted. A trial was done with four columns to compare the original sand washed and unwashed with new washed sands of two different grades. Results of this trial are in **Figure 1.22**.

Two sand columns were set up as described previously: one as a two-phase system (oil and water) and the second as a three-phase (air, oil and water) system. The 20/30 sand was chosen as a good new model medium and used for a 3-phase trial with no PFAS. Octanol and water concentrations were obtained for one column packed the new medium. Octanol and deionized water were used as oil phase and aqueous phase, respectively. In the two-phase experiment, 10 mL of octanol was placed on top of the water. The drainage line was then opened, allowing slow drainage in the sand

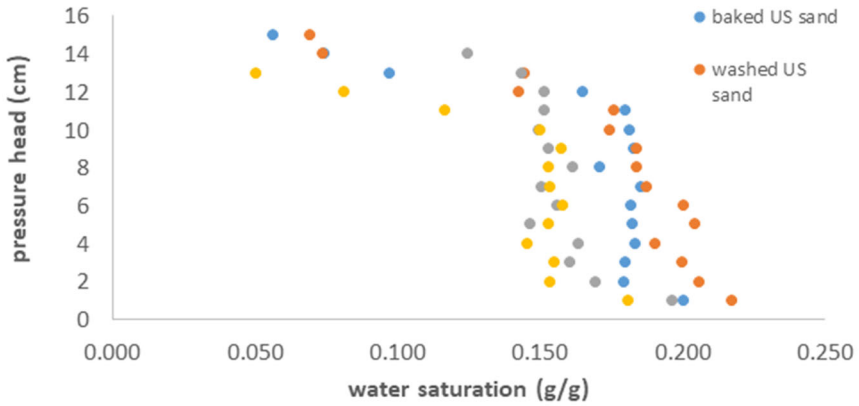

Figure 1.22. Gravimetric water saturation with pressure head for four different column-packing media.

column. Drainage was stopped just before all the octanol entered the sand column (a thin layer of octanol was above the sand column). In the three-phase experiment, 3 mL of octanol was placed on top of the water. Then the drainage line was opened, allowing slow drainage in the sand column. Drainage was stopped just after all the octanol entered the sand column. The 12 sand column slices were analyzed for water and octanol by CDM Smith after a 6-day equilibration period.

Three-phase experiments. Three-phase experiments were performed twice. In each case, octanol was used as the model NAPL and PFOS at 1000 ng/L was added to triplicate columns. The first set of columns with only 10 'slices' did not yield useful data, so the second column set was performed with 16 slices. Despite our best efforts, we were unable to obtain usable data from three-phase experiments with octanol as a model NAPL. Experiments were terminated at this point.

Batch Partitioning Studies.
Given the limited success of the three phase laboratory experiments, we undertook a study aimed at quantifying PFAS partitioning into LNPAL in laboratory batch experiments using relatively low PFAS concentrations (2,000 – 100,000 ng/L).

Experiments. A previously characterized AFFF as part of ESTCP ER18-C1-1259 was used as a model AFFF. The synthetic freshwater recipe used to produce a water with a conductivity of approximately 180 uS/cm. Jet Fuel A was purchased from Corvallis Municipal Airport (Corvallis, OR). Eight-point partition isotherms were made in triplicate at initial PFAS concentration ranges from 0 – 100,000 ng/L and at 3% AFFF dilutions from 1:50,000 to undiluted. A 1:1 synthetic fresh water and Jet Fuel A ratio was used in a 15 mL polypropylene tube. All PFAS were spiked into 1.5 mL of water and vortexed for 30 s. After vortexing, 1.5 mL of Jet Fuel A was added to the tube. Tubes were set to shake on an orbital shaker table for 72 hours to thoroughly mix and then let stand for 48 hours to finish equilibrating prior to sampling.[13,14]

Sampling of the bulk Jet Fuel A and the underlying bulk aqueous phase was done via pipette. All samples were diluted 1:10 or 1:100 to bring their concentrations within detectable range of the instrument (20-10,000 ng/L) and analyzed directly. For aqueous samples dilutions were into MeOH. For LNAPL samples dilutions were into ethyl acetate. The accuracy of the whole method for target PFAS with matched surrogate standards ranged from 77 – 130%, as indicated by the average recovery, while precision ranged from 2-30% for most analytes. Samples were spiked with

0.75 ng of isotopically labeled internal standard before analysis for quantification and final sample volumes were 1.5 mL. Separation was done with an Agilent 1100 and detection with a Waters TQ Detector triple quadrupole mass spectrometer for acquisition.

All partitioning experiments included a method blank which consisted of unspiked water and Jet Fuel A subjected to the partition experiment described above. Method and solvent blanks were analyzed at the start of each analytical sequence and fell below ½ of the limit of quantification. Adsorptive losses of PFAS to polypropylene tubes in both NAPL and water are negligible. Spike and recovery experiments in polypropylene tubes have been previously performed with recoveries of select PFASs in water ranging from 75-130% and recoveries for PFAS in NAPL ranging 79 – 125% depending on the individual PFAS used in this study.

Jet Fuel A – water partition coefficients (K_n) were calculated as single points between equilibrated water and Jet Fuel A concentrations across the range of initial water concentrations:

$$K_n = \frac{C_{eq\ jet}}{C_{eq\ water}} \qquad \textbf{(Equation 1.4)}$$

In addition, Jet Fuel A – water interfacial coefficients were determined by mass balance within the system by subtracting the total initial PFAS mass in the aqueous (e.g., total mass in system) by the mass in the equilibrated aqueous phase and the mass in the equilibrated Jet Fuel A phase:

$$m_{interface} = m_o - m_{eq\ water} - m_{eq\ jet} \qquad \textbf{(Equation 1.5)}$$

Values for K_{nw} were determined for PFASs between equilibrated aqueous concentration (units of ng/cm^3) and calculated interfacial mass per unit area (ng/cm^2) through linear regression and Freundlich curve fitting. The Freundlich model has been shown to better represent PFAS K_{aw} values at lower PFAS concentrations.[15]

Results and Discussion

Jet Fuel A – Synthetic Freshwater Partitioning. Schaefer et. al. showed that simple mixes of low concentration of PFAS (e.g., below the critical micelle concentration) could be represented by single solute K_{aw} and that K_{aw} results from a simple mixture were not statistically different from a single solute K_{aw}.[15] A similar approach was taken for these batch experiments. PFOS as a single solute was partitioned in triplicate according to the methodology described above. The average concentrations of PFOS between the single solute and PFAS mixture in both the synthetic fresh water and jet fuel A and the associated t-statistic which indicated that over the range of concentrations equilibrated concentrations between the single solute and the mix were not different. It was therefore concluded that a simple mixture of PFAS could be used for batch partitioning experiments, which greatly reduced the total number of LC-MS/MS analyses.

Carbon chain length was the determining factor for presence of PFASs in Jet Fuel A. However, polyfluorinated substances (e.g., fluorotelomer chemistry) showed decreased partitioning compared to perfluorinated substances. No detectable Jet Fuel A concentrations were observed for PFBA, PFPeA, PFPrS, and PFBS. Approximately 90% of PFBA and PFPeA and 60 – 70% of PFPrS and PFBS was accounted for in the synthetic freshwater at the highest concentration. Short chain PFASs are less hydrophobic due to their decreased carbon chain length and are more mobile

in the environment, this combined with the hydrophilic headgroup and oleophobic properties of the fluorinated tail could explain why partitioning into the Jet Fuel A was not observed.

Detectable PFAS concentrations, defined as greater than the limit of detection (LOD) and less than the limit of quantification (LOQ), in Jet Fuel A were observed for PFHxA, PFHpA, and PFHxS. Approximately 85% of mass for these analytes was accounted for in synthetic freshwater at the highest concentration. Perfluorinated substances with six and seven carbon chain lengths represent the transition point where the PFASs are detectable in the Jet Fuel A.

Quantifiable PFAS concentrations in Jet Fuel A were observed for PFOA, PFNA, PFDA, PFUdA, PFDoDA, PFTrDA, PFTeDA, PFOS, and PFNS. Carbon chain length played a large role in determining PFAS partitioning to Jet Fuel A with approximately 1% of PFOA/PFOS mass accounted for in the Jet Fuel A to approximately 40% of PFTeDA mass accounted for in the Jet Fuel A at the highest initial concentration of 100,000 ng/L. Synthetic freshwater concentrations also showed decreases with increasing chain length from approximately 80% of PFOA/PFOS mass accounted for in the water to only 5% for PFTeDA, again at the highest concentration. Single point K_n values were calculated for analytes where possible across the concentration range and are reported in **Table 1.12**. For all analytes K_n (e.g., partitioning into bulk Jet Fuel A) decreased with increasing initial PFAS concentration indicating non-ideal partitioning of PFAS between synthetic freshwater and Jet Fuel A, example PFOS (**Figure 1.23**). Non-ideal partitioning has been observed in surfactants between water and NAPL both above[16] and below CMC.[17,18] Belhaj et. al. 2019[18] related the decrease of alkylpolyglucoside, a nonionic surfactant, partitioning with increasing concentration to interfacial tension, noting that the rate of surfactant partitioning is higher when the mass at the interface is lower. However, as the interface begins to accumulate more mass surfactant migration between phases is impeded.[18]

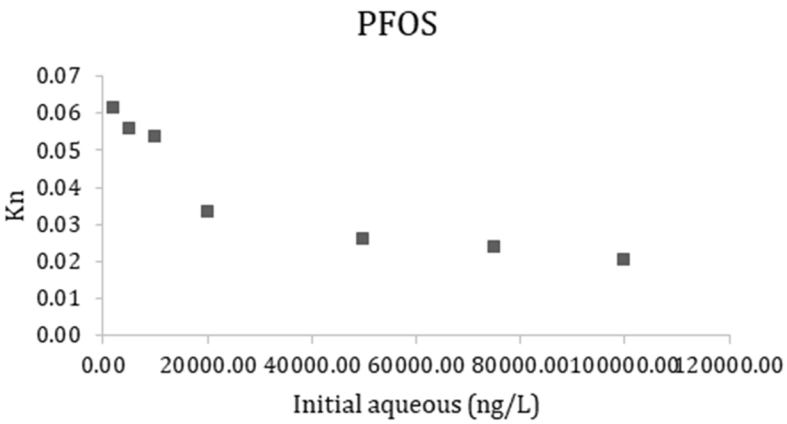

Figure 1.23 PFOS K_n values over the concentration range.

Figure 1.24 shows K_n values for 100,000 ng/L initial PFAS concentrations according to carbon chain length for the PFCAs and PFSAs and shows increasing partitioning with increasing carbon chain length. The decrease in synthetic freshwater concentrations for longer chain PFAS is consistent with literature material sorption studies which have indicated that long chain PFAS partitioning and adsorption increases with increasing chain length and is driven by hydrophobicity.

Jet Fuel A – Synthetic Freshwater Interfacial Sorption. Interfacial sorption regardless of the interface type are typically derived experimentally via interfacial tension measurements and typically use high (mg/L) surfactant concentrations.[13,15] However, when measured by mass difference, as was performed here, interfacial sorption can be determined at lower PFAS concentrations. By determining no sorptive losses to the polypropylene tube in water and Jet Fuel

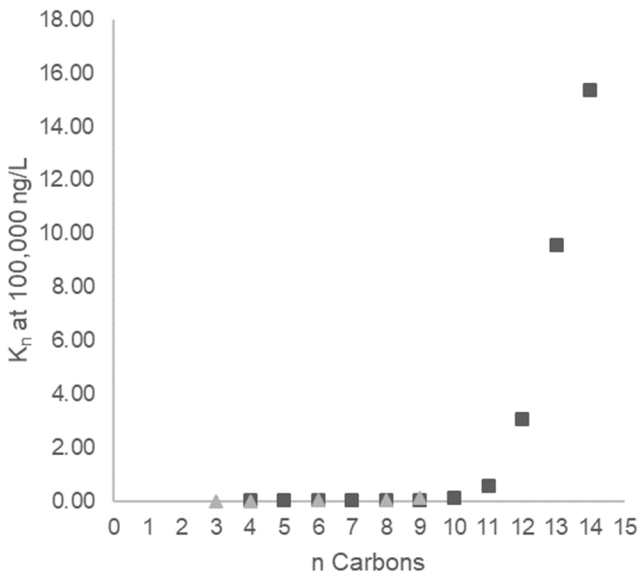

Figure 1.24 K_n values for PFCAs and PFSAs at 100,000 ng/L initial PFAS concentrations according to carbon chain length.

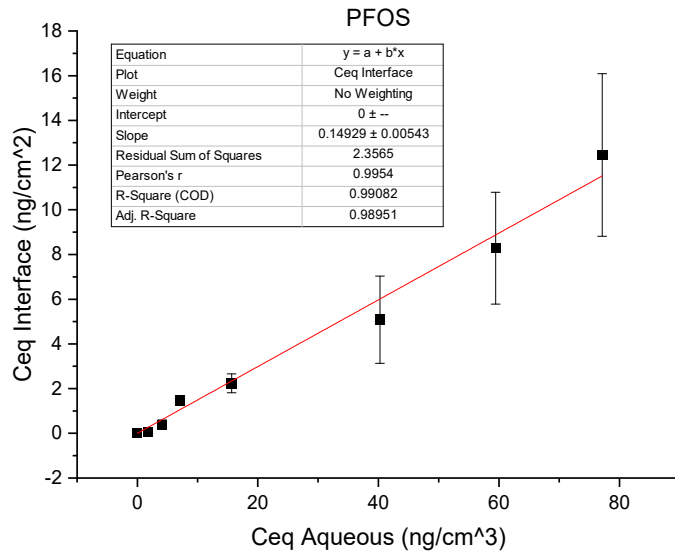

Figure 1.25 PFOS interfacial adsorption isotherm.

A systems, described above in the methods, and assuming that the Jet Fuel A – air interface is negligible we are able to consider that the interfacial mass measured by difference is associated with the synthetic freshwater – Jet Fuel A interfacial area.

For C4 – C10 PFCAs and C6, C8, and C9 PFSAs, the mass attributed to the interface was approximately 10% and best fit by linear regression (e.g., PFOS, **Figure 1.25**). Short chain PFPrS and PFBS both showed enhanced interfacial adsorption, although the 95% confidence intervals on the PFBS ranged from 7 – 33%. To ensure that this was not due to the PFAS mixture, an additional PFPrS single solute partitioning experiment was performed and showed interfacial uptake within the 95% confidence interval to the PFAS mix although the trend was of a lower slope. A similar observation was made by Guelfo and Higgins with short chain PFCA sorption to soil where they saw increased K_d values for PFPeA and PFBA.[14] As these findings departed from the hydrophobic mechanism typically tied to soil sorption the authors concluded that ion exchange or some other mechanism must be dominant for soil sorption of these PFAS. The results here, although not observed for PFBA and PFPeA, indicate that a mechanism other than hydrophobicity is determining short chain sulfonate interfacial adsorption with Jet Fuel A.

For C11 – C14 PFCAs, mass attributed to the interface increased with increasing chain length and decreased with increasing PFAS concentration. This relationship generated curved isotherms that were fitted to the Freundlich model (e.g., PFTeDA, **Figure 1.26**). Increased interfacial sorption with increasing PFAS chain length at the water – NAPL interface has been observed previously.[13] Calculated K_{nw} values here are two to three orders of magnitude higher than previously reported measurements.[13,19,20] The most recent and similar of which were performed by Silva et. al. using kerosene and synthetic groundwater reporting K_{nw} for C5 – C10 PFCAs, where PFOA K_{nw} =

0.000386 cm[13] and here we have calculated K_{nw} = 0.10 +/- 0.01 cm. These findings are similar to air – water interfacial adsorption results described by Schaefer et. al 2019.[15]

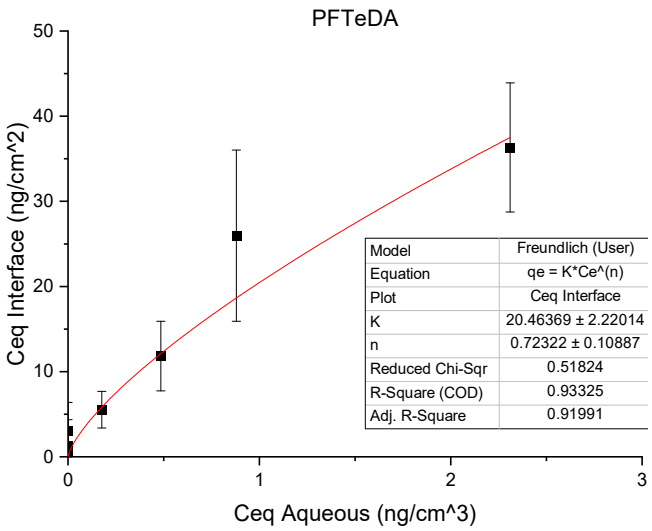

Figure 1.26 PFTeDA interfacial adsorption fitted to a Freundlich isotherm.

By quantifying PFASs in both the water and Jet Fuel A we were able to, by difference, determine the Jet Fuel A – water interfacial sorption coefficients (K_{nw}) and make inferences about NAPL – water partitioning (K_n). For PFAS with chain lengths of less than 10 carbons data were best fit to a linear model and K_{nw} ranged from 0.06 – 0.26 cm, which is two to three orders of magnitude higher than previously reported literature values. PFCAs with 11 – 14 carbons were better fit to the Freundlich model and showed greater accumulation at the interface, with PFTeDA (C14) K_{nw} = 20 cm. Partitioning into bulk Jet Fuel A was not observed for PFASs below eight carbons and increased with increasing carbon chain length with PFTeDA (C14) showing the highest mass partitioned at approximately 40%. Single point K_n values decreased with increasing PFAS concentration indicating non-ideal partitioning for these PFASs and this relationship became more pronounced with increasing carbon chain length.

Through direct measurement, we verified PFAS partitioning into bulk Jet Fuel A from synthetic freshwater. No PFASs below a carbon chain length of eight could be quantified in the Jet Fuel A, which is consistent with bioaccumulation literature. Mass of PFAS partitioned varied greatly with chain length with PFOA and PFOS exhibiting approximately 1% of mass partitioning to Jet Fuel A compared to 40% for PFTeDA at the highest concentration. Thus, we confirmed that PFAS partitioning into Jet Fuel A is determined by PFAS chain length and that the partitioning is non-ideal, with K_n decreasing as PFAS concentrations increase. We have determined by mass balance K_{nw} that are two to three orders of magnitude higher than previously reported values in the literature. The data generated were from experiments with a synthetic freshwater. Ionic strength is known to impact partitioning of PFASs in sediments and produced changes to interfacial adsorption between PFASs and kerosene; thus, is therefore presumed to be a factor in PFAS partitioning to NAPL. Additional research will need to be performed to evaluate PFAS partitioning, interfacial adsorption, and the linear relationships between initial and equilibrated concentrations at ionic strengths similar to what may be found in brackish groundwaters.

Table 1.12 Single point K_n values calculated across the concentration range.

	PFOA		PFNA		PFDA		PFUnDA		PFDoDA		PFTrDA		PFTeDA		PFOS		PFNS	
	K_n	95% CI	K_n	95% CI	K_n	95% CI	K_n	95% CI	K_n	95% CI	K_n	95% CI	K_n	95% CI	K_n	95% CI	K_n	95% CI
0	NA	NA	NA	NA	NA	NA	N A	NA	N A	NA	N A	NA	N A	NA	NA	NA	NA	NA
2000	0.00 0	NA	0.00 0	NA	0.1 8	NA	1.7	0.06	N A	NA	N A	NA	N A	NA	0.06 2	0.02 0	0.2 9	0.080
5000	0.00 9	NA	0.01 3	0.01 5	0.1 9	0.01	1.4	0.06	9.8	0.92	N A	NA	N A	NA	0.05 6	0.00 6	0.3 1	0.036
10000	0.00 4	NA	0.00 7	0.00 8	0.1 5	0.02	1.3	0.05	7.3	0.51	N A	NA	N A	NA	0.05 4	0.00 3	0.2 5	0.006
20000	0.00 8	0.00 4	0.00 5	0.00 6	0.1 3	0.03	1.0	0.04	6.4	0.31	N 21	2.4	N A	NA	0.03 3	0.00 2	0.2 5	0.012
50000	0.00 1	0.00 9	0.00 1	0.00 1	0.1 1	0.01	0.9	0.02	6.3	0.22	16	3.5	60	8.1	0.02 6	0.00 9	0.1 6	0.021
75000	0.00 3	0.00 1	0.00 0	0.00 1	0.1 0	0.01	0.7	0.00	5.2	0.22	15	3.4	39	0.8	0.02 4	0.00 1	0.1 6	0.009
100000	0.00 3	0.00 1	0.00 1	0.00 1	0.0 9	0.01	0.6	0.03	3.5	0.21	10	1.3	16	2.4	0.02 1	0.00 1	0.1 1	0.013

Table 1.13 Interfacial sorption coefficients from linear regressions.

	K_{nw}	± SE	R^2
PFBA	0.12	0.01	0.97
PFPeA	0.11	0.003	0.99
PFHxA	0.08	0.01	0.96
PFHpA	0.11	0.01	0.97
PFOA	0.10	0.01	0.95
PFNA	0.06	0.01	0.88
PFDA	0.09	0.01	0.95
PFPrS	0.36	0.02	0.98
PFBS	0.26	0.02	0.95
PFHxS	0.06	0.01	0.96
PFOS	0.15	0.01	0.99
PFNS	0.11	0.01	0.95

Table 1.14 Interfacial sorption coefficients from Freundlich models.

	K_{nw}	± SE	n	± SE	R^2
PFUdA	0.62	0.20	0.84	0.12	0.88
PFDoDA	2.6	0.16	0.83	0.06	0.95
PFTrDA	12	2.0	0.60	0.14	0.90
PFTeDA	20	2.2	0.72	0.11	0.93

Critical Micelle Concentration (CMC) determination for AFFFs. Three AFFFs were chosen based on the known characterization of the fluorinated surfactants previously reported,[2,3] as well as the known hydrocarbon surfactant compositions discovered in the current work. The three AFFFs include a 1989 3M, Ansul, and National Foam AFFF, which contain PFASs as well as multiple hydrocarbon surfactant classes. From each AFFF, eleven dilutions in tap water were used to make interfacial tension measurements (**Figure 1.27**). Two model non-aqueous phases, octanol and jet fuel A were tested.

Plots of interfacial tension (nM/m) versus concentration were constructed and linear regression was used to generate the intersection of the two lines, which indicates the CMC. Simple linear regressions of the two lines in the plot are used to visually estimate the CMC.

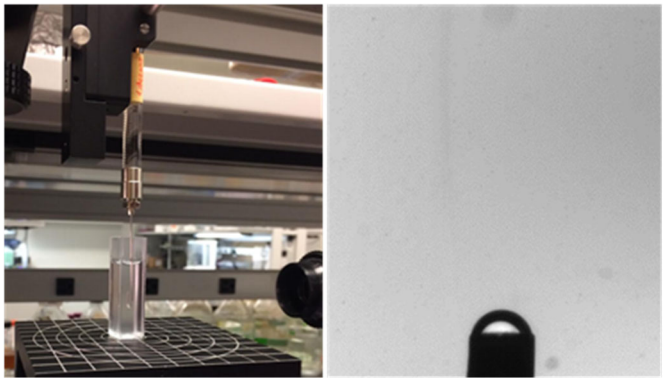

Figure 1.27 Pendant drop apparatus (left) and NAPL drop entering AFFF solution (right).

Each AFFF gave an estimated CMC that was below the recommend 3% AFFF application rate (marked by black vertical line in plots; **Figure 1.28**), which indicates that micelles are present when AFFFs are applied to fires. The presence of micelles indicates the potential for NAPL and other co-contaminant transport. In addition, AFFF-impacted waters after application have reduced surface and interfacial tensions, thus potentially increasing soil wetting and infiltration.

At the recommended dilution of 3%, the PFOS concentration in the 3M AFFF is 240 mg/L, which contrasts to the published CMCs for PFOS in its neat salt forms, which range from 5 – 8.5 mM (Li^+, Na^+, K^+, NH_4^+ salts) or 2,500-4,200 mg/L.[21] This finding indicates that published values should not be used for estimating the properties or behavior of AFFFs. The lower CMC is likely due to the synergistic blend of PFAS and hydrocarbon surfactants.

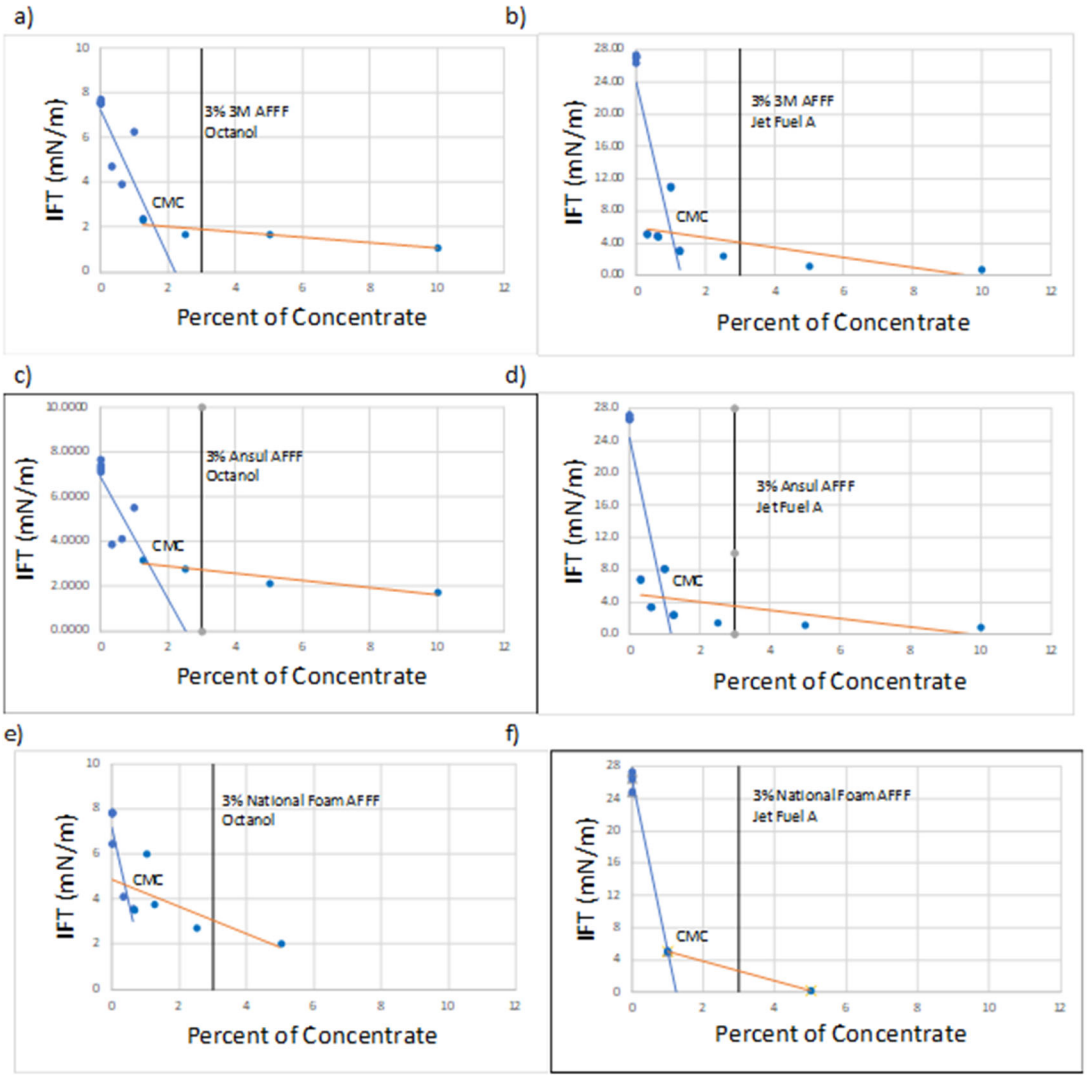

Figure 1.28 Interfacial tension (mN/m) versus AFFF concentration dilution to estimate the critical micelle concentration (CMC) of 3M AFFF and octanol (a), and Jet Fuel A (b), Ansul AFFF and octanol (c) and Jet Fuel A (d), and National Foam AFFF in octanol (e) and Jet fuel A (f). The 3% dilution (AFFF application rate) is marked by vertical black line and the CMC is marked by the intersection.

Task 1.4. Geochemical factors impacting the release of PFASs. As groundwater ionic strength and pH affect interactions between PFASs, surfactants, aquifer solids and NAPL, the release of PFASs from field-collected solids was evaluated under varied pH and ionic strength conditions. The ionic strength and pH ranges examined were selected to explore ranges of values representative of ambient field conditions and applied remedial conditions (e.g., bioremediation, ISCO). The same experimental apparatus and soils were used as in Task 1.2. To simulate the effect of varied pH under natural field conditions, the release of PFASs from Soil A was examined pH 5 and 9, while to simulate the effects of remedial conditions, Soil B was subjected to AGW at pH 3, at pH 10 with elevated NaCl, and at pH 10 with elevated $CaCl_2$ (**Figure 1.29**). The contents of the synthetic groundwaters used are detailed in **Table 1.15** and **Table 1.16**. As in Task 1.2, effluents were collected over 150-200 pore volumes and were measured for PFASs, pH, total organic carbon, UV-visible absorbance, as well as major solution constituents. PFAS concentrations were also determined in soils following PFAS release experiments. Each experimental condition was evaluated in duplicate, though for simplicity data from only a single column of each treatment is shown.

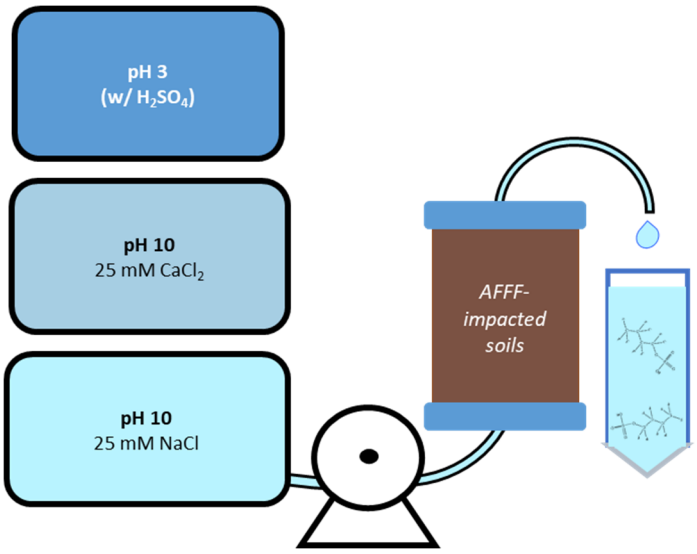

Figure 1.29 Schematic of experimental apparatus and conditions used in Task 1.4 column experiments with Soil B.

Table 1.15 Components of AGW used in Task 1.4 column experiments with Soil A to identify the role of pH in determining PFAS release under natural conditions.

Component	pH 5 Synthetic Groundwater	pH 9 Synthetic Groundwater
$MnSO_4$ * H2O	1 mg / L	1 mg / L
Na_2SO_4	180 mg / L	180 mg / L
NaCl	113 mg / L	113 mg / L
$NaHCO_3$	40 mg / L	40 mg / L
Concentrated HCl	As needed to adjust pH to 5	-
NaOH	-	As needed to adjust pH to 9

Table 1.16 Components of AGW used in Task 1.4 column experiments with Soil B to identify the role of pH in determining PFAS release under remedial conditions.

Component	High NaCl, pH 3	High NaCl, pH 10	High $CaCl_2$, pH 10
$MnSO_4$ * H2O	1 mg / L	1 mg / L	1 mg / L
Na_2SO_4	180 mg / L	180 mg / L	180 mg / L
NaCl	113 mg / L	1460 mg / L	-
$CaCl_2$	-	-	2780 mg/L
$NaHCO_3$	40 mg / L	40 mg / L	40 mg / L
H_2SO_4	As needed to pH 3	-	-
$Na_2B_4O_7$	-	1000 mg / L	1000 mg / L
NaOH	-	As needed to pH 10	As needed to pH 10

Results.

The pH 5 and 9 AGWs pumped through the Soil A columns in Task 1.4 resulted in effluent pHs that were similar to those observed in Task 1.2 (**Figure 1.30**, left).While passing pH 3 AGW through Soil B produced similar effluent pHs as observed in Task 1.2, passing high ionic strength groundwaters, buffered at pH 10, through Soil B columns resulted in initially lower pHs than observed in the Task 1.2 columns followed by a sudden increase in effluent pH after 5-10 pore volumes of AGW had eluted (**Figure 1.30**, right). The sudden increase in effluent pH from the columns exposed to pH 10 AGW may indicate that the soil buffering capacity had been exhausted.

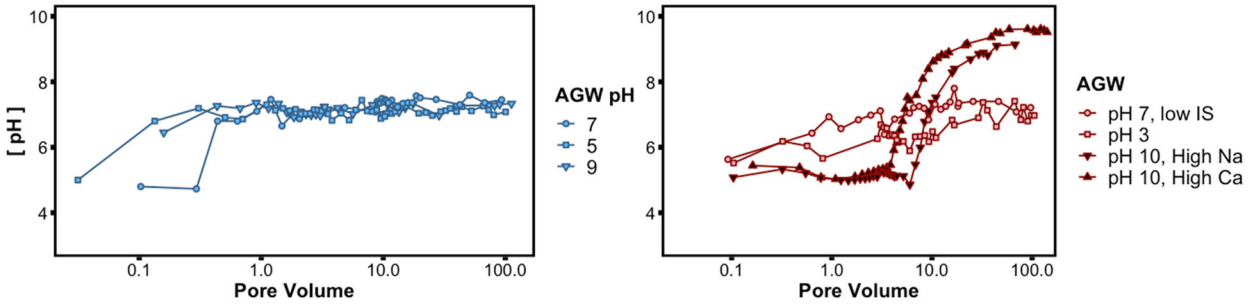

Figure 1.30 Effluent pH of columns packed with Soil A (left) or B (right) and exposed to AGWs of various pHs. The data from columns with pH 7 artificial groundwater was collected as part of Task 1.2, while the other data was collected as part of Task 1.4.

PFAS effluent concentration profiles (**Figure 1.31**) and cumulative masses released (**Figure 1.32**) of rapidly released PFASs, such as PFHxA, as well as slowly released PFASs, such as PFOS, were similar in columns filled with Soil A regardless of initial AGW pH. In these columns, the low buffering capacity of the various AGWs likely resulted in the pH within the columns being similar across all treatments.

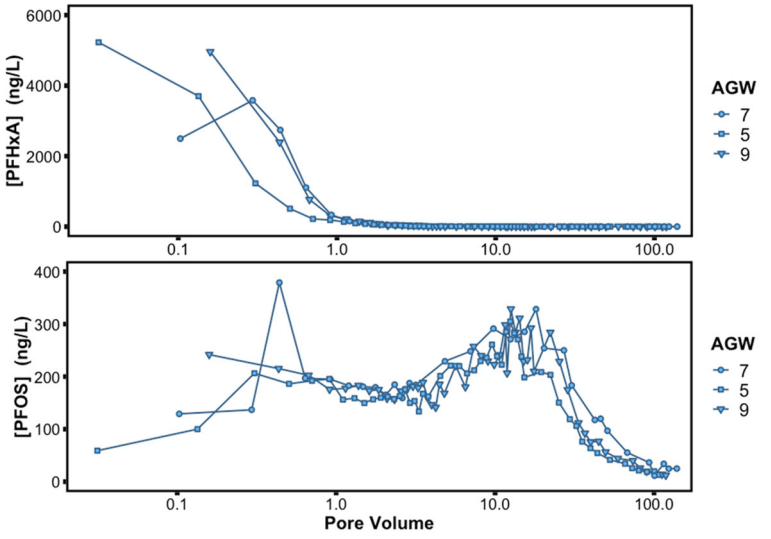

Figure 1.31 Effluent concentrations of PFHxA (top) and PFOS (bottom) from columns packed with Soil A and exposed to AGWs of various pHs. The data from columns with pH 7 AGW was collected as part of Task 1.2, while the other data was collected as part of Task 1.4.

Soil B columns were exposed to AGWs with a wider range of pHs and much higher buffering capacities and there were clear differences in effluent PFAS concentration profiles and cumulative PFAS masses released between treatments (**Figure 1.33** and **Figure 1.34**). While rapidly eluted PFASs, such as PFHxS, showed little difference in elution profile between the different treatments, PFASs with concentration maxima after 5-10 pore volumes when exposed to pH 7 AGW exhibited very different effluent concentration profiles when exposed to pH 10 AGW (**Figure 1.33**). For these more slowly released PFAAs, such as PFOS, as

well sulfonamide-containing PFASs such as MeFOSAA or FOSA, effluent concentrations peaked immediately after effluent pH concentrations increased in the pH 10 AGW columns, in both high Na and high Ca treatments. This resulted in PFASs with very different effluent concentration profiles when exposed to pH 7 AGW having simultaneous effluent concentration maxima with each other. Additionally, all three of these more slowly released PFASs exhibited lower effluent concentration maxima in the high Na treatment than in the high Ca treatments.

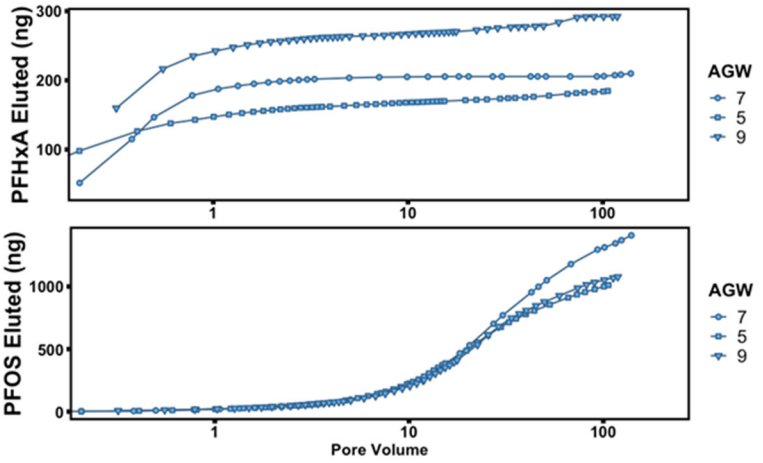

Figure 1.32 Cumulative mass of PFHxA (top) and PFOS (bottom) eluted from columns packed with Soil A and exposed to AGWs of various pHs. The data from columns with pH 7 AGW was collected as part of Task 1.2, while the other data was collected as part of Task 1.4.

PFAS with later effluent concentration peaks in pH 7 AGW had much higher effluent concentration peaks when exposed to pH 10 AGW. For example, PFOS had effluent concentration peaks after 6 pore volumes in pH 7 AGW and had effluent concentration maxima that were approximately 4 times higher in pH 10 AGW with high Ca, while FOSA, which had not yet reached an effluent concentration peak 150 pore volumes in pH 7 AGW, had effluent concentration maxima that were over 50 times higher when exposed to pH 10 AGW with high Ca.

The cumulative mass released was similar across treatments for PFASs that were rapidly released from Soil B, such as PFHxS, as well as for slightly more slowly released PFASs such as PFOS (**Figure 1.34**). However, for PFASs that were very slowly released from Soil B, much more mass was released by the experimental conclusion when exposed to high pH AGW (**Figure 1.34**). PFASs that were the most slowly released, such as FOSA, had the largest differences between masses released at high pH versus those at low or neutral pH. However, the difference in cumulative MeFOSAA and FOSA mass released between Soil B columns exposed to neutral and high pH AGWs may simply indicates that experiments with pH 7 AGW were concluded before the bulk of some PFASs were released.

Exposure to high or low pH AGW appeared to only produce differences in effluent PFAS profiles after the soil pH buffering capacity was exhausted. However, large effluent concentration peaks of diverse PFASs occurred immediately after the soil pH buffering capacity was exhausted. For slowly released PFASs, the effluent concentration peaks meant that more mass was released before the experimental conclusion. Columns exposed to high Ca pH 10 AGW had earlier pH breakthroughs and corresponding earlier PFAS effluent concentration peaks than those exposed to high Na pH 10 AGW, though the earlier PFAS effluent concentration peaks did not result in dramatically higher cumulative masses released. These data suggest that soil buffering capacity is highly relevant to PFAS transport and that remedial actions that produce large groundwater pH shifts may cause the rapid release of PFASs that are typically less mobile in the subsurface.

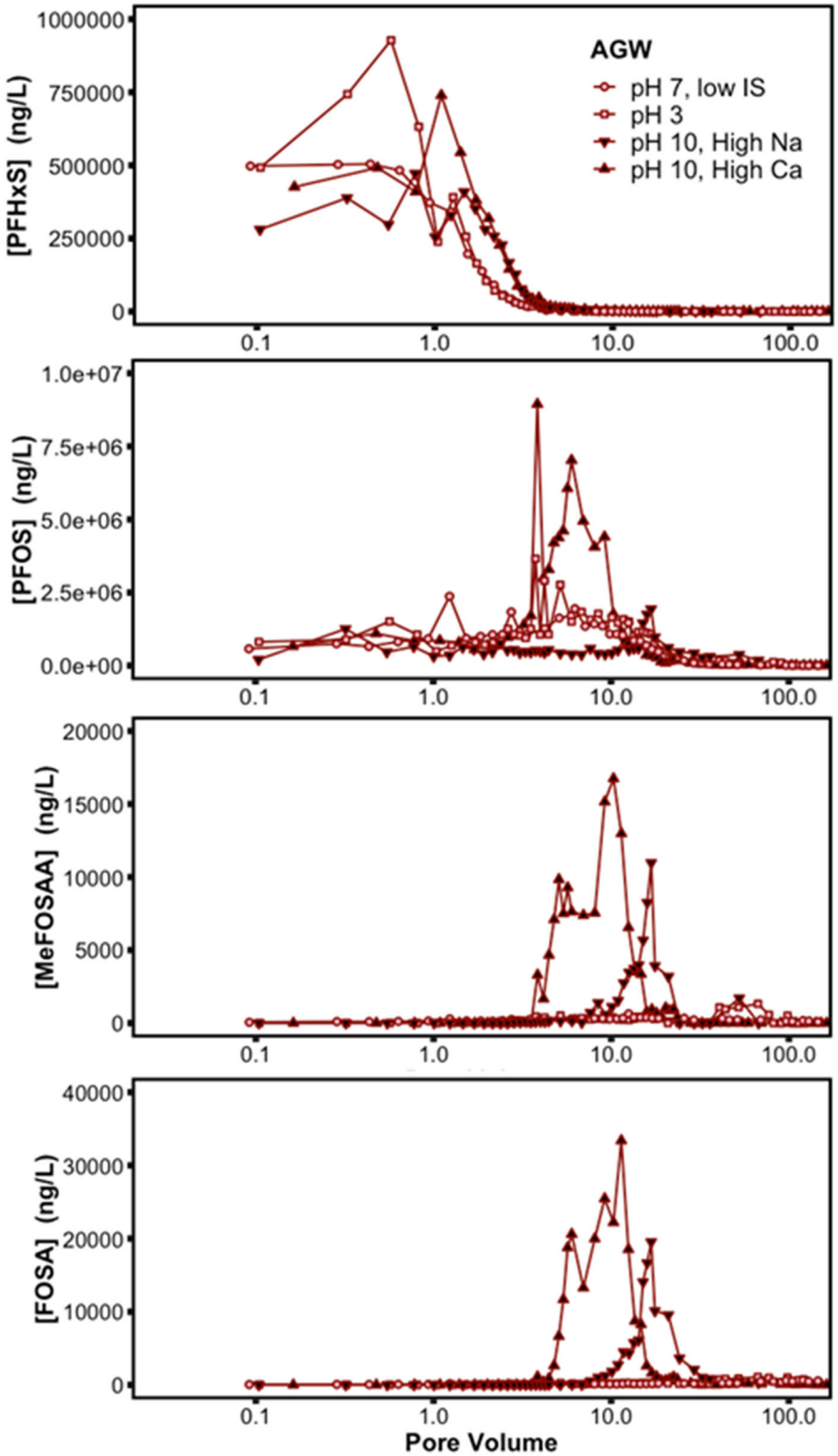

Figure 1.33 Effluent concentrations of PFHxS (top), PFOS (second from the top), MeFOSAA (third from the top), and FOSA (bottom) from columns packed with Soil B and exposed to AGWs of various pHs. The data from columns with pH 7 AGW was collected as part of Task 1.2, while the other data was collected as part of Task 1.4.

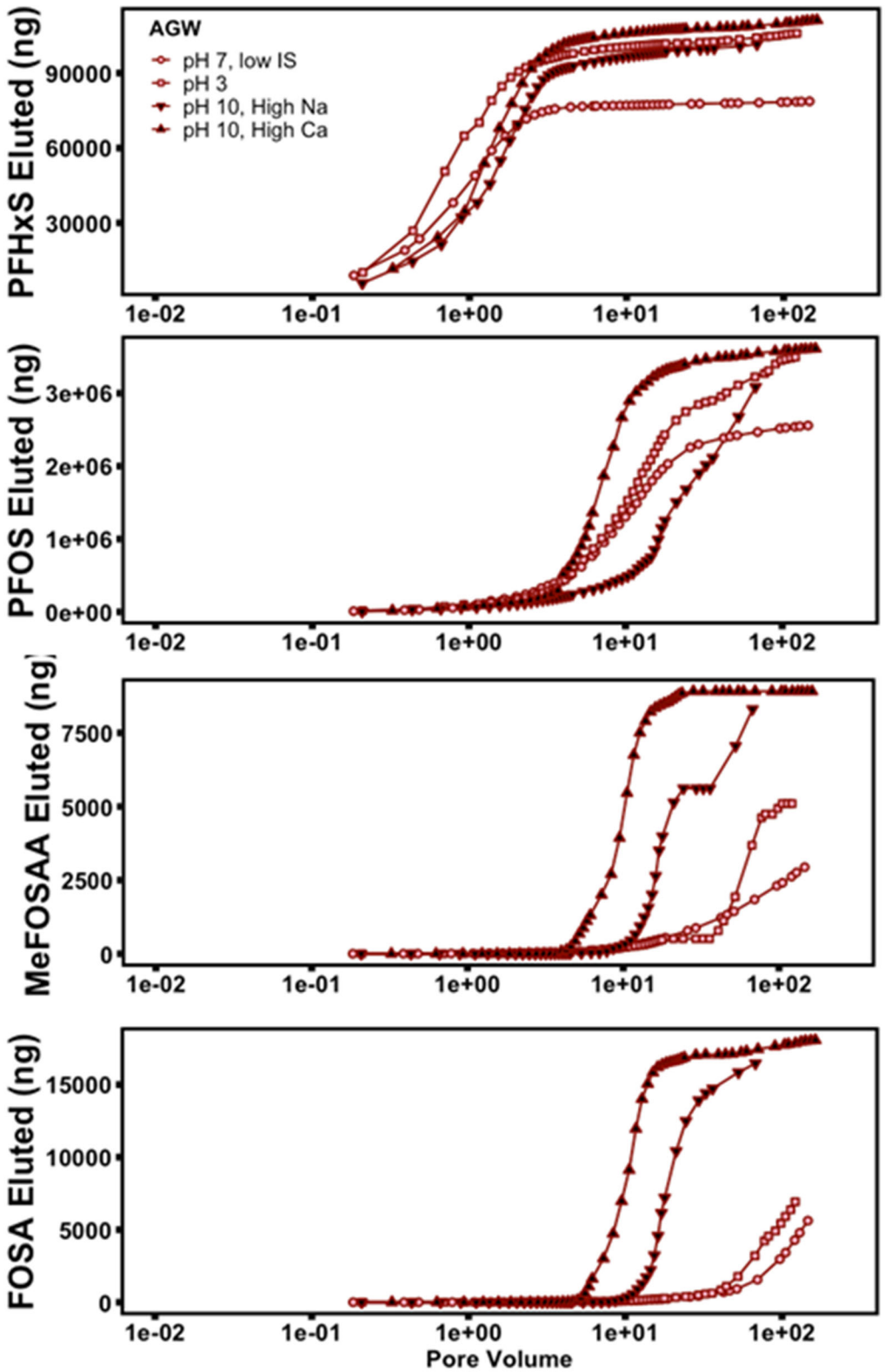

Figure 1.34 Cumulative released mass of PFHxS (top), PFOS (second from the top), MeFOSAA (third from the top), and FOSA (bottom) from columns packed with Soil B and exposed to AGWs of various pHs. The data from columns with pH 7 AGW was collected as part of Task 1.2, while the other data was collected as part of Task 1.4.

TASK 2. COUPLED DIFFUSION AND ABIOTIC REACTIONS OF PFASS WITHIN CLAYS

Task 2.1. ***Determine Aqueous Diffusivity of PFASs***. Aqueous diffusivities were measured for selected PFAAs using the capillary method.[22] Borosilicate capillary tubes (5 cm long, 0.05 cm inner diameter) were used for all diffusion experiments. A synthetic groundwater (100 mg/L $NaNO_3$, 1 mg/L $MnSO_4$, 180 mg/L Na_2SO_4, 113 mg/L NaCl, 40 mg/L $NaHCO_3$) was used as the aqueous medium. PFAA concentrations initially in the capillary tubes are provided in **Table 2.1**. The PFAA concentrations were selected to approximate the relative levels of PFAAs observed in groundwater,[2,23] although the PFHpS concentration in **Table 2.1** is elevated relative to the levels observed in groundwater. All PFAAs were purchased from Sigma Aldrich (St. Louis, MO), with the exception of PFHpS, which was purchased from Wellington Laboratories (Ontario, Canada). It is noted that these PFAA concentrations are generally 100-fold lower than the critical micelle concentrations.[24,25] All diffusion experiments were performed at a room temperature of approximately 20°C.

Table 2.1 PFAAs and their initial concentration in each capillary tube for Task 2.1 diffusivity experiments.

PFAAs*	Concentration (mg/L)	Aq. Diffusivity (cm^2/s)	R^2
PFBA	1.0	$2.5 \pm 0.6 \times 10^{-5}$	0.88
PFPeA	2.4	$1.2 \pm 0.2 \times 10^{-5}$	0.96
PFHxA	6.6	$0.78 \pm 0.2 \times 10^{-5}$	0.94
PFHpA	0.70	$0.93 \pm 0.3 \times 10^{-5}$	0.88
PFOA	4.3	$0.49 \pm 0.09 \times 10^{-5}$ (0.44×10^{-5})**	0.90
PFBS	1.4	$1.1 \pm 0.3 \times 10^{-5}$ (0.9×10^{-5})***	0.91
PFHxS	5.0	$0.45 \pm 0.1 \times 10^{-5}$	0.84
PFHpS	8.6	$0.64 \pm 0.07 \times 10^{-5}$	0.87
PFOS	4.3	$0.54 \pm 0.04 \times 10^{-5}$	0.93

* *PFBA= perfluorobutanoic acid, PFHxA=perfluorohexanoic acid, PFHpA = perfluoroheptanoic acid, PFOA=perfluorooctanoic acid. PFBS = perfluorobutane sulfonic acid, PFHxS = perfluorohexane sulfonic acid, PFHpS = perfluoroheptane sulfonic acid, PFOS = perfluorooctane sulfonic acid*
** *data from* Nordstierna et al. (2006)[26]
*** *data from Kim et al. (2014)*[27]

Three capillary tubes filled with the PFAA solution were then placed in a 1.7 L glass container containing 0.2 L of PFAA-free water (**Figure 2.1**). A glass coated stir bar was used to keep the bulk aqueous solution well mixed. The glass container and stir bar were pre-rinsed with methanol and deionized water prior to use. The bulk aqueous phase was sampled (5 mL per sampling event) as a function of time for 4 to 10 days. Collected samples were placed in 15 mL polypropylene tubes (pre-rinsed with methanol and deionized water) and analyzed for PFAAs. The diffusion experiment was performed in duplicate. To ensure that there was no multicomponent solute effect on

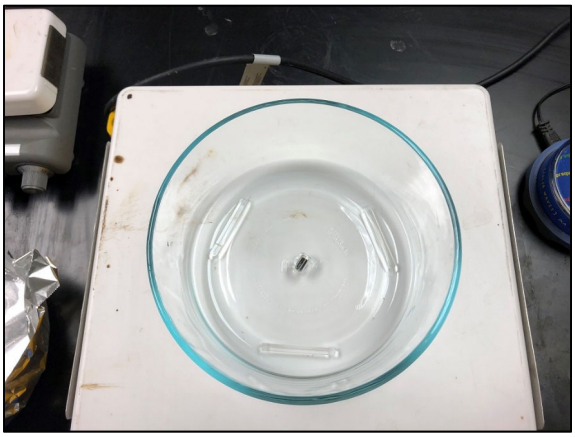

Figure 2.1. Capillary tube apparatus used for measuring aqueous diffusion coefficients.

the observed aqueous diffusivities, an additional experiment (performed in duplicate) was conducted using PFBS only; any solute-solute interactions would likely be most noticeable for the smallest PFAA molecules as evidenced by an apparent decrease in its aqueous diffusivity.[22,28]

Diffusion samples were extracted using the micro liquid-liquid extraction technique described by Backe et al. 2013.[2] In brief, 3.0 mL of diffusion sample was added to a 15 mL polypropylene centrifuge tube (VWR, Radnor, PA) containing 0.97 – 1.0 g of sodium chloride. Samples were acidified with 10 µL of 6 M HCl and extracted with 10% (v/v) 2,2,2-trifluoroethanol in ethyl acetate. Extract were analyzed using orthogonal chromatography as described by Barzen-Hanson et al.[3] and Robel et al.[29]. Briefly, a 900 µL aliquot of extract was injected onto an Agilent 1100 series HPLC fitted with two Zorbax diol (Agilent, Santa Clara, CA; 4.6 x 12.5 mm x 6 µm) and Zorbax silica (Agilent; 4.6 x 12.5 mm x 5 µm) guard columns that were connected in-line to a Zorbax Eclipse Plus C18 analytical column (Agilent; 4.6 x 100 mm x 3.5 µm). Mobile phases consisted of 3% methanol in HPLC-grade water and 10 mM ammonium acetate in HPLC-grade methanol.[29] Analyte identification and quantification followed that of Allred et al. 2015.[30] Each analytical sequence consisted of solvent and extraction process blanks that were spiked with 0.72 ng of isotopically labeled standards; all blanks gave responses that fell below the limit of quantification. The analytical sequence consisted of a minimum 5 point calibration curve over the range of 5-10,000 ng/L for all analytes. Accuracy was determined from the analysis of a second source of standards and ranged from 72 – 127%. Precision, as indicated by the relative standard deviation calculated from four replicate extraction and analyses, ranged from 4-18%. The limit of detection (LOD) was (3-15 ng/L) and was calculated by normalized-weighted regression (1/X), which the limit of quantification was calculated as 3.3 x the LOD and ranged from 10-50 ng/L.[2]

Aqueous diffusivities were calculated based on the measured increase in PFAA concentrations in the bulk aqueous solution, relative to the PFAA mass initially in the capillary tube, as follows:[22]

$$\frac{M}{M_T} = \frac{8}{\pi^2} \sum_{n=1}^{\infty} \frac{1}{(2n-1)^2} \exp\left[\frac{-\pi^2 (2n-1)^2 Dt}{4L^2}\right] \qquad \textbf{(Equation 2.1)}$$

where M and M_t are the masses of each PFAS species at time t and initially in the capillary tubes (respectively), D is the PFAS aqueous diffusivity (cm^2/s), t is time, and L is the length of the capillary tube. The mass that exited the capillary tube at a given time t was determined based on the measured PFAS concentration in the 0.2 L water reservoir.

Results. A typical diffusive release curve, along with the regression of **Equation 2.1** to the experimental data, is shown in **Figure 2.2**. The regressed aqueous diffusivities and R^2 values for each PFAA are provided in **Table 2.1** (data regressed to **Equation 2.1**), where the ± values indicate the 95% confidence intervals. Values in parentheses are from previous studies. The aqueous diffusivities obtained for PFOA and PFBS are in reasonable agreement with their previously measured values.[26,27] The aqueous diffusivity measured for the PFBS-only system ($1.0 \pm 0.2 \times 10^{-5}$ cm^2/s) showed no statistical difference from that measured in the PFAA mixture, indicating that solute-solute interactions were negligible with respect to diffusion.

Figure 2.3 shows the PFAA aqueous diffusivities plotted as a function of their molar volumes, where the PFAA molar volumes were calculated based on the group contribution method, with a

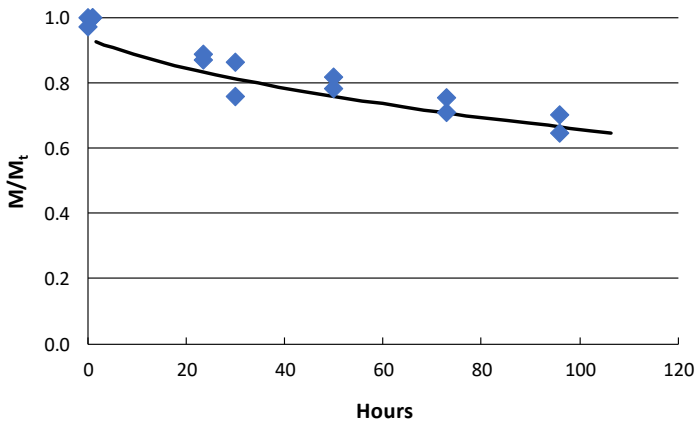

Figure 2.2. Diffusive release of PFHpS during the capillary experiment. Results from duplicate experiments are shown. The solid line represents the regression of Equation 1 to the experimental data (with time units converted from hours to seconds).

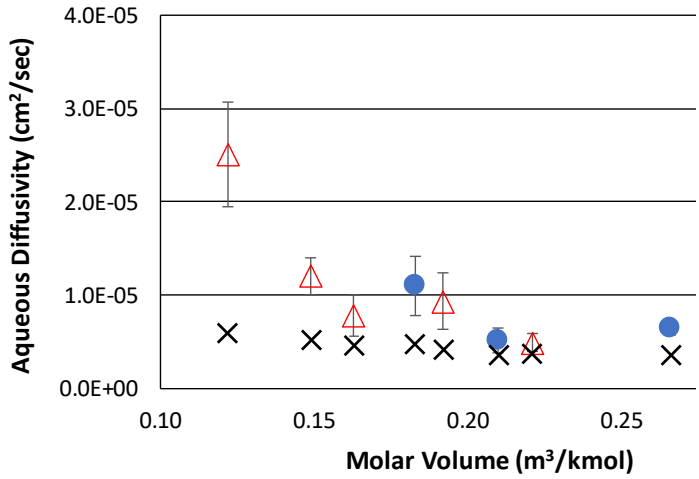

Figure 2.3. Measured aqueous diffusivities for the PFCAs (open triangles) and PFSAs (filled circles) as a function of the molar volume. The error bars represent the 95% confidence intervals. The X's represent the estimated aqueous diffusivities based on a molecular weight-based empirical model that Xiao et al. (2017) used in their activated carbon kinetic sorption model.[10]

C-F contribution term of 12.3.[31,32] The expected trend of increasing aqueous diffusivities with decreasing molar volumes is generally observed for the PFCAs, with the exception of PFHpA which has an average diffusivity value slightly higher than what this trend would suggest. However, for the PFSAs, the expected trend of increasing aqueous diffusivities with decreasing molar volume is not observed, although PFBS (with a molar volume of 0.18 m^3/kmol) shows a significantly greater aqueous diffusivity than the other PFSAs.

To further evaluate the experimental results and trends observed in **Figure 2.3**, results from Xiao et al. (2017) were examined.[10] In their work, Xiao et al. measured the diffusive uptake rate of several PFAAs into activated carbon, where the rate of uptake was proportional to the aqueous diffusivity (D) divided by a tortuosity factor.[10] The aqueous diffusivities were estimated based on a basic empirical model;[33] the PFAA diffusivities predicted from this model were generally in poor agreement with the diffusivities measured herein (**Figure 2.3**). To describe their sorption data, Xiao et al. used the dimensionless tortuosity as a fitting parameter for each PFAA, with tortuosity values ranging from 2.7 to 7.6. Typically, when describing the diffusive uptake of organic contaminants in to activated carbon, the tortuosity is a function of the carbon,[34] and is not expected to vary substantially for the range of PFAAs tested. Thus an alternate approach for evaluating the data from Xiao et al., with the purpose of determining the PFAA aqueous diffusivities, was considered.

The estimated diffusivity value used by Xiao et al. (2017) for PFOA (0.37 x 10^{-5} cm^2/s)[10] is in reasonably agreement to the value measured herein (0.49 x 10^{-5} cm^2/s). Thus, the tortuosity value for PFOA (7.6) was assumed to be the representative value for the activated carbon for all the PFAAs tested. Assuming a tortuosity value of 7.6 for all of the PFAAs examined by Xiao et al., the PFAA aqueous diffusivities for each compound were re-calculated as follows:

$$D = D^* \frac{7.6}{\tau} \qquad \textbf{(Equation 2.2)}$$

where D^* is the originally estimated PFAA aqueous diffusivity used by Xiao et al. and τ is the tortuosity for each PFAA determined by Xiao et al. Thus, **Equation 2.2** calculates the aqueous diffusivities from the data of Xiao et al. with the assumption that the tortuosity for all PFAAs is constant at a value of 7.6. The resultant aqueous diffusivities are plotted in **Figure 2.4**, and are in reasonable quantitative agreement with the values measured herein using the capillary method. Interestingly, the irregular trend in the aqueous diffusivity data using the data from Xiao et al. (modified by **Equation 2.2**) show a nearly identical trend in D as a function of the PFAA molar volumes compared to that measured herein. Thus, the data from Xiao et al. provide a confirmation of the non-uniform trend in PFAA aqueous diffusivities relative to their molar volumes.

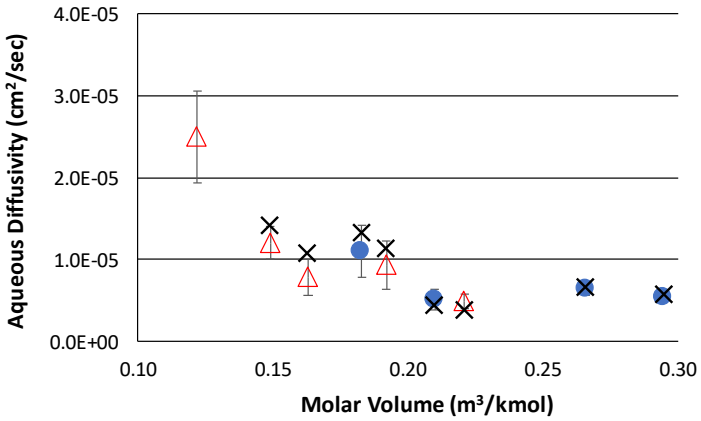

Figure 2.4. Measured aqueous diffusivities for the PFCAs (open triangles) and PFSAs (filled circles) as a function of the molar volume. The error bars represent the 95% confidence intervals. The X's represent the data from Xiao et al. (2017), transformed as described in **Equation 2.2**. Data for PFBA from Xiao et al. were not available.

Experimental data were also compared to the semi-empirical and widely-used Wilke-Chang correlation for prediction of D:[34,35]

$$D = \frac{7.4x10^{-8}(\varphi M)^{0.5}\, T}{nV^{0.6}} \qquad \textbf{(Equation 2.3)}$$

where φ is an empirical factor (equal to 2.6 when water is the solvent), M is the molecular weight (g/mol), T is the temperature (K), n is the viscosity (g/cm/s), and V is the molar volume (cm^3/mol). Comparison of **Equation 2.3** to the experimental data in **Figure 2.5** shows that Wilke-Chang model substantially underestimates the magnitude of the negative slope for the PFCAs, and does not capture the non-uniform trend in the PFSAs. The Wilke-Chang prediction for the PFBA aqueous diffusivity shown in **Figure 2.5** differs from the experimental data by up to nearly a factor of 3. In addition to the prediction for D by the Wilke-Chang model, **Figure 2.5** shows molecular diffusion simulations performed by Pereira et al. (2014).[36] These molecular simulations for PFOA and PFOS are within 13% and 23%, respectively, of the experimental values, indicating a reasonable prediction of the experimental data for these compounds. However, it is currently unclear if such molecular modeling would describe the trend in the aqueous diffusivities observed for the smaller-chained (and smaller molar volume) compounds shown in **Figure 2.5**.

The non-uniform trends in D as a function of the molar volume shown in **Figure 2.5** are not typical, as most compounds show a trend that is at least reasonably described by empirical models such as Equation 6. However, similar unique behavior in properties have been observed for PFAAs. For example, Kim et al. (2015) observed non-uniform trends in the vapor pressure and Henry's Law constant for PFAAs as a function of their molar volumes.[37] The unique behavior of highly fluorinated compounds compared to non-fluorinated compounds may be due to their relatively small van der Walls interactions,[38] but this would not explain the irregular trend behaviors observed for the PFAAs.

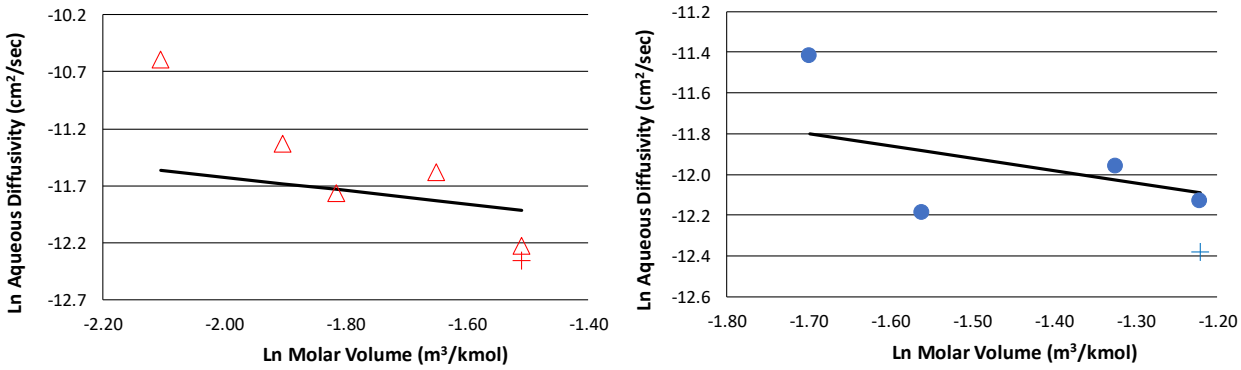

Figure 2.5 Measured aqueous diffusivities for the PFCAs (top) and PFSAs (bottom) as a function of the molar volume. The + symbols represent molecular simulations for PFOA (top) and PFOS (bottom). The solid lines represent the Wilke-Chang model predictions (**Equation 2.3**).

Task 2.2 *Assess Abiotic Reactions.*

Using methods similar to those previously employed,[39] the extent to which ferrous minerals facilitate the abiotic transformation of polyfluorinated PFASs was measured in batch systems: abiotic reactions involving the PFAAs are not expected. In this Task, batch experiments were performed using AFFF-impacted groundwater. Mineral reactants within the batch systems included both pure ferrous minerals (e.g., pyrite) and natural clays containing ferrous minerals. Based on our previous/ongoing work on SERDP Projects ER-1685 and ER-2530, such materials are expected to facilitate abiotic reactions. Experiments were performed under both oxic and anoxic conditions, with the headspace inside the batch reactors (60 mL serum bottles, **Figure 2.6**) consisting of either air or nitrogen. For the anoxic experiments, water was sparged with nitrogen to limit any dissolved oxygen. Under oxic conditions, parallel bottles were prepared to measure the generation of •OH using a compound that fluoresces upon exposure to •OH; alternately, •OH-scavenging compounds were used. Microbial inhibitors and/or sterilization were used to limit microbial activity. The aqueous phase was monitored as a function of time to determine PFAS transformation. Parallel experiments were also performed with BTEX/solvent co-contaminants. First-order rate constants and sorption coefficients to mineral phases were determined.

Initial batch testing to assess the extent to which ferrous minerals facilitate the abiotic transformation of PFAA precursors was performed using pyrite as a model ferrous mineral. Batch experiments were prepared to assess abiotic precursor transformation under both aerobic and anaerobic conditions.

Pyrite (Ward's Science, Cat #470118-152) was prepared by crushing the mineral into small pieces with a screwdriver and hammer. The small pieces were subsequently ground using a ceramic mortar and pestle and then passed through different sized stainless-steel sieves. The crushed material was separated into 3 different particles sizes: <0.85, 0.85-2.0, and 2.0-3.35mm. The 0.85-2.0mm particle size pyrite was chosen to perform these experiments. Approximately 200g of 0.85-2.0mm crushed pyrite was rinsed twice with 1M hydrochloric acid (HCl). The acid-cleaned crushed pyrite was then rinsed with deionized (DI) water until the pH of the supernatant from the solution measured >6.7 standard units (SU). The cleaned crushed pyrite was transferred to a glass bowl and then into the anaerobic chamber to dry anaerobically. Anaerobic chamber conditions were verified to be <0.3% oxygen.

Figure 2.6. Experimental serum bottles filled with ferrous minerals, clays, or neither (controls).

Three treatments (three different waters) were tested: deionized water spiked with 6:2 FTS (final concentration of 0.32 mg/L), AFFF-impacted groundwater from Site A, and AFFF-impacted groundwater from Site C. Each of these waters was sparged with nitrogen for a minimum of 1 hour, while being stirred with a glass stir bar. The bottles were quickly capped with a chlorobutyl rubber stopper (Bellco Glass, Cat# 2048-11800), crimp sealed, and then transferred into the anaerobic chamber. Sparged solutions remained in the anaerobic chamber until the experimental setup was complete.

Polypropylene 50 mL (VWR, Cat#89039-660) and 15 mL (VWR, Cat#89004-368) conical tubes were rinsed with methanol, deionized water (3 times), and then left to air dry under a fume hood. The 50 mL conical tubes were wrapped in aluminum foil and transferred into the anaerobic chamber. Test conditions containing DI were spiked with 1.0 mL of 9.6 mg/L 6:2 FTS and diluted with 29 mL of anaerobic deionized water. The bottles used for the anaerobic conditions remained in the anaerobic chamber through the duration of the study.

The bottles used for the aerobic conditions were removed from the anaerobic chamber and uncapped to allow atmospheric air into the headspace of the conical tubes. The aerobic conditions were then recapped and hand shaken for a minimum of 30 seconds. The bottles were then uncapped, recapped, and shaken every other day to ensure that the test vessels remained aerobic. The aerobic bottles were placed on a shaker table and continuously mixed at 70 revolutions per minute (RPM). Bottles were placed on their sides to facilitate dissolution of oxygen into the water, and its subsequent contact with pyrite mineral surfaces.

Both anaerobic and aerobic bottles were stored in the dark. Samples were periodically collected from the test vessels by collecting 1 mL of solution and diluting it into 11 mL of deionized water in methanol-rinsed 15 mL conical tubes.

No measurable abiotic precursor transformation was observed using crushed pyrite. Subsequent testing of the pyrite with chlorinated solvents indicated that the pyrite used in our testing had very limited reactivity. Subsequent experiments using reactive FeS particles under anoxic and oxic conditions were performed similarly to the experiments previously described using pyrite.

Reactive FeS particles were prepared as described by Hyun and Hayes in an anaerobic chamber.[40] Batch reactors were prepared in 160 mL glass serum bottles containing 50 mL of deoxygenated buffer solution (Trizma base tris hydroxymethyl aminomethane, Trizma HCl tris hydroxymethyl aminomethane hydrochloride, and NaCl). One milliliter of FeS solution (in deoxygenated water) was added to each bottle. In addition, bottles were amended with either 6:2 fluorotelomer sulfonate (6:2 FTS) for a final concentration of 10 µg/L in the bottles or 3M AFFF (1:1000 dilution in the bottles). Anoxic bottles were sealed with a chlorobutyl stopper and crimp capped in the anaerobic chamber, while the oxic samples were covered with parafilm with several holes punched through the opening to allow for entry of air during sample incubation. The microcosms were then transferred outside of the anaerobic chamber to a shaker table and left to mix in the dark under a cover. All samples, including control containing no FeS, were prepared in duplicate.

At each sampling point (1, 5, 9, 19 or 41 days), the microcosms were transferred back into the anaerobic chamber. When sampling, 2 mL of solution from a microcosm was pipetted out into a 15 mL conical tube. After each microcosm was sampled, the 15 mL conical tubes were taken out of the anaerobic chamber and centrifuged at 10,0000 RPM for 5 minutes. The conical tubes were then transferred back into the chamber and 1 mL of supernatant from each condition was then pipetted into another 15 mL conical tube. The supernatant was then diluted with 11 mL of deoxygenated DI water. All samples were wrapped with aluminum foil and parafilm at the cap before being sent for PFAS analysis at Mines.

Results.

The results of the experiments using FeS particles showed no enhanced reductive or oxidative transformation of precursors to PFAAs. Under 6:2 FTS and AFFF-spiked conditions, no precursor transformation or generation of PFAAs were observed in the control (no FeS) bottles. Visual comparison of the oxic and anoxic FeS-amended bottles showed that (as expected) substantial oxidation of the FeS was occurring under oxic conditions, which is consistent with the generation of hydroxyl radicals (**Figure 2.7**). For both the oxic and anoxic FeS amended bottles, no measurable decreases in 6:2 FTS concentrations were observed over the 19 day monitoring period, nor were any potential transformation products (analyzed by suspect screening HRMS) observed.

Figure 2.7 Anoxic (left) and oxic (right) FeS-amended bottles. Clear visual evidence of FeS oxidation in the presence of oxygen was observed.

Precursor transformation, and subsequent PFAA formation, was negligible over a 20-day period for the AFFF-spiked water in FeS-

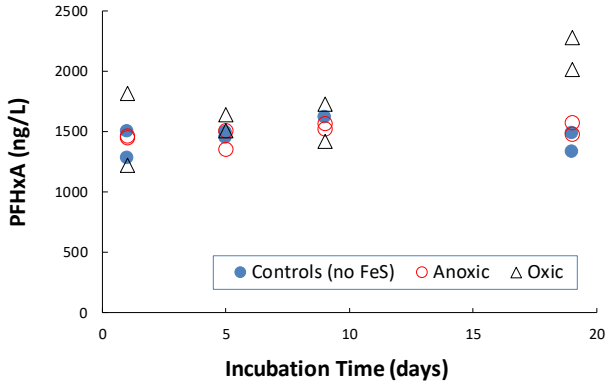

Figure 2.8. PFHxA concentrations in the oxic FeS-amended bottles. Results of duplicate experiments are shown.

amended bottles. The exception was PFHxA formation under oxic conditions (**Figure 2.8**), suggesting that hydroxyl radicals (formed via reaction of dissolved oxygen with the FeS particles) oxidized and transformed PFHxA precursors. Generation of PFHxS precursors (MeFHxSAA and PFHxSi) was also observed, which is consistent with a hydroxyl radical facilitated transformation pathway.

To further assess the oxidative formation of PFHxA in the oxic FeS bottles, screening of suspect analytes was performed. Results, shown in **Figure 2.9**, indicate that increases in both MeFHxSAA and PFHxSi were observed during the 19-day duration of the study. Both of these precursor compounds have been shown to be part of the oxidation pathway that leads to formation of perfluorinated carboxylic acids. Thus, these results suggest a clear oxidation pathway facilitated by FeS-induced formation of hydroxyl radicals under oxic conditions.

Additional experiments using PFOSi were performed to further explore abiotic precursor transformation coupled with PFAA formation. Results of this study, performed identically to the earlier FeS study, are shown in **Figure 2.10**. PFOSi was rapidly transformed under oxic conditions with or without FeS; PFOSi remained stable under anoxic conditions even in the presence of FeS. The PFOSi decrease in the oxic control was accompanied by an increase in PFOS in the oxic control, indicating that PFOS was the primary oxidative product under these conditions (**Figure**

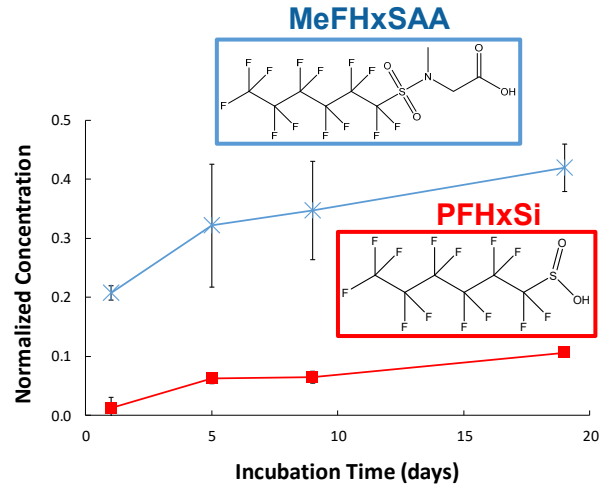

Figure 2.9 Increases in the normalized peak areas of MeFHxSAA and PFHxSi over time in the oxic FeS-amended bottles. Error bars represent the standard deviation of duplicate bottles.

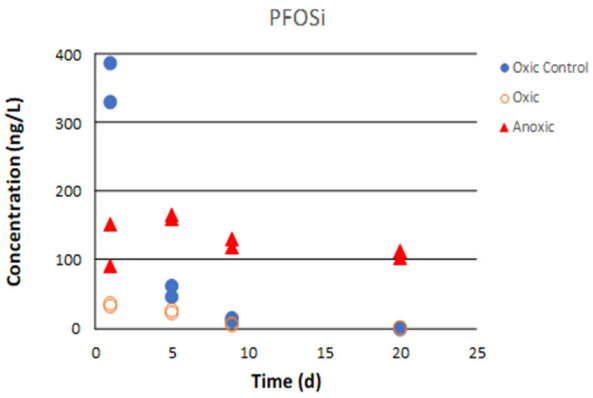

Figure 2.10 PFOSi in the oxic control (which contained no FeS), and the oxic and anoxic treatments (both of which contained FeS). The lower PFOSi initial concentrations are likely due to adsorption to the FeS.

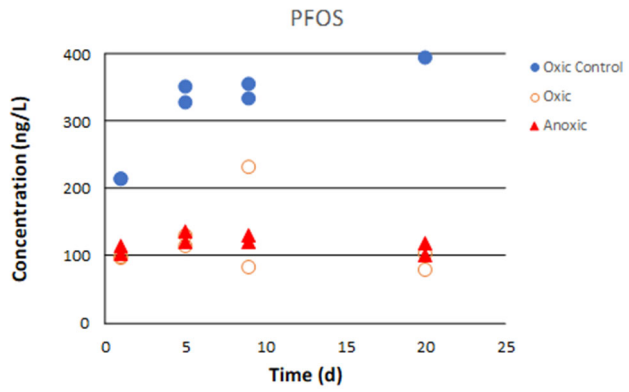

Figure 2.11 PFOS in the oxic control (which contained no FeS), and the oxic and anoxic treatments (both of which contained FeS). The lower PFOS initial concentrations are likely due to adsorption to the FeS.

2.11). PFOS generation was not observed in the anoxic FeS treatment, presumably due to adsorption of the PFOSi and/or PFOS on to the FeS particles.

Overall, these results suggest reactive iron induced reductive transformation of PFAA precursors in AFFF is unlikely to be an important mechanism at most AFFF-impacted sites. However, ferrous iron minerals may play a small role in precursor transformation under oxic conditions due to generation of hydroxyl radicals (which has been shown for chlorinated solvents). Perhaps more importantly, results shown in **Figure 2.9** and **Figure 2.10** suggest that PFOSi is very unstable under oxic conditions and rapidly oxidized to PFOS. This oxidative process may be important for AFFF-impacted sites where PFASs in anoxic source areas undergo transformation as the downgradient plume becomes aerobic.

Task 2.3 ***Coupled Diffusion and Reaction in Low Permeability Materials***

Contaminant flux from high permeability zones into lower permeability zones, or conversely, from low to high permeability zones, can significantly impact the fate and transport of dissolved plumes. To characterize how low permeability zones impact the fate and transport of a mixed contaminant plume, the aqueous diffusivities of the individual contaminants must first be well defined. While aqueous diffusivities for BTEX and chlorinated solvents have been previously determined, to our knowledge, aqueous diffusivity data for PFASs are comparatively limited. Furthermore, the unique physiochemical nature of PFASs limits the use of model compounds in approximating aqueous diffusivities, as colloidal aggregation of micelles and surfactant behavior complicates the diffusion of PFASs in porous media. In an effort to better inform long-term plume behavior and mass discharge at AFFF impacted sites, the tests described herein were executed to develop a fundamental understanding of diffusive behavior and long-term release of PFASs from low permeability zones. First, bromide tracer tests were performed on two clays to determine empirically derived distribution coefficients. Batch kinetics tests were performed using PFASs to determine the time required for PFASs to reach equilibrium between solid and aqueous phases. After the data from the bromide diffusion columns and batch kinetics tests were analyzed, the batch isotherm and PFAS diffusion columns were carried out. Batch isotherm tests and PFAS diffusion columns were executed in parallel to develop aqueous diffusivities for the compounds evaluated.

Bromide Tracer Tests. Bromide tracer tests were performed in duplicate for two natural clayey soils (from Grand Forks AFB and Cidra Superfund Site in Puerto Rico), for a total of 4 experimental columns. A 30-mL plastic syringe with the dispensing end sawed off and plunger removed were used as a column. Each clay was homogenized in a separate Pyrex dish and saturated with a spray bottle containing a 0.05M $CaCl_2$ solution. Approximately 10 cubic centimeters of saturated clay (6 cm in length) was packed into each of the columns and the mass

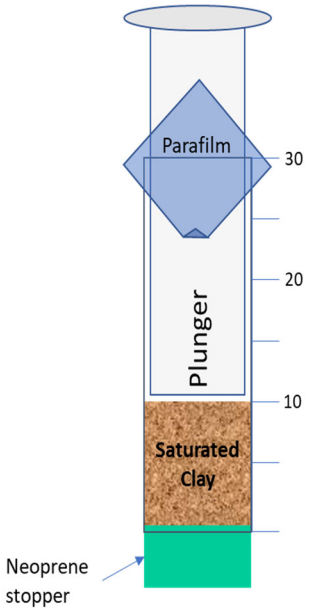

Figure 2.12 Experimental Schematic of bromide diffusion columns.

was recorded. A number 4 neoprene stopper was used to plug the bottom of the column. 50 µL of a 100 g/L bromide solution was applied to the top of each column representing a "source zone". The plunger was placed flush with the soil and parafilm was placed at the top of the column to prevent evaporation. The bromide solution diffused for 2 days. See **Figure 2.12** for the experimental setup.

After the bromide has diffused for two days, the parafilm and stopper were removed from the column and the plunger was used to extrude the clay approximately 1.5 g at a time. Each section of the column was sliced off using a razorblade and weighed out into a 50 mL conical tube. 45 mL of DI water was mixed with the clay using a vortex until the clay was completely disaggregated. The water was filtered using a 0.45µm filter and the resulting bromide was measured at CDM Smith Laboratory using modified EPA Method 300.1.

An analytical solution was used to approximate the concentration of bromide along the length of the column:[41]

$$C = \left(\frac{M}{\pi D t^{\frac{1}{2}}}\right) \exp\left(-\frac{x^2}{4Dt}\right) \qquad \textbf{(Equation 2.4)}$$

Where: $D = \frac{D_{eff}}{R}$ and: $R = 1 + \frac{\rho K_d}{\theta}$. The model result was fit to the observed bromide data by non-linear regression of the aqueous diffusion coefficient.

Batch Kinetics Test. Two kinetic microcosm experiments were prepared in duplicate (**Table 2.2**). Four 250 mL HDPE bottles containing a 4:1 mass ratio of PFAS solution to clay (40mL PFAS solution and 10g clay) were incubated for 120 hours. The PFAS solution was prepared with 0.05M $CaCl_2$ and contained 0.2µM of 6:2 FtS, PFHxS, PFOS, PFHxA, PFHpA, PFOA, and PFNA. Samples of supernatant were collected at 24, 48, and 120 hours where 1mL of sample was added to a 15 mL conical tube containing 7mL of DI. These samples were sent to Colorado School of Mines for analysis. The results of the batch kinetics test were used to inform experimental design and execution of the batch isotherm and diffusion column tests.

Table 2.2 Batch Kinetic Test Matrix

	PFAS Concentrations (uM)	Time points (hours)	Number of samples
Cidra A	0.2	24, 48, 120	3
Cidra B	0.2	24, 48, 120	3
Grand Forks A	0.2	24, 48, 120	3
Grand Forks B	0.2	24, 48, 120	3
TOTAL			12

Batch Isotherm Test. Batch isotherm tests were executed for each clay and a no soil control at 5 different PFAS concentrations in duplicate (total of 30 microcosms; **Table 2.3**). Bottles were prepared as described in the batch kinetics test (4:1 solution to clay mass ratio) except with with 0.1, 0.5, 5, 50, 500 µg/L PFAS (**Table 2.3**). The isotherm bottles were sampled after they reached equilibrium (as determined by the batch kinetic test). 1mL of sample was added to a 15 mL conical tube containing 7mL of DI and sent to the Colorado School of Mines for analysis.

Diffusion Columns. PFAS diffusion columns were prepared in parallel with the batch isotherm experiments in 30mL syringes as described in the bromide tracer test and **Figure 2.13**. Approximately 22.5 g (~15 cm^3) of saturated clay was packed into the syringe, and 10 mL of a mixed PFAS solution containing 50 ppb each of PFOS, 6:2 FtS, PFHxS, PFHxA, PFHpA, PFOA, and PFNA was dispensed on top of the column representing a semi-infinite source (**Figure 2.13**). This reservoir was replaced with fresh stock after 24 hours, 48 hours, and then approximately every 3 days afterwards until the end of the incubation.

Table 2.3. Batch Isotherm Test Matrix

	PFAS Concentrations (µg/L)*	Time (hours)	Time points	Samples
Cidra A	0.1, 0.5, 5, 50, 500	24	1	5
Cidra B	0.1, 0.5, 5, 50, 500	24	1	5
Grand Forks A	0.1, 0.5, 5, 50, 500	24	1	5
Grand Forks B	0.1, 0.5, 5, 50, 500	24	1	5
No Soil A	0.1, 0.5, 5, 50, 500	24	1	5
No Soil B	0.1, 0.5, 5, 50, 500	24	1	5

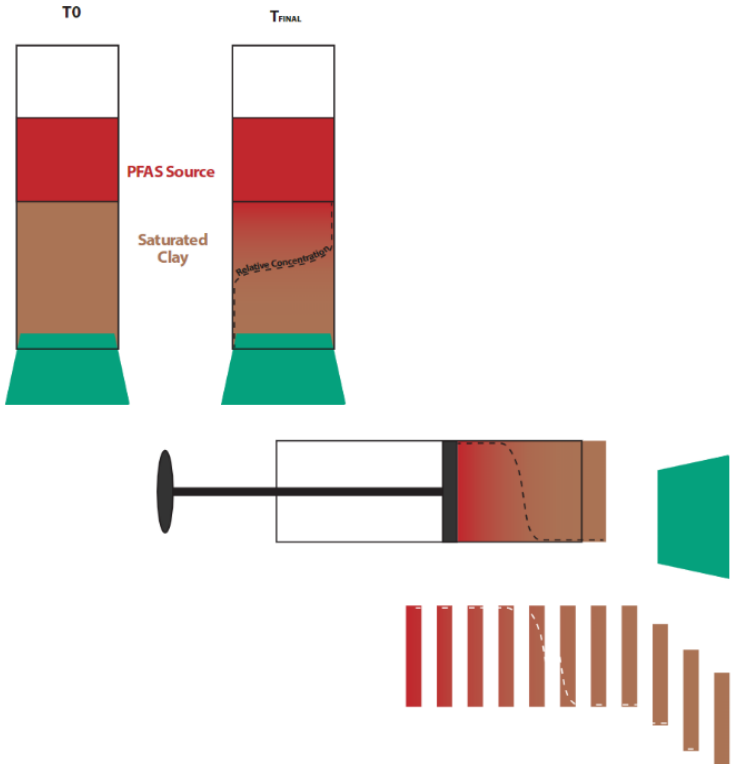

Figure 2.13 PFAS diffusion column with a semi-infinite PFAS source (red).

After 25 days of incubation the reservoir was pulled off the top of the column and disposed. The stopper was removed and using a clean plunger the clay was extruded about 1 cm at a time and sliced using a clean razor blade. It is worth noting the plunger did not come in contact with the clay during extrusion as the clay and plunger formed air tight seals (**Figure 2.14**). Of the 22.5 g of clay in the column 21.9 g was recovered from 15 slices. Each slice was placed in a clean 50 mL centrifuge tube and sent to the Colorado School of Mines for analysis.

To predict the diffusion for each PFAS through the column, the following unsteady-state mass balance equation was employed for each substance:

$$\frac{c_1 - c_{10}}{c_{1\infty} - c_{10}} = \mathrm{erf}\frac{z}{\sqrt{4D_{obs}t}} \qquad \textbf{(Equation 2.5)}$$

where C_1 is the PFAS concentration (ng cm^{-3}), C_1 is the constant PFAS concentration at the top of the column (ng cm^{-3}), $C_{1\infty}$ is the PFAS concentration an infinite distance away from the top of the column (assumed to be zero), z is the distance from the top of the column (cm), t is the time (s), D_{obs} is the observed PFAS diffusivity (cm^2 s^{-1}). Further, this can be related to D_{aq} via:

$$D_{obs} = \frac{\frac{D_{aq}}{\tau}}{1+\frac{\rho K_d}{\epsilon}} \quad \textbf{(Equation 2.6)}$$

with D_{aq} is the PFAS aqueous diffusivity (cm^2 s^{-1}), τ is the tortuosity (dimensionless), ρ is the clay bulk density (measured at 1.35 g cm^{-3}), ε is the water-filled clay porosity (0.4 based on the saturated water content of the clay), and K_d is the linear PFAS adsorption coefficient to the clay (cm^3 g^{-1}).

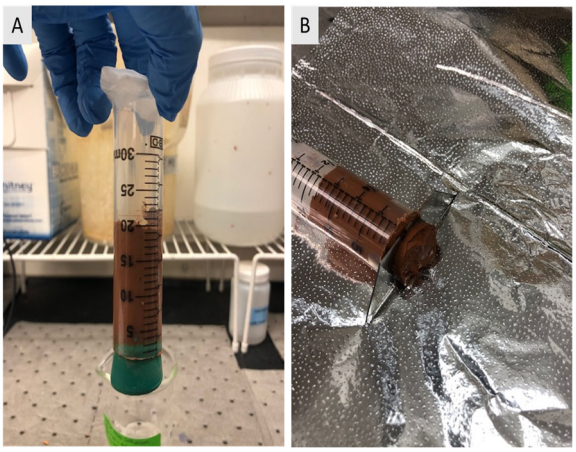

Figure 2.14 PFAS diffusion column before slicing (A), and during slicing procedure (B).

Model Development. Assuming a constant PFAA concentration at the top of the column (z=0), no PFAAs in the soil at t=0, and a no flux condition at the bottom of the column, the observed diffusion coefficient for each PFAA through the soil is described as follows:[41]

$$C = C_0 \sum_{n=0}^{\infty}\left[(-1)^n erfc\left(\frac{(2n+1)L-z}{2\sqrt{D_{obs}t}}\right)\right] + C_0 \sum_{n=0}^{\infty}\left[(-1)^n erfc\left(\frac{(2n+1)L+z}{2\sqrt{D_{obs}t}}\right)\right] \quad \textbf{(Equation 2.7)}$$

where C is the PFAA aqueous concentration (µmol cm^{-3}), C_0 is the PFAA aqueous concentration at z=0 (µmol cm^{-3}), L is the length of the soil column (cm), z is the distance along the soil column from the PFAA source (cm), t is the time (s), and D_{obs} is the observed diffusion coefficient (cm^2 s^{-1}). Assuming that D_{obs} consists of contributions from both aqueous diffusion in the pores and clay surface diffusion, D_{obs} is defined for each PFAA as follows for a system described by a linear equilibrium adsorption isotherm:[42–44]

$$D_{obs} = D_{obs,p} + D_{obs,s} = \frac{\frac{D_{aq}}{\tau}}{1+\frac{\rho K_d}{\varepsilon}} + \frac{\rho K_d D_s}{\varepsilon} \quad \textbf{(Equation 2.8)}$$

where $D_{obs,p}$ and $D_{obs,s}$ are the observed PFAA pore and surface diffusion coefficients, respectively (cm^2 s^{-1}), D_{aq} is the aqueous diffusivity (cm^2 s^{-1}), τ is a dimensionless tortuosity factor to account for the reduction in diffusivity in clay relative to water only, ρ is the dry soil bulk density (1.04 g cm^{-3}), K_d is the PFAA linear adsorption coefficient determined from the batch adsorption isotherm (cm^3 g^{-1}), ε is the water-filled porosity (0.31), and D_s is the PFAA surface diffusivity (cm^2 s^{-1}).

Values for D_{aq} are based on measurement of PFAA aqueous diffusivities performed by Schaefer et al. (2019).[45]

The value for τ was determined based on the bromide diffusion experiments, where τ was calculated by dividing the D_{aq} for bromide (2.1×10^{-5} cm^2 s^{-1})[22] by the D_{obs} measured for bromide in the diffusion columns. The value of τ calculated from the bromide diffusion experiments and used in **Equation 2.6** was 2.6.

The value of D_s was fit to the experimental diffusion curve for PFOS. PFOS was selected for this regression because D_s is expected to be most pronounced for the most strongly sorbing PFAA, consistent with previously developed models.[42,46] To estimate D_s for the other PFAAs, it is assumed that D_s scales with the value for D_{aq} for each PFAA, which is a reasonable assumption based on previously observed relationships between D_{aq} and D_s.[47,48] Thus, for the 6 PFAAs used in this study, only the single parameter D_s for PFOS was regressed to the experimental data.

Results. Results of the batch adsorption isotherms and linear regressions (K_d) for each of the PFAAs are presented in **Figure 2.15**. Comparison of PFHxA adsorption with and without PFOS present showed that PFHxA was not measurably impacted by the presence of PFOS (data not shown), as PFHxA adsorption on the soil was identical whether PFOS was present or not. While this single-point is not an exhaustive assessment of PFAA sorptive competition on the soil, comparison of the most strongly sorbing compound (PFOS) to one of the more weakly sorbing compounds (PFHxA) suggests that competitive adsorption effects are likely minimal at the concentrations examined herein.

PFAA K_d values generally increased with increasing chain length. The exception was PFHpA, which had a K_d value that was greater than that measured for PFOA. Comparing PFOS to PFNA, which both have the same perfluorinated chain length but differ in head group, the sulfonate had a greater K_d than the carboxylate. However, comparison of PFHxS to PFHpA, shows that the K_d values are statistically identical for the sulfonate and the carboxylate, suggesting that increased adsorption of perfluorinated sulfonates relative to perfluorinated carboxylates of the same perfluorinated chain length may not be true for all chain lengths for the soil examined herein.

Diffusion Experiments. PFAA aqueous concentrations are shown as a function of distance from the top of the column in **Figure 2.16**. PFAA aqueous porewater concentrations are calculated from the measured PFAA soil concentrations (which include both aqueous and sorbed PFAAs) for each soil slice for each PFAA via the following mass balance equation:

$$C = \frac{M}{V_w + K_d S} \qquad \textbf{(Equation 2.9)}$$

where M is the total (soil + aqueous phase) PFAA molar mass, V_w is the volume of water (calculated based on a measured moisture content of 32%), and S is the soil mass. For all PFAAs evaluated, measurable diffusion into the soil column over the 20-day incubation period occurred.

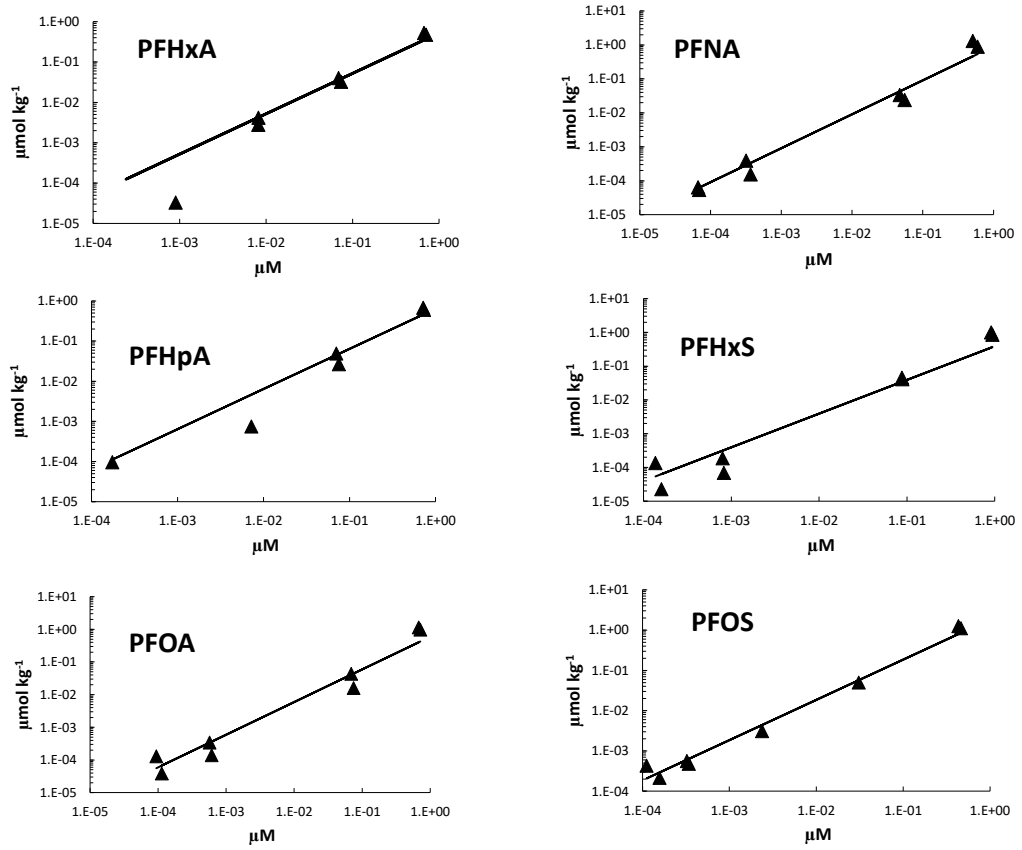

Figure 2.15. Adsorption isotherms.

The solid lines shown in **Figure 2.16** represent the model (**Equation 2.7** and **Equation 2.8**) prediction considering aqueous diffusion only (i.e., $D_{obs,s}$, $D_s = 0$). Values of $D_{obs,p}$ and D_{aq} used for this model prediction are shown in **Table 2.4**; all other values in **Table 2.4** apply to the model which includes coupled aqueous and surface diffusion. The D_{obs} values (11 to 23 x 10^{-7} cm^2 s^{-1}) observed for benzene and toluene in natural soils containing 12 to 20% clay[43] are (with the

Table 2.4. Parameters for the diffusion model. As discussed in the text, the dry bulk density is 1.04 g cm^{-3}, the porosity is 0.31, the tortuosity is 2.6, and the K_d values are provided in **Figure 2.15** and **Table 2.5**. D_s for PFOS is the only regressed parameter. Units for all diffusivities and diffusion coefficients are in cm^2 s^{-1}.

Parameter	PFHxA	PFHpA	PFOA	PFNA	PFHxS	PFOS
D_{obs}	14 x 10^{-7}	11 x 10^{-7}	7.8 x 10^{-7}	5.8 x 10^{-7}	8.6 x 10^{-7}	3.2 x 10^{-7}
$D_{obs,p}$	12 x 10^{-7}	8.9 x 10^{-7}	6.3 x 10^{-7}	4.4 x 10^{-7}	7.4 x 10^{-7}	2.9 x 10^{-7}
$D_{obs,s}$	1.1 x 10^{-7}	1.6 x 10^{-7}	0.96 x 10^{-7}	1.4 x 10^{-7}	0.59 x 10^{-7}	3.3 x 10^{-7}
$D_{obs,p}$ / $D_{obs,s}$	11	5.6	6.6	3.1	13	0.88
D_{aq}*	78 x 10^{-7}	73 x 10^{-7}	49 x 10^{-7}	47 x 10^{-7}	45 x 10^{-7}	54 x 10^{-7}
D_s**	0.77 x 10^{-7}	0.91 x 10^{-7}	0.48 x 10^{-7}	0.46 x 10^{-7}	0.44 x 10^{-7}	0.53 x 10^{-7}
Log normalized RMSE***	0.12 (0.097)	0.089 (0.12)	0.17 (0.21)	0.37 (0.95)	0.11 (0.14)	0.17 (2.4)

* Values of D_{aq} are from Schaefer et al. (2019). D_{aq} for PFNA and PFHpA estimated based on non-linear trend of C5, C6, and C8 perfluorinated carboxylates.

** D_s for PFOS determined based on regression to the diffusion data. Ds for the other PFAAs are assumed to scale with the values of the aqueous diffusivity D_{aq}.

*** Calculated using **Equation 2.10**. Values in parentheses are for the model case where D_s and $D_{obs,s}$ are set equal to zero.

Table 2.5. Values of K_d ± the 95% confidence intervals

PFAA	K_d (L/kg)
PFHxA	0.43 ± 0.15
PFHpA	0.64 ± 0.22
PFOA	0.59 ± 0.35
PFNA	0.91 ± 0..40
PFHxS	0.39 ± 0.30
PFOS	1.8 ± 0.53

exception of PFHxA and PFHpA) 2- to 3-times greater than the D_{obs} values for PFAAs shown in **Table 2.4**. This discrepancy is primarily due to the relatively small D_{aq} values for the PFAAs.[45]

Evaluation of the dashed line model predictions in **Figure 2.16** shows that neglecting surface diffusion results in a visible (>10-times) underprediction of predicted PFOS aqueous concentrations beginning at approximately a 2 cm distance from the top of the soil column. Similarly, for PFNA, model predictions underestimate aqueous concentrations by approximately 10-times by z = 3 cm. **Figure 2.17** shows that the error between predicted (neglecting surface diffusion) and measured PFAA concentrations increases with K_d based on a log normalized root mean square error (RMSE):

$$\text{log normalized RMSE} = \sqrt{\frac{\sum_{i=1}^{q}\left(logC_i - logC_{m,i}\right)^2}{q}} \qquad \textbf{(Equation 2.10)}$$

where C_i and $C_{m,i}$ are the measured and modeled aqueous PFAA concentration, respectively, and q is the number of datapoints (or, soil slices). Use of log-normalized concentrations serves to more evenly weight data at both high and low aqueous PFAA concentrations. The trend in **Figure 2.17**

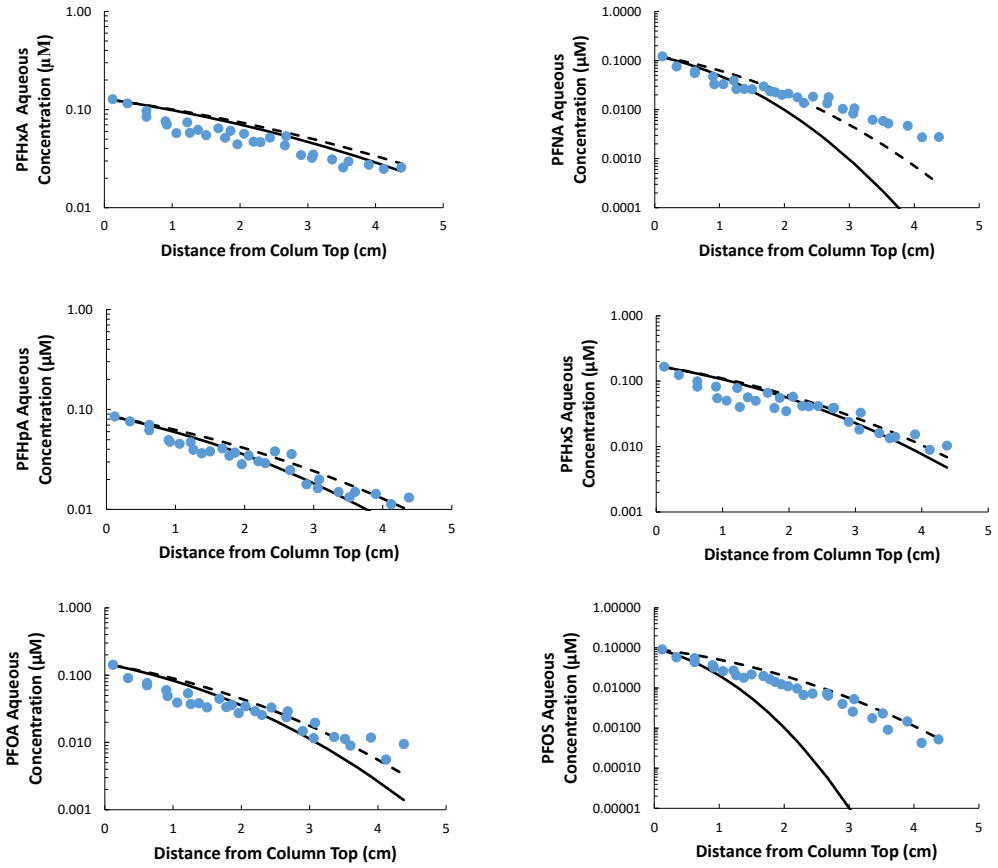

Figure 2.16. Measured PFAS concentrations in the diffusion columns compared to model predictions.

is expected, as modeling efforts have shown that surface diffusion increasingly contributes to D_{obs} as K_d increases.[42,46] Thus, **Figure 2.17** highlights the need for including surface diffusion for PFOS and PFNA, which have the highest K_d values. For the PFAAs and soil examined herein, surface diffusion contributions become important (>10% of the overall diffusion) at K_d values greater than approximately 0.5 L kg^{-1}.

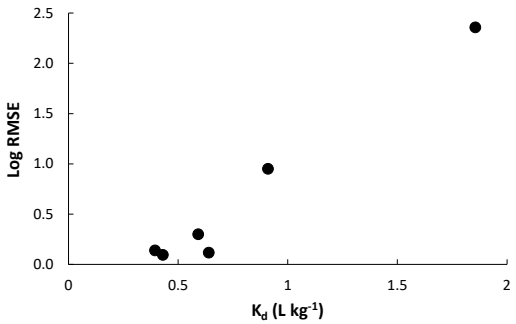

Figure 2.17. Log RMSE (**Equation 2.10**) as a function of PFAA K_d value when comparing the diffusion model (neglecting surface diffusion) to the diffusion column data.

The dashed lines in **Figure 2.16** represent the model considering both aqueous pore ($D_{obs,p}$) and surface diffusion (D_s) contributions. Diffusion coefficient values used in the model are provided in **Table 2.4**. The value of D_s for PFOS was regressed to the data using logarithmic values of the measured and modeled PFOS aqueous concentrations, with a regressed value of $5.3 \pm 0.1 \times 10^{-8}$ cm^2 s^{-1}. As discussed in the Model Development, D_s values for the other PFAAs subsequently were scaled by the ratio of their values of D_{aq} (**Table 2.4**). The value of D_s for PFOS was within the range of D_s values measured for phenol (phenol has a D_{aq} value within approximately a factor of two of that for PFOS (Bhatia et al., 1990))[49] on activated carbon by Ocampo-Pérez et al. (2013)[50].

Visual inspection of the models relative to the experimental data readily indicates that, for PFOS and PFNA, inclusion of surface diffusion resulted in substantial improvement in the model predictions. This improvement is most apparent at large values of z (i.e., as diffusion distance increases). Comparison of the log-normalized RMSE with and without inclusion of surface diffusion confirms the visual observations, particularly for PFOS and PFNA (**Table 2.4**). Inclusion of surface diffusion results in a decrease in the RMSE for all PFAAs, with the exception of PFHxA, where surface simulated surface diffusion impacts are minimal.

The ratio $D_{obs,p}/D_{obs,s}$ is greatest for PFHxS, and generally decreases with increasing K_d (**Table 2.5**). This observation is consistent with previously developed models such as Yoshida et al., Do and Rice, and Gimmi and Kosakowski (**Equation 2.8)**.[42,44,46] For PFOS, which has the largest K_d (1.8 L kg^{-1}) among the PFAAs examined herein, surface diffusion processes account for approximately 53% of the overall diffusive flux; for PFNA, which has the second largest K_d (0.91 L kg^{-1}) surface diffusion processes account for approximately 24% of the overall diffusive flux.

In addition, for the anionic surfactant SDBS, surface diffusion accounted for 45-70% of the overall observed diffusion coefficient in activated carbon; this is in reasonable agreement with the surface contribution observed for PFOS (52%). The fraction D_s/D_{aq} is approximately 10^{-2} for all the PFAAs examined herein. This value is well within the range determined by Gimmi and Kosakowski (2011) for several cations on a wide range of clay rock and clay sediment, although Gimmi and Kosakowski examined cations rather than the anionic PFAAs examined herein.[44]

TASK 3. BIOTIC TRANSFORMATION

Task 3.1 *Assess Biotic Reactions Under Varied Redox Conditions.*

Aerobic Microcosms with 3M California Guardian and National Foam AFFF. It has been reported that N-containing precursors are persistent in the environment.[51] The objective of Task 3.1 was to compare the biotransformation potential between N-containing ECF precursors and N-containing fluorotelomers in AFFF formulations. Aerobic microcosms containing 3M California Guardian AFFF or National Foam AFFF were performed to assess their biotransformation. A soil slurry made from soil collected from a former AFB (Soil D) was added (2% g solids/ liquid final concentration) to a mineral salts medium containing 3M California Guardian AFFF or National Foam AFFF. The AFFFs were amended at a 1:1000 dilution of the commercial grade mixtures (3%). On average, the concentrations of 3M and National Foam AFFF PFCA precursors, quantified by the Total Oxidizable Precursor assay[52] in triplicate, were ~20-40 μM. PFCA precursor concentration measured by the TOP assay can provide an upper estimate of biotransformable PFAS.[52] During the first carbon amendments, diethyl glycol monobutyl ether (DGBE), also known as butyl carbitol, was added (1.5 mmol/L) as an additional carbon source because of its widespread occurrence in AFFF formulations and its biodegradability. Heat-killed controls were prepared by autoclaving a Soil D soil slurry (10% g solids/liquid in 0.9% saline) and subsequently freezing the slurry for four consecutive days. The bottles were incubated in the dark at 30 °C in an orbital shaker (100 rpm). All treatments and controls were run in triplicate.

Liquid samples were retrieved with aseptic technique and centrifuged (10 min, 15000g). After centrifugation, the supernatants were separated for PFAS analysis (stored in methanol 1:1) and TOC analyses. LC-MS/MS analyses using multiple reaction monitoring (MRM) were performed according to DoD QSM Method DOD QSM 5.1.1 Appendix B Table B-15. Initial characterization of the cationic and zwitterionic PFAS components present in this 3M California Guardian showed that AmPr-FHxSA ($[M+H]^+$ 485) was a major component, accounting for ~90% of peak areas of visible mass features detectable along the chromatogram. For National Foam, 6:2 fluorotelomer sulfonamido betaine (FTSA-PrB) accounted for the majority of the PFAS composition. For these cationic/zwitterionic precursors, relative responses were calculated by normalizing the peak areas to [$^{14}C_4$]-PFOS using pole-switching.

In 3M microcosms, we suspected AmPr-FHxSA could yield PFAA products.[51,53] In microcosms with Soil D inoculum (**Figure 3.1**), the decrease in relative response of AmPr-FHxSA over the first few days across all the treatments and controls was attributed to adsorption. After the first week, the concentration stabilized in the medium and autoclaved controls, while the live treatment continued to decrease. No PFCAs were detected as a product of transformation.

TOC decreased in the live control between days 20-40 but then recovered to the initial concentration and was comparable to the medium-only and autoclaved controls. In the microcosms, 1.5 mmol/L of DGBE was present (accounting for ~144 mg-C/L of the TOC) and was not consumed. This suggests that 3M California Guardian inhibits biodegradation of readily available carbon sources, such as DGBE.

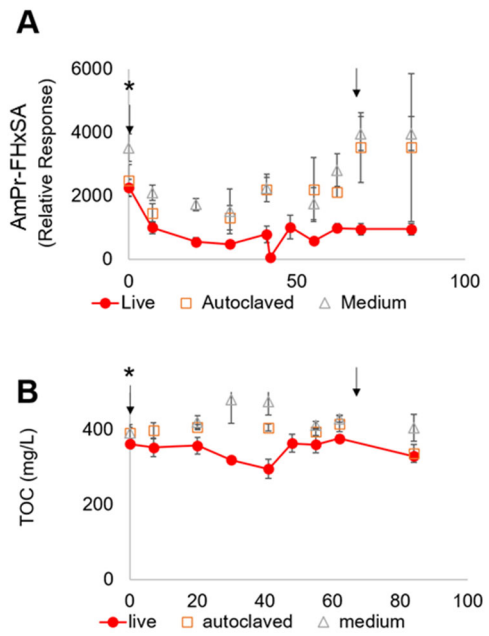

Figure 3.1 3M aerobic biotransformation microcosm with Soil D inoculum. Panel A: Relative response of perfluorohexane sulfonamido amine (AmPr-FHxSA) normalized to mass-labeled PFOS. Panel B: Total Organic Carbon (TOC). The arrows indicate amendment with 3M California Guardian AFFF. The asterisks denote amendment with 1.5 mM DGBE.

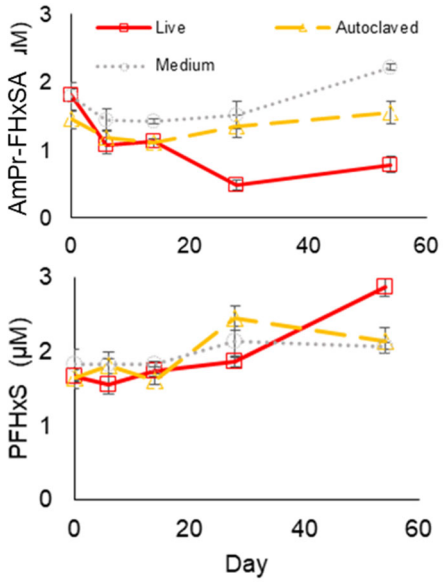

Figure 3.2 Butyl carbitol amended aerobic biotransformation microcosms of Peterson AFB bucket AFFF.

Aerobic microcosms with California Guardian 3M AFFF and Soil A, which has lower PFAS concentrations than the Soil D, showed biological activity within 10 days via the consumption of non- fluorinated organics. However, little biological transformation was observed for 3M polyfluorinated precursors. We hypothesize that the biotransformation was stalled by the high levels of PFOS in the AFFF.

Biotransformation experiments were also conducted with an AFFF mixture collected at Peterson Air Force Base, which contains lower concentrations of PFOS but still has a substantial amount of 3M precursors. Aerobic microcosms with Soil A and amended with butyl carbitol or BTEX (1% soil to medium) showed decreases in AmPr-FHxSA in both treatments (**Figure 3.2**). However, the BTEX microcosms stalled and there was no evidence of targeted transformation products. The butyl carbitol microcosms showed slight increases in PFHxS concentrations.

National Foam Microcosms. The National Foam microcosms showed decreases in 6:2 FTSA-PrB during the first 50 days, but there were no significant differences in concentrations between the live treatment and the controls. However, 6:2 FTSA-PrB was continuously removed from solution over 150 days of experimentation. No PFCAs or 6:2 FtS were detected as products of biotransformation in the LC-MS/MS analyses.

Unlike the 3M California Guardian microcosms, the National Foam microcosms (**Figure 3.3**) showed depletion of the majority of TOC in the system within 25 days, suggesting that the readily available carbon sources were consumed without any inhibitory effects. Several amendments of National Foam were made to replenish the carbon source in the system. After 100 days of incubation, the autoclaved and medium-only controls showed a decrease in TOC. This decrease does not seem to be due to biological cross contamination based on visual examination, but could be due to precipitation of some components in National Foam.

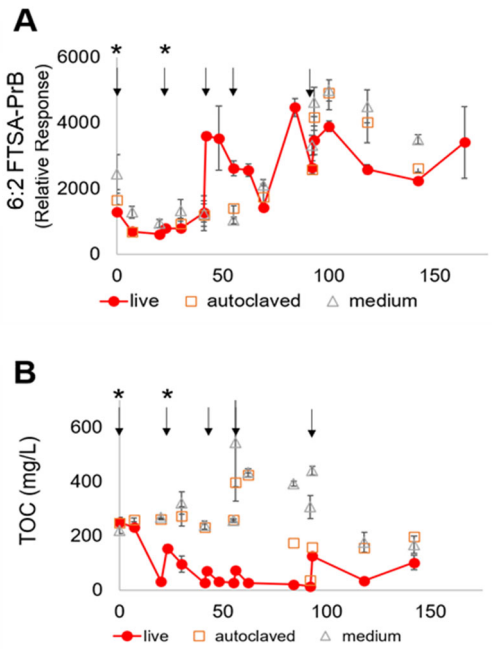

Figure 3.3 National Foam aerobic biotransformation microcosm with Soil D inoculum. Panel A: Relative response of 6:2 fluorotelomer sulfonamido betaine (FTSA-PrB) normalized to mas-labeled PFOS. Panel B: Total Organic Carbon (TOC). The arrows indicate amendment with National Foam AFFF. The asterisks denote amendment with 1.5 mM DGBE. In the amendments between days 0 and 50, only the live treatment was spiked with National Foam AFFF.

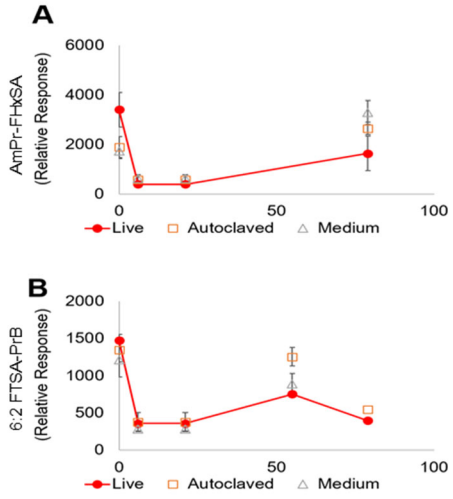

Figure 3.4 Methanogenic microcosms. Panel A: 3M California Guardian microcosms showing the relative response of AmPr-FHxSA. Panel B: National Foam microcosms showing the relative response of 6:2 FTSA-PrB.

Methanogenic Incubations of 3M and National Foam Anaerobic Microcosms. Anaerobic methanogenic incubations were set up with some modifications to the experimental setup described in the aerobic microcosms. The mineral salts medium included cysteine as a reducing agent, and resazurin as a redox indicator. The bottles also were amended with Vitamin B12. The mineral salts medium was boiled and flushed with N_2 gas to remove O_2 from the system. The headspace in all microcosms was flushed with 80%/20% N_2/CO_2.The bottles were incubated in the dark at 28 ºC without shaking. Liquid samples were retrieved for PFAS analysis as described in the aerobic microcosms experimental section.

The methanogenic microcosms showed little activity during 75 days of incubation (**Figure 3.4**), and there was no significant difference between the treatments and controls. The initial decrease across all treatments and controls in 3M and National Foam microcosms was attributed to adsorption. The following weeks did not show continued decreases for AmPr-FHxSA or 6:2 FTSA-PrB.

Aerobic biotransformation of AmPr-FHxSA with carbon source enrichments. We performed biotransformation assays with AmPr-FHxSA alone because the background PFHxS concentrations in AFFF formulations masked the amount produced by biotransformation. Soil B enrichments were developed by amending with four carbon sources during 2 months (BTEX, DGBE, acetate, and methane).

Over the course of 70 days, AmPr-FHxSA was transformed into FHxSA, and to a lesser extent PFHxS (**Figure 3.5**). The methanotrophic and acetoclastic enrichments had the highest amounts of FHxSA (up to 40% of initial AmPr-FHxSA in the methanotrophic) and PFHxS (up to 5% of the initial AmPr-FHxSA in the methanotrophic enrichment) produced. The BTEX and the DGBE enrichments resulted in less PFHxS, and less than 5 nM FHxSA. Interestingly, the autoclaved controls also showed removal of AmPr-FHxSA despite showing no significant ATP formation (**Figure 3.6**), indicating that the decrease was not

attributed to biological processes in these controls. The autoclaved controls did not form detectable levels of FHxSA or PFHxS.

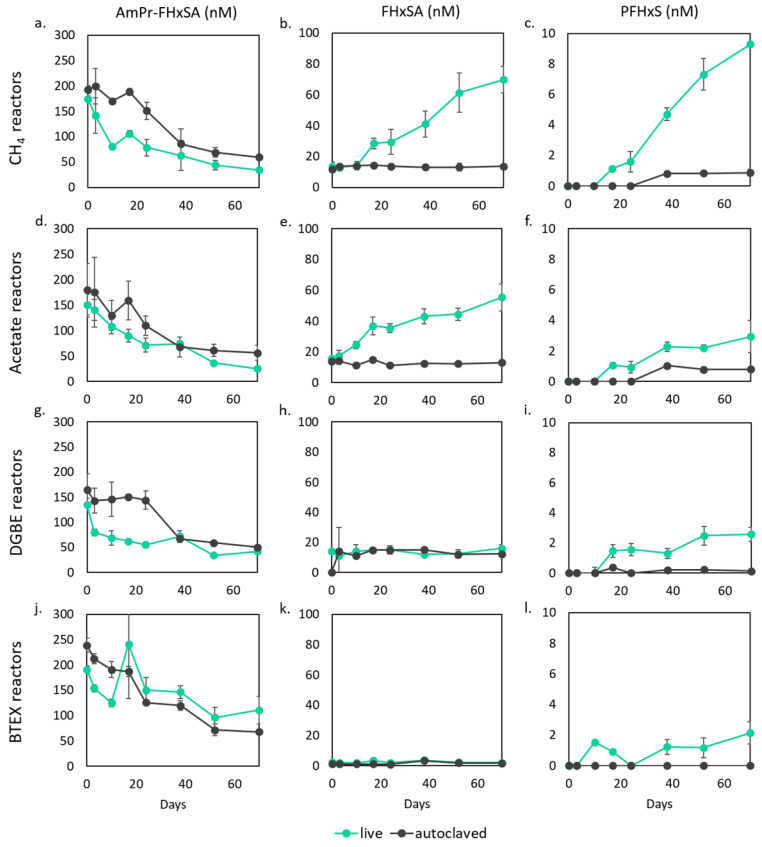

Figure 3.5 AmPr-FHxSA depletion and FHxSA and PFHxS production (from left to right) over 70 days under aerobic conditions with four different carbon sources: a-c) CH_4, d-f) sodium acetate, g-i) DGBE, and j-l) BTEX. Error bars represent standard deviation of triplicate reactors

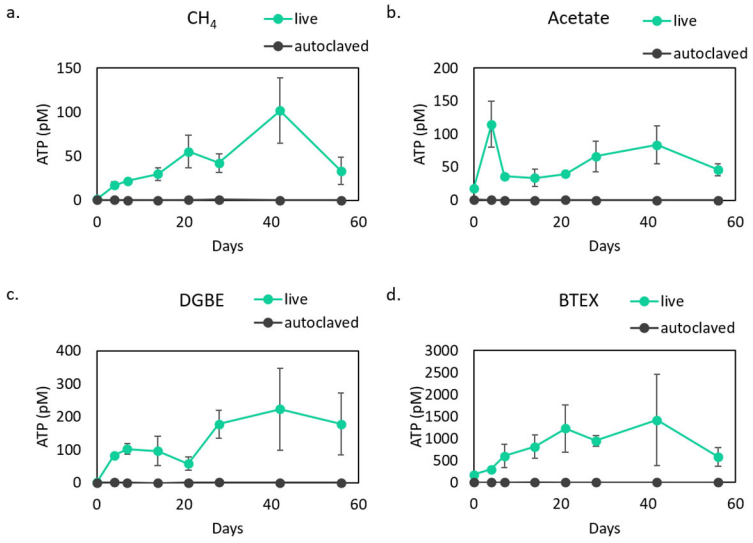

Figure 3.6. ATP concentrations in BTEX (a), Acetate (b), DGBE (c), and BTEX (d) enrichments during aerobic biotransformation experiments.

Carbon source (BTEX, DGBE) effects on aerobic 6:2 FtTAoS biotransformation. In parallel to experiments with ECF-precursors, we also evaluated the impact of carbon sources on a fluorotelomer precursor—6:2 fluorotelomer thioether amido sulfonate (6:2 FtTAoS, aka 6:2 FTTh-PrAd-DiMeEtS). Aerobic biotransformation of 6:2 FtTAoS formed 6:2 FtS, which is further transformed to a mixture of PFBA, PFPeA, and PFHxA, consistent with previous aerobic biotransformation studies.[54] Although all the treatments generated the same transformation products, the presence of BTEX increased the yield of PFCAs (**Figure 3.7**). This increase was not observed in treatments amended with an equivalent amount of carbon in the form of DGBE (**Figure 3.7** Panel A2 vs B2), indicating that the increase in PFCA yield was not attributed to more carbon for the microorganisms. The sum of PFCAs and 6:2 FtS recovered in all treatments with BTEX was greater than in the treatments without BTEX.

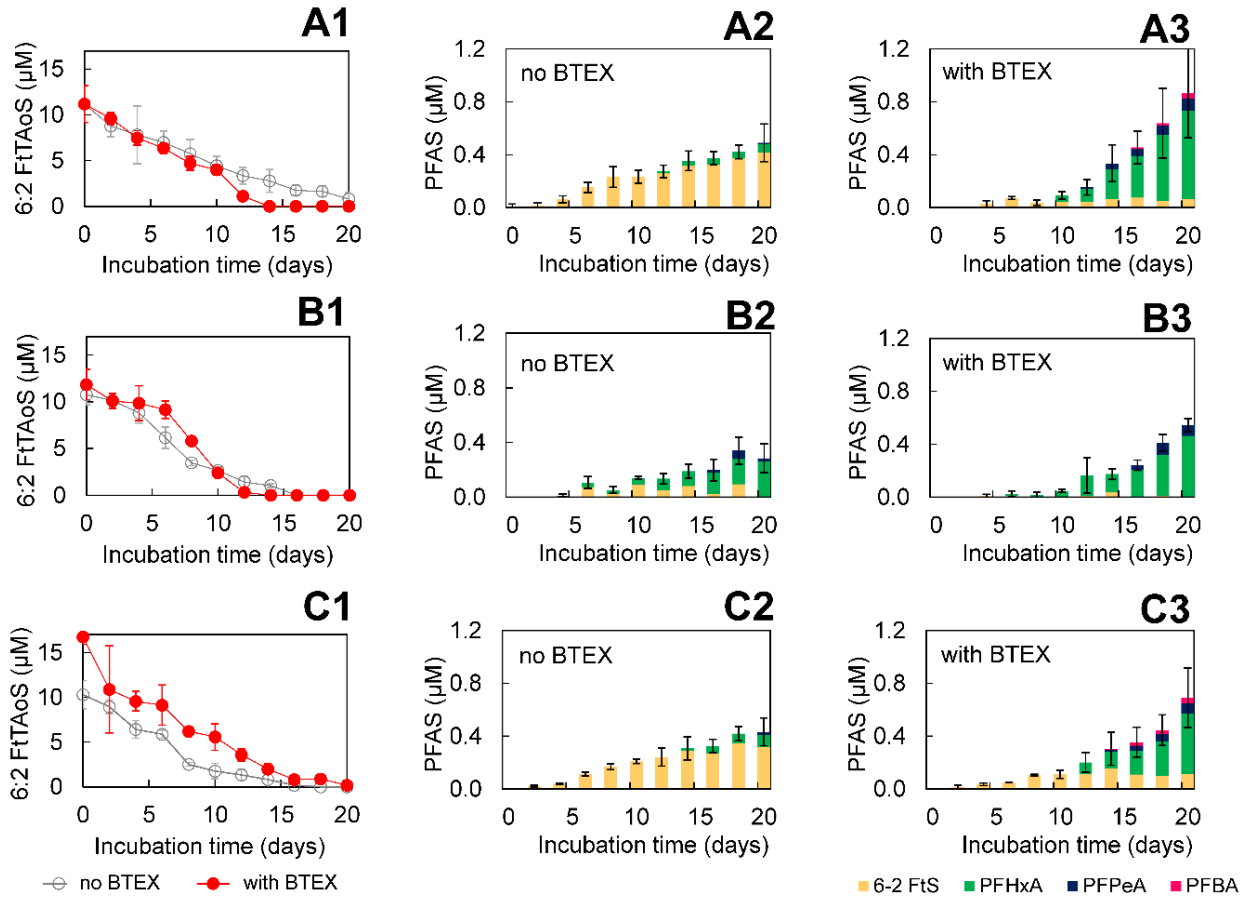

Figure 3.7 Biotransformation of 6:2 FtTAoS with (red filled circles) or without (gray open circles) BTEX in microcosms inoculated with 10% AFFF impacted soil. Microcosms amended with: (A1) 6:2 FtTAoS only (transformation products: A2, A3); (B1) 6:2 FtTAoS plus DGBE (transformation products: B2, B3); and (C1) Ansul AFFF plus DGBE (transformation products: C2, C3). Monitored transformation products: 6:2 FtS (yellow), PFHxA (green), PFPeA (navy blue), PFBA (pink). Error bars represent standard deviation (n=3).

Task 3.2 *Effect of PFASs on Biotic Degradation of Chlorinated Ethenes and BTEX Degradation.*

The objective of Task 3.2 was to assess the impacts of a range of PFAS concentrations (low mg/L to high mg/L) on the dechlorination of chlorinated ethenes, as well as aerobic and anaerobic BTEX

biodegradation. In this task we performed experiments with two AFFFs, 3M California Guardian and Peterson AFB Bucket AFFF. California Guardian had a higher proportion of PFOS to AmPr-FHxSA than Peterson AFB Bucket AFFF.

California Guardian Inhibition of Aerobic BTEX biodegradation. Upon exposure of 3M California Guardian (~20-50 µM of PFCA precursors as measured by the TOP assay), no benzene, toluene, ethyl-benzene or o-xylene degradation was observed during ~20 days, during which significant BTEX biodegradation was observed in the AFFF-free treatment (**Figure 3.8**). A previous study on toxicity effects to *Rhodococcus jostii*, a BTEX degrader, reported no decrease in toluene biodegradation rate in mixtures of PFAAs up to 110 mg/L.[55] The difference with our findings could be in the additional components of AFFF (polyfluorinated substances or non-PFAS substances) that might pose an inhibition to BTEX degrading microorganisms.

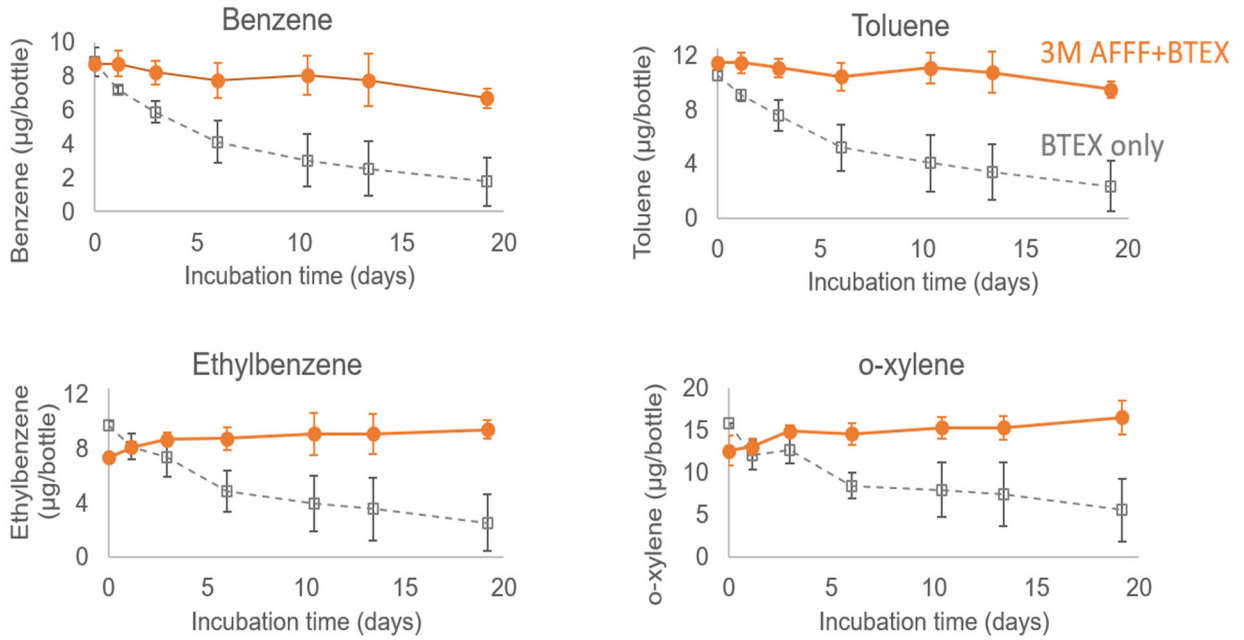

Figure 3.8 Inhibition of aerobic BTEX biodegradation in Soil D enrichments exposed to 3M California Guardian (~20-50 µM PFCA precursors measured by the TOP assay).

California Guardian Inhibition of TCE anaerobic dehalogenation. We performed inhibition experiments with a co-culture consisting of *D. mccartyi* 195 (195) and *D.* Hildenborough (DvH). The TCE experiments evaluated four treatments: 1) 100 mg/L diethyl glycol monobutyl ether (DGBE), 2) 100 mg/L DGBE + 10 mM AmPr-FHxSA, 3) Peterson Bucket AFFF (containing ~100 mg/L DGBE and 10 mM AmPr-FHxSA), 4) Peterson Bucket AFFF with an additional 10 mM AmPr-FHxSA. The treatments with spiked AmPr-FHxSA had slower TCE dehalogenation rates, suggesting that there was an inhibition caused by the precursor to TCE dehalogenation rates (**Figure 3.9**). Unlike previous experiments with TCE, there was no lag phase, suggesting that the inhibition remained and that the microorganisms do not seem to recover from the inhibition. However, the addition of DGBE individually or via AFFF resulted in stimulation of TCE dehalogenation, presumably because of glycol fermentation. These findings suggest that TCE dehalogenation could be affected in places with high concentrations of AmPr-FHxSA, but if

DGBE has not been consumed by other microorganisms, this could counteract the inhibitory effects.

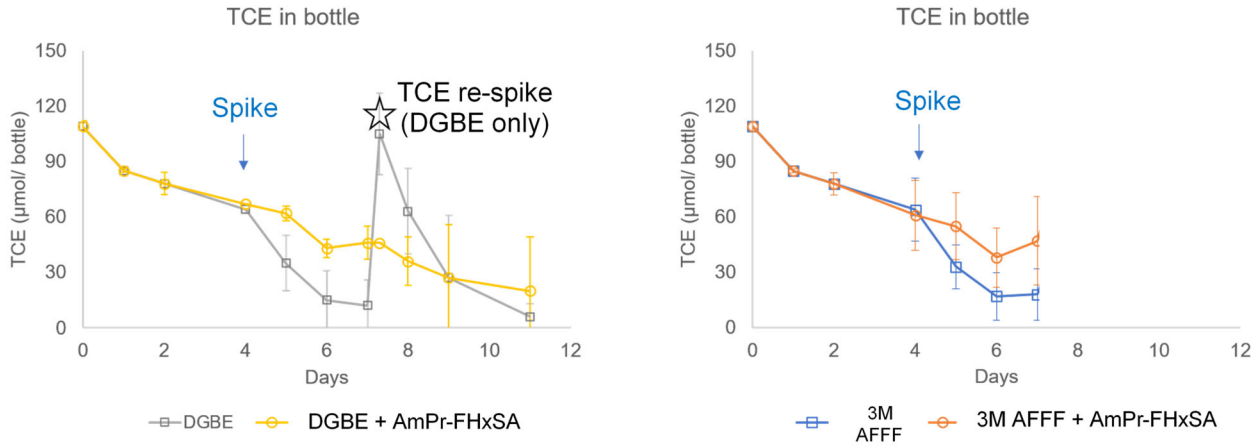

Figure 3.9 TCE dehalogenation in 195+DvH co-culture exposed to AmPr-FHxSA and Peterson Bucket AFFF (which contains AmPr-FHxSA). Arrows show spike of each treatment (DGBE, DGBE+AmPr-FHxSA, Peterson, Peterson+AmPr-FHxSA), and the star denotes re-addition of TCE in the DGBE treatment.

Peterson Bucket AFFF inhibition of anaerobic dehalogenation. We performed TCE dehalogenation inhibition experiments with different concentrations of Peterson AFB AFFF (1:100 ~200 µM PFAS ; 1:1000 ~ 20 µM, 1:10000 ~ 1 µM dilutions) in co-culture of 195 and DvH. The dilution (1:10000 resulting in the least amount of PFAS had a stimulatory effect compared to the control, as seen by an earlier peak of vinyl chloride, a transformation product of TCE (**Figure 3.10**). This stimulatory effect was attributed to DGBE and other fermentable organics present in the formulation. For the 1:1000 dilution, an increase in vinyl chloride concentration was observed but no ethene was formed during 20 days of incubation. The highest concentration (1:100 dilution) had no observable dehalogenation of TCE (**Figure 3.10**). These findings suggest that the TCE dehalogenation coculture (195 and DvH) is able to withstand a wide range of AFFF concentrations (up to ~20 µM PFAS), but the highest concentration ~200 µM PFAS did inhibit the co-culture.

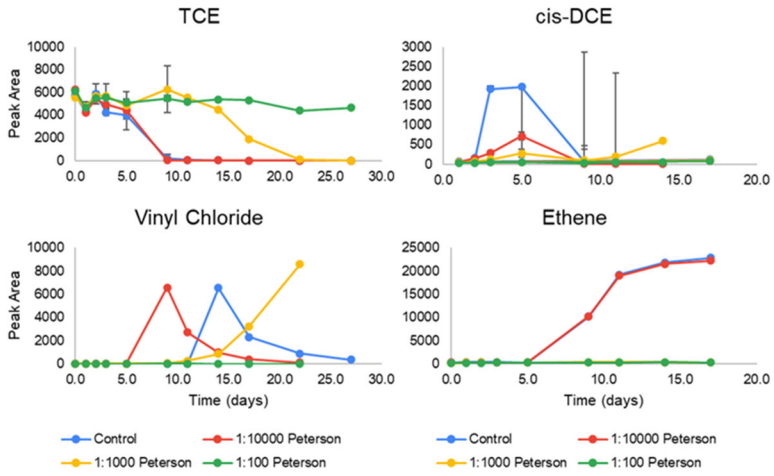

Figure 3.10 Anaerobic dehalogenation of TCE (TCE → cis-DCE→ vinyl chloride → ethene) during exposure of different dilutions of Peterson AFB AFFF.

Peterson Bucket AFFF Inhibition of Aerobic BTEX biodegradation. Similar to the anaerobic inhibition experiments, we performed aerobic BTEX biodegradation inhibition experiments exposed to different concentrations of Peterson Bucket AFFF **(Figure 3.11**). The 1:1000 dilution

(~ 20 µM PFAS) slowed down the biodegradation of benzene, toluene, and o-xylene compared to the control. The higher concentrations (1:100 dilution, 1:100 dilution + additional AmPr-FHxSA) also stalled the biodegradation of benzene and toluene. Overall, these findings suggest that BTEX biodegradation can be impacted by the presence of ECF AFFF.

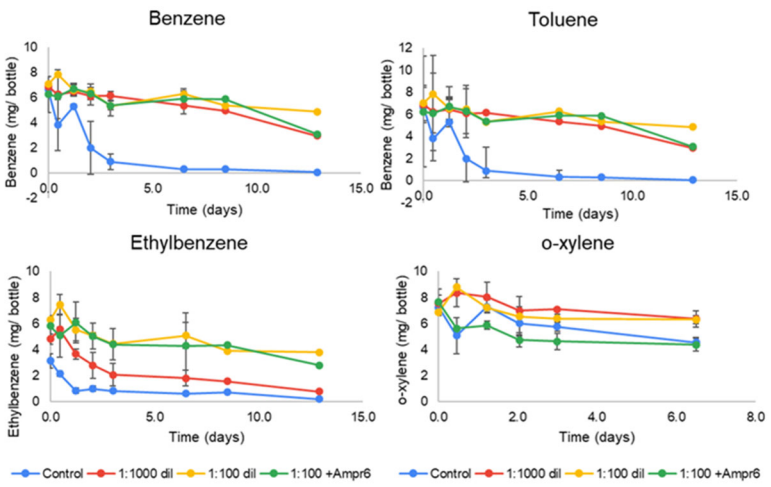

Figure 3.11 BTEX biodegradation in Peterson Bucket dilutions (red-1:1000; yellow 1:100; green 1:100 + additional AmPr-FHxSA)

Peterson Bucket AFFF Inhibition of Anaerobic BTEX biodegradation. Microbial incubations under anaerobic (denitrifying, sulfate-reducing) redox conditions were also performed. Saturated soil collected from a former AFB (Soil D) was characterized for water content (159.9±15.2% water/dry weight solids) and organic carbon content (9.3±1.8%). These solids were incubated (10% solids/liquid) in a mineral salts medium and 25 mM of nitrate or sulfate, for denitrifying and sulfate-reducing conditions, respectively. During the first week of incubation, no toluene was added to ensure labile organic matter was consumed with the electron acceptors. Then, 2.5 mM of toluene was supplemented to all bottles as the electron donor and carbon source. Toluene was replenished upon depletion to ensure continued biomass growth and toluene biodegradation. Upon continued successful toluene depletion, the incubations were transferred (5% inoculum into fresh anaerobic medium) to develop the enrichment.

We performed exposures of these enrichments to 1:100 (~200 µM PFAS) to 1:10000 (~2 µM PFAS) dilutions of Peterson AFB AFFF and compared to the controls (in triplicate). Surprisingly, toluene degradation for all cases tested did not inhibit toluene anaerobic degradation (**Figure 3.12**), which was strikingly an opposite finding to the aerobic case. DvH has been reported to develop biofilms composed of protein-based filaments,[56] which might also protect the coculture from any toxic effects of PFAS.

Overall, our findings with anaerobic and aerobic systems suggest that anaerobic microorganisms (TCE coculture, anaerobic BTEX biodegradation) are more tolerant of AFFF than the aerobic system (BTEX biodegradation). This could be attributed to fermentation of non-fluorinated organics in the formulation, such as DGBE. A second possibility that needs to be further studied is the production of extra polymeric substances that might shield the microorganisms from toxic compounds.

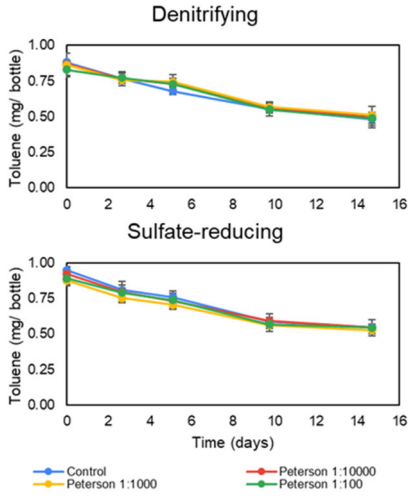

Figure 3.12 Anaerobic BTEX biodegradation under sulfate and denitrifying conditions in Peterson Bucket AFFF (red 1:10000 dilution – ~2 µM PFAS, yellow 1:1000 ~20 µM PFAS; green 1:100 dilution ~2 µM PFAS).

Task 3.3 ***Elucidate Impacts of Bioremediation Strategies on PFAS***

To study the inhibition of AmPr-FHxSA in context of its transformations products FHxSA and PFHxS, we performed microbial inhibition experiments with each of these PFAS species alone. We tested two co-contaminant microbial biodegradation systems: aerobic BTEX biodegradation with an enrichment developed from an AFFF-impacted site as well as an aerobic TCE dehalogenation coculture (195 + DvH).

Aerobic BTEX inhibition by AmPr-FHxSA, FHxSA, and PFHxS. We evaluated inhibition to aerobic BTEX biodegradation by the zwitterionic precursor AmPr-FHxSA and its transformation products: FHxSA and PFHxS (1 µM for all compounds). We also included a non-fluorinated surfactant, SDS, to compare general surfactant inhibition mechanisms with PFAS specific ones. The rates of degradation of BTEX in treatments containing PFAS were compared to the toxicant-free control. In addition, supernatant samples were taken for metabolomics analysis, based on Fiehn et al.[57] 0.5 mL of culture samples (pre-filtered 0.2 µm for extracellular metabolites) were extracted into cold isopropanol/acetonitrile (1:1.5:1.5 sample:isopropanol:acetonitrile), vortexed (20 min), centrifuged (2 min, 12800 g, 4 ºC), and the supernatant was transferred to a new vial. Samples were vacuum vortexed (5 hours, 30 ºC) and reconstituted with 200 µL (1:1 acetonitrile:water) and analyzed by LC-MS/MS based on a target list of metabolites.

At 1 µM there was no visible inhibition by AmPr-FHxSA and its transformation products FHxSA and PFHxS compared to the control (**Figure 3.13**). However, a 1:10000 dilution of Peterson AFB AFFF (~ 2µM PFAS) did slow down benzene, toluene, and o-xylene biodegradation. This suggests that the inhibition observed in the AFFF could not be attributed alone to AmPr-FHxSA or either of its transformation products, FHxSA and PFHxS. One possibility is that PFOS (the PFAS species with highest concentration in the Peterson Bucket AFFF), other PFAS in the mixture, and/or non-fluorinated surfactants. A second possibility is that the mix has synergistic inhibition effects that

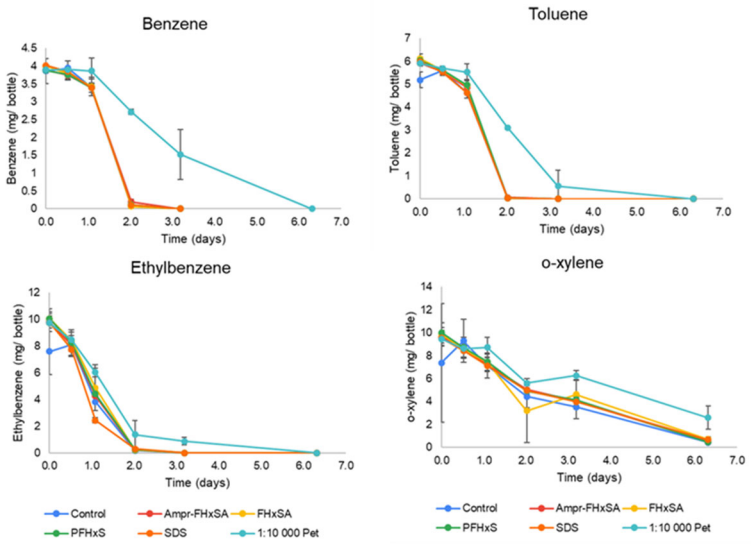

Figure 3.13 BTEX biodegradation by Peterson AFB enrichment exposed to PFAS (red Ampr-FHxSA, yellow FHxSA, green PFHxS) or SDS (orange) at 1 µM orange SDS and 1:10000 dilution of Peterson AFB Bucket AFFF.

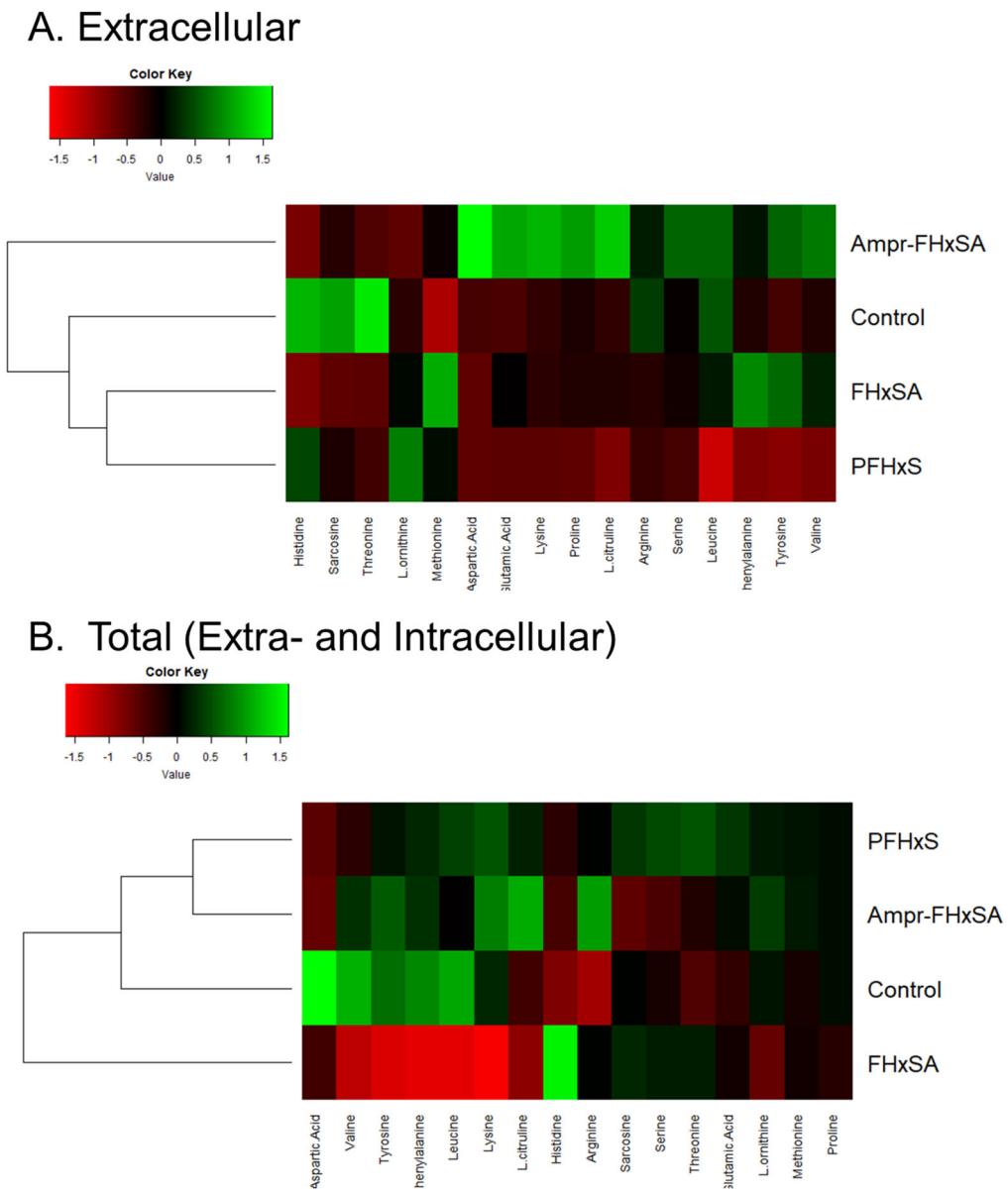

Figure 3.14 Aerobic BTEX biodegradation enrichment metabolite profile and clustering metabolite based on relative abundance. Signals are scaled based on standard deviation of the mean (n=3). Green -more abundance, red- less abundance.

are not expressed with each PFAS alone. Despite no inhibition based on biodegradation physiological data, there were differences in extracellular and total (extra- and intracellular) metabolite abundances between AmPr-FHxSA, FHxSA, and PFHxS treatments compared to the PFAS-free control (**Figure 3.14**). The AmPr-FHxSA treatment had a higher abundance of extracellular metabolomics compared the control and other PFAS, suggesting that it has surfactant properties that can make the cell membrane leaky, releasing these metabolites. This is supported by the metabolite profiles considering both extra- and intracellular metabolites. The zwitterionic nature of AmPr-FHxSA[3] may allow for different electrostatic interactions to disrupt the cell membrane and make the cell leak more of internal components. The control had the largest amount of total metabolites (**Figure 3.14B**) based on the number of metabolites with green color. Interestingly, FHxSA had the least abundance of metabolites (red color) and clusters further away from the rest of the treatments, suggesting an inhibitory interaction.

Anaerobic Dehalogenation inhibition by AmPr-FHxSA, FHxSA, and PFHxS. Previous anaerobic TCE inhibition experiments with Peterson AFB AFFF showed that the AFFF mixture had inhibitory effects due to AmPr-FHxSA as well as stimulatory effects from fermentable organics. To study the inhibition of AmPr-FHxSA, TCE dehalogenation experiments were performed with co-cultures exposed to AmPr-FHxSA and the inhibition potential compared to its transformation products, FHxSA and PFHxS. No complete inhibition of TCE dehalogenation was observed at this concentration, although the AmPr-FHxSA treatment had the slowest ethene formation rate of the three PFASs (**Figure 3.15**). Because of the physiological similarities between all exposures and the control, we analyzed the metabolomic profile of total (extra- and intracellular) metabolites (**Figure 3.16**). AmPr-FHxSA and FHxSA had the lowest abundance of metabolites, and PFHxS clustered with the control. This suggests that AmPr-FHxSA and FHxSA are more likely to cause an inhibitory interaction with the TCE dehalogenation co-culture. Unknown m/z 393 is suspected to be a lipid, which may be a biomarker of PFAS toxicity because it has very low concentrations in the controls. No extracellular metabolites were separately analyzed because of the low biomass concentration of the 195+DvH co-culture compared to the BTEX enrichment.

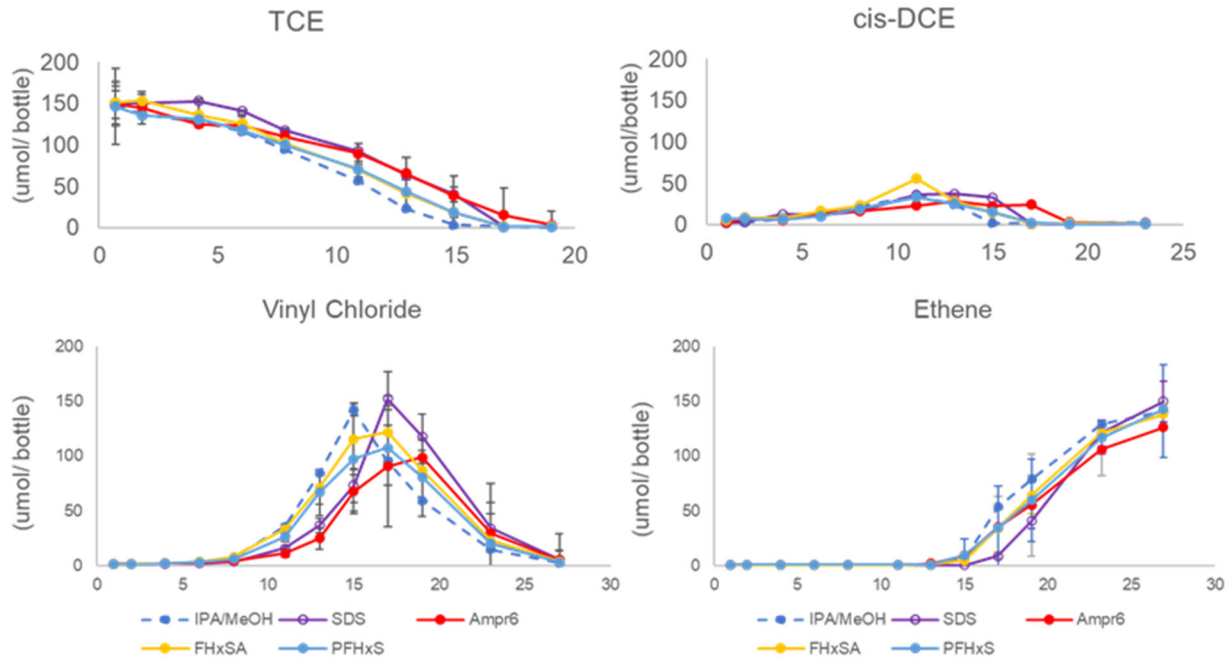

Figure 3.15 TCE dehalogenation (TCE→ cis-DCE → vinyl chloride → ethene) exposed to 1 µM of AmPr-FHxSA, FHxSA, PFHxS and the non-fluorinated surfactant SDS. IPA/MeOH is the control with just the solvent vehicle added (<1% total volume).

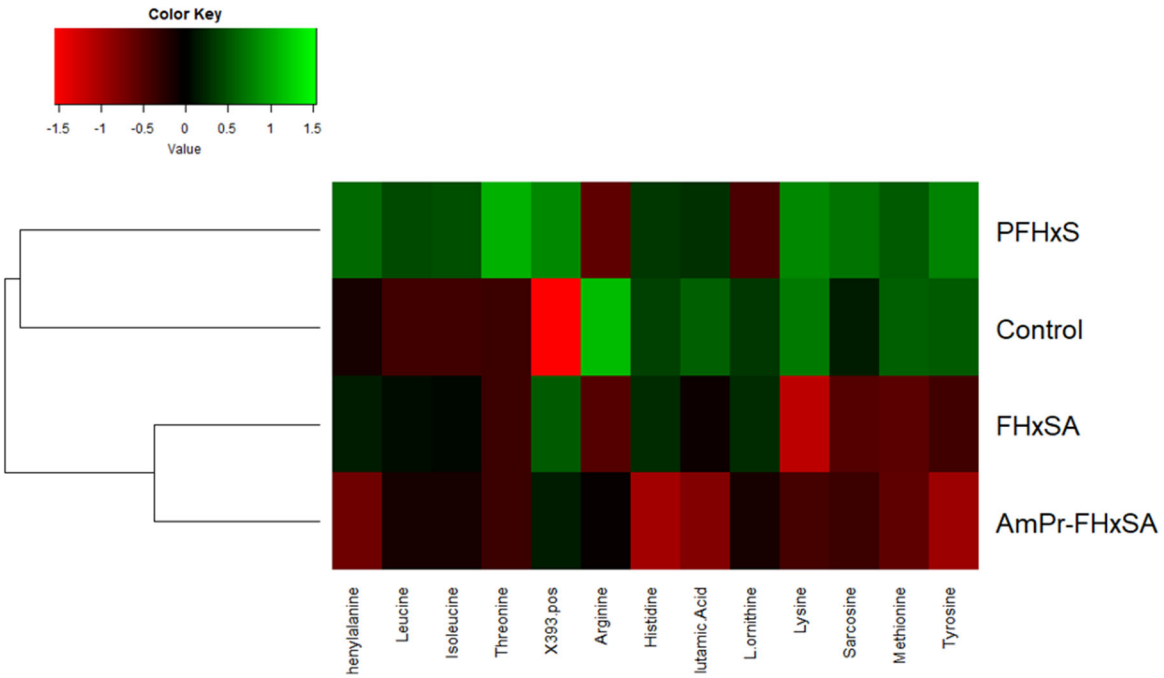

Figure 3.16 Anaerobic TCE dehalogenation co-culture metabolite profile and clustering metabolite based on relative abundance. Signals are scaled based on standard deviation of the mean (n=3). Green -more abundance, red- less abundance.

TASK 4. IMPACTS OF REMEDIAL ACTIVITIES ON PFAS RELEASES

Task 4.1 *Microbial Stimulation Experiments*

The objective of Task 4.1 was to stimulate biosparging of an AFFF-impacted soil to understand how remediation of co-contaminants such as BTEX can influence PFAS release and transformation. The setup of this experiment was based on Tasks 1.2 and 1.4 in which only AGW was pumped through the same soil (previously referred to as Soil B). Four glass columns (48 x 150 mm; Chromaflex, Kimble-Chase) with 20 µm HDPE bed supports were packed with dry soil approximately one cm at a time by tamping down and vortexing. To reduce residual air in the columns, packed columns were flushed with carbon dioxide for 30 minutes prior to starting water flow. A peristaltic pump with PharMed (Cole Parmer) tubing pumped AGW continuously into the bottom of each vertical column. AGW was adjusted to pH 7.00±0.10. Two columns received oxygen (O_2)-sparged AGW (DO>13 mg/L) and two columns received nitrogen (N_2)-sparged AGW (DO<3 mg/L). The O_2-sparged AGW contained monopotassium phosphate and ammonium chloride to encourage microbial growth, but concentrations were limited to prevent column clogging (AGW composition in **Table 4.1**). A syringe pump was used to pump a 420 mg/L toluene solution via four 10 mL gastight glass syringes (one per column). Syringes were refilled at least every five days with autoclaved DI water and toluene. The syringe pump contributed ~1% of the peristaltic pump rate into a union with the main AGW line prior to entering the column through a single piece of tubing. The total influent flow rate for each column was ~0.12 mL/min (~7 mL/hour) with a toluene concentration of approximately 4 mg/L. The first seven pore volumes (four days) of the experiment had no toluene addition nor sparging, after which toluene was added continuously except for when the syringes were being refilled. All tubing and fittings were PEEK.

Table 4.1. Components of the artificial groundwater solutions pumped through the columns

Compound	Concentration in AGW (mg/L)
$MnSO_4*H_2O$	2
Na_2SO_4	360
NaCl	226
$NaHCO_3$	80
KH_2PO_4	5
NH_4Cl	30

Columns were sampled continuously for the first 17 pore volumes (five-hour sampling duration) with an automated Arduino fractionator, then sampling frequency decreased with time. All samples for PFAS analysis were collected in 50 mL polypropylene centrifuge tubes and stored at -4°C until a few days prior to PFAS analysis and thawed at 4°C prior to analysis. Influent and effluent samples for toluene analysis were collected once per week directly in GC vials by placing the influent or effluent tubing through a pierced septum to minimize volatile losses. Toluene was analyzed by headspace GC-MS (Trace 1310 GC coupled with TSQ 8000 Evo MS/MS and TriPlus RSH autosampler, Thermo Fisher Scientific) using a method based on Cao et al.[58] DO and pH measurements were taken at least once per week in a N_2-sparged centrifuge tube sealed with parafilm. Due to the slow flow rates, effluents were collected for approximately one hour to obtain sufficient volume for the DO and pH probes.

After 130 pore volumes (2 months after flow start), the N_2-sparged columns started to clog due to presumed iron sulfide precipitation. The majority of sulfate was taken out of the AGW composition to prevent further clogging. Operation of Column N_2-sparged-1 was terminated at 136 pore volumes because of continued leaking. Operation of column N_2-sparged-2 was discontinued at

pore volume 196 due to leaking. O_2-sparged-1 and O_2-sparged-2 columns continued to flow until 278 and 253 pore volumes, respectively. After operation of both N_2-sparged columns was terminated, an aerobic BTEX-degrading enrichment culture developed from a different AFFF-impacted site was pumped into the two O_2-sparged columns. The enrichment culture contained negligible concentrations of PFAS compared to the concentrations present in the soils (<5 ng total PFAS added to each column). Once the experiment concluded, columns were taken apart, roughly sectioned from influent to effluent end, and the soil stored in 50 mL polypropylene centrifuge tubes at -4°C until analysis. The post-elution soils and the original soil were extracted and analyzed via the method in Nickerson et al.[1]

The mass of PFAS eluted per sample was calculated by the product of sample PFAS concentration and sample volume. The mass eluted between samples was estimated by the product of concentration means and estimated volumes (based on flow rates) in the preceding and following samples. Data were compared to unaltered column data from Task 1.2.

Results.

DO, pH, and toluene trends. The DO of the N_2-sparged column influents was 0.1-3 mg/L throughout the experiment. Influent DO of the O_2-sparged columns was at least 13 mg/L throughout the experiment and usually over 20 mg/L (DO meter only showed readings up to 20 mg/L). Influent DO varied slightly with time because the AGW solutions were typically sparged once per day. DO decreased in all column effluents once sparging and toluene addition began, and it remained between 0-3 mg/L until pore volume 196 (**Figure 4.1**). DO increased to 5 mg/L after the BTEX-degrading aerobic microbial enrichment was inoculated in the two O_2-sparged columns at pore volume 196. This rise in DO suggests that the inoculated microbial culture was not successfully established. Since the enrichment culture was developed from a different AFFF-impacted site (Soil A), it may have been sensitive to the high concentrations of PFOS in this soil. Moreover, effluent DO readings may be biased high due to the sampling limitations: sample containers were not perfectly sealed while collection was ongoing for approximately one hour. Effluent pH at the start of the experiment was 5.37-6.00 and remained near neutral (7.12±0.34) after the first 15 pore volumes.

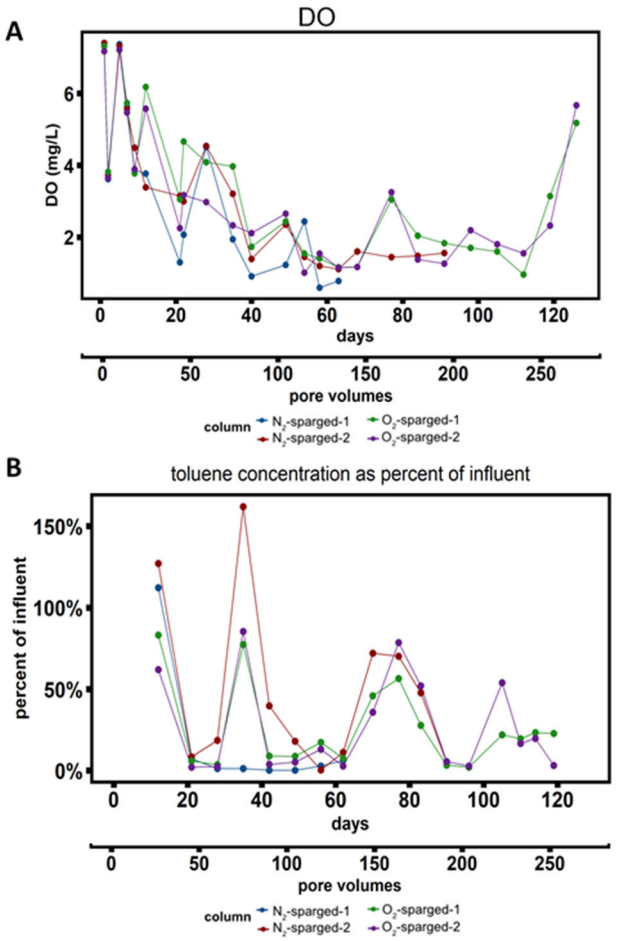

Figure 4.1 A) DO (mg/L) and B) toluene concentration as percent of influent toluene concentration for each column. Pore volumes are shown as a secondary x-axis; pore volume values are approximate because each column flowed at a slightly different rate.

The two N_2-sparged columns experienced intermittent leaking and clogging, and the soil near the effluent side turned nearly black, likely signifying biogenic iron sulfide. Cracks formed in the saturated soil with black precipitates evident near the effluent side of the N_2-sparged columns. Precipitation of iron sulfides confirmed reducing conditions within these columns.[59] When the columns were taken apart, a strong sulfide smell was also noted. All columns were confirmed to be microbially active by measuring adenosine triphosphate (ATP) of the column effluents two months after start of flow (**Table 4.2**).

Table 4.2. ATP measurements of column effluents two months after start of flow (~100 pore volumes).

Sample	ATP (pM)
N_2-sparged-1	13.61
N_2-sparged-2	10.35
O_2-sparged-1	3.45
O_2-sparged-2	3.43

Toluene concentrations undulated for both O_2-sparged columns and N_2-sparged-2, whereas the concentration of toluene remained low (<10% of influent concentration) in N_2-sparged-1 after the initial decrease (**Figure 4.1B**). Toluene degradation in the N_2-sparged columns was not intentionally stimulated, but reducing conditions may have encouraged toluene degradation via the anaerobic pathway,[60] especially since anaerobic toluene degradation and sulfate-reduction can be coupled.[61] The microbial communities in this soil that were not inhibited by high PFAS concentrations may have been more capable of anaerobic degradation. Since redox conditions were not uniform throughout the columns and some oxygen may have been present (up to 3 mg/L DO), toluene may have been degraded by both aerobic and anaerobic processes in the N_2-sparged columns at different temporal and spatial points. Despite undulating toluene concentrations, the O_2-sparged columns showed decreased toluene at most sampling times, demonstrating that the conditions within the columns were representative of aerobic biosparging. No significant change in toluene concentration was observed after addition of an aerobic BTEX-degrading enrichment culture at pore volume 196. High PFOS concentrations may have inhibited the culture that was developed from Soil A with much lower PFOS concentrations.

Higher concentrations of some PFASs eluted from O_2-sparged columns. When the elution profiles are compared between the O_2-sparged and N_2-sparged columns, 14 PFASs eluted at higher concentrations from the O_2-sparged columns around pore volumes 11-20 (days 5-10; examples provided in **Figure 4.2**). This was shortly after the introduction of toluene and the beginning of sparging at pore volume 7 (day 4). The increase in concentration of many PFASs in the O_2-sparged

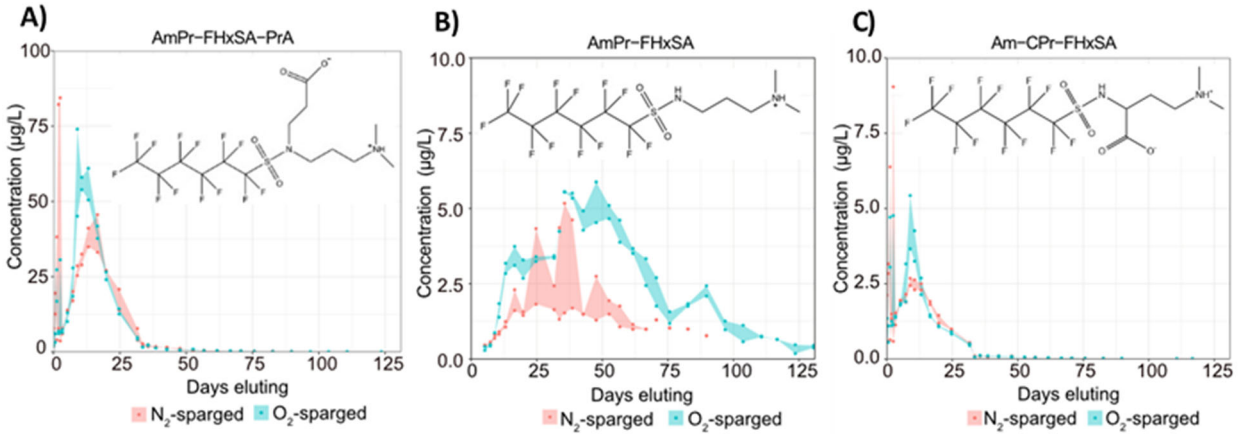

Figure 4.2 Concentrations of three zwitterionic PFASs vs days eluting for N_2-sparged (red) and O_2-sparged (blue) columns: (A) AmPr-FHxSA-PrA, (B) AmPr-FHxSA, (C) Am-CPr-FHxSA. Ribbons depict the minimum and maximum concentration of the two O_2-sparged or N_2-sparged columns at each time point.

column effluents at this time suggests that sparging with oxygen increased the release of these PFASs. This pattern was observed for zwitterions such as N-dimethylammoniopropyl-perfluorohexane sulfonamide (AmPr-FHxSA), N-dimethylammoniocarboxypropyl-perfluorohexane sulfonamide (Am-CPr-FHxSA), and AmPr-FHxSA-PrA, as well as other homologs of these compounds (**Figure 4.2**). These three zwitterions account for about 10% of the C6 mass; although they were not the highest concentration compounds in this soil, they were significant enough that altered release from the soil could be important in a field setting. Two anionic fluorotelomer PFASs, 8:2 FTS and 8:2 FTSO2PrAd-DiMeEtS, also had increases in effluent concentrations at similar times (**Figure 4.3**). Other PFAS with the same elution pattern included FHxSA, N-trimethyl ammoniopropyl perfluorobutane sulfonamido propanoic acid (TAmPr-FBSAPrA), N-trimethyl ammoniopropyl perfluorobutane sulfonamide (TAmPr-FBSA), 6:2 FTSA-PrB, and other homologs of these classes. The increased concentration of FHxSA eluting from the O_2-sparged columns is particularly important because this compound makes up a large percentage of the overall mass (38% of C6 mass) and may be a transformation product of other sulfonamide-based structures. The reason for the spike in N_2-sparged concentrations around

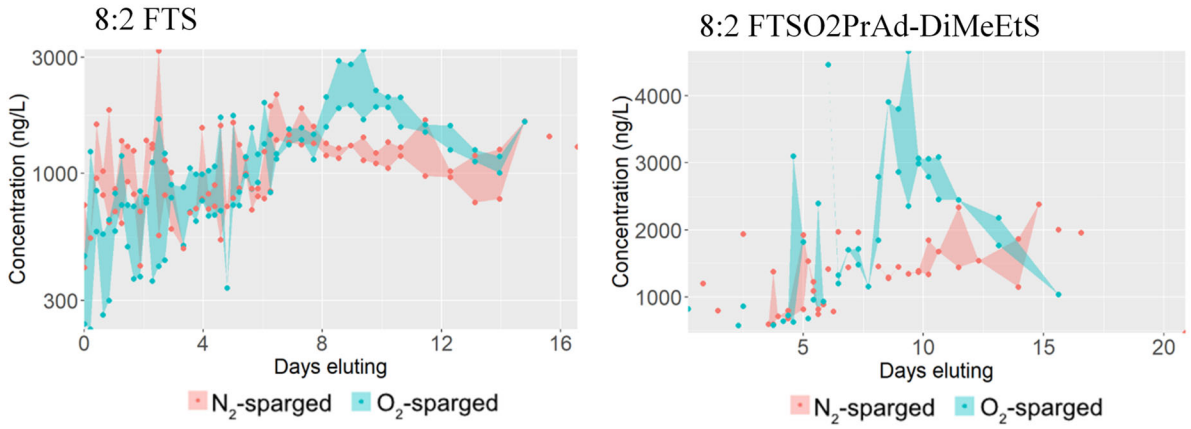

Figure 4.3 Ribbon plots of 8:2 FTS and 8:2 FTSO2PrAd-DiMeEtS concentrations (ng/L) vs days eluting for N_2-sparged and O_2-sparged columns.

pore volume 3-4 (day 2) remains unclear; it cannot be attributed to changes in redox conditions or the presence of co-contaminants, since this was prior to the start of sparging.

Fraction eluted of original soil PFAS mass. The fraction of PFAS mass eluted from each column was calculated by the cumulative mass eluted in water divided by the original mass of each PFAS in soil. Fractions eluted are only indicative of mass eluted in the aqueous phase, not the total mass balance – total mass balances including mass on post-elution soil will be discussed in a subsequent section. Since the O_2-sparged columns ran for longer than the N_2-sparged and unaltered columns, only data up to pore volume 196 were used in this comparison.

The fraction eluted of PFCAs and PFSAs were similar between all three sets of columns (**Figure 4.4A-C**). Even after 250+ pore volumes, the data suggest that a portion of long chain PFSAs remained on the soil. A maximum of 64% and 24% of PFOS and PFNS eluted, respectively, while PFDS and PFDoS were not detected in any column effluent samples. PFASs present at relatively low concentrations in the original soil, such as these long chain PFSAs, may not have been measurable in water effluents due to the high sample dilution factor and resulting high LOQs. For

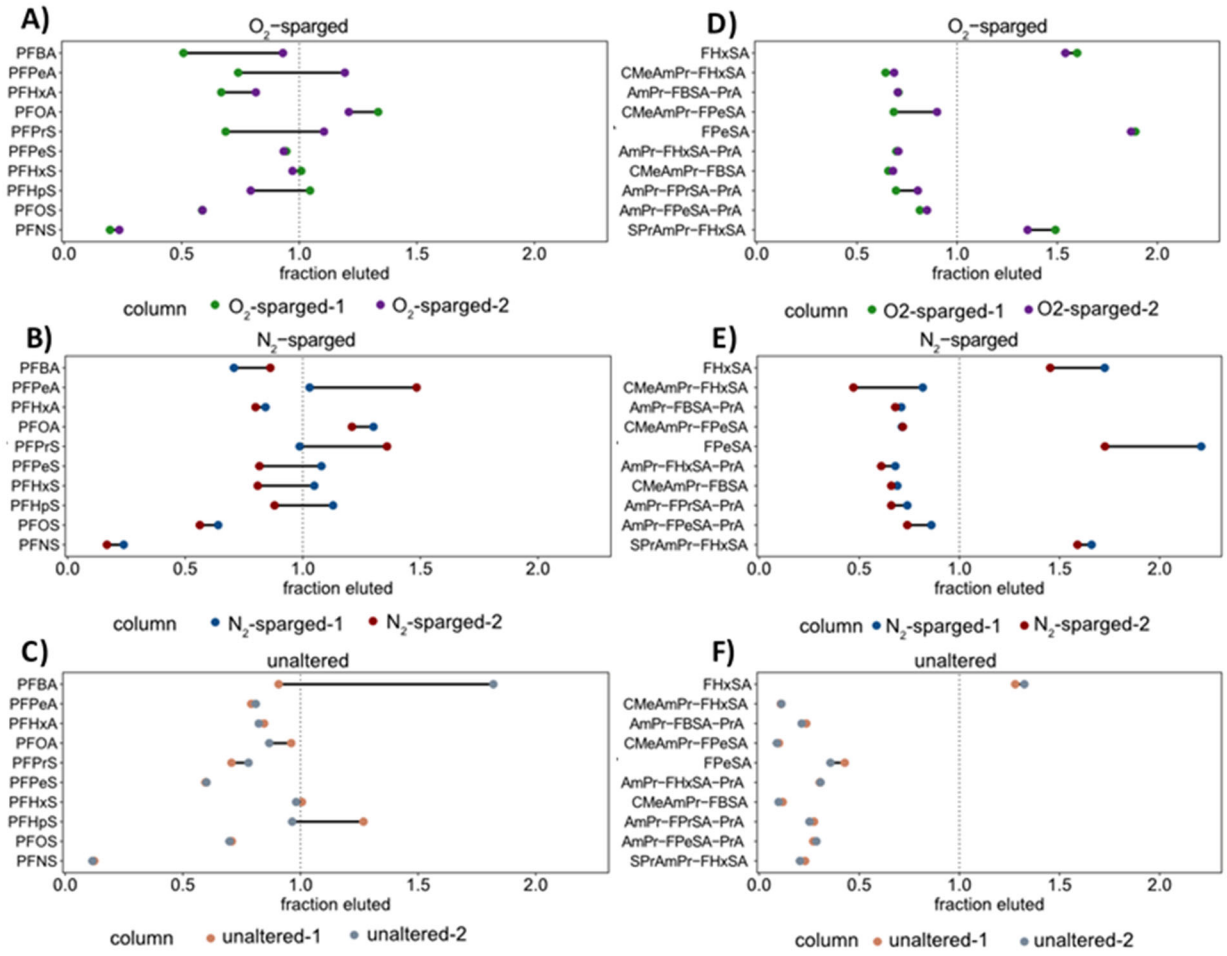

Figure 4.4 Mass fraction eluted of (A-C) PFCAs and PFSAs and (D-F) the top ten concentration PFASs other than PFCAs and PFSAs for the O_2-sparged, N_2-sparged, and unaltered columns. Compounds in D-F are shown in highest to lowest concentration order. Data for unaltered columns from Task 1.2. The range of values is shown for each column pair.

example, when the LOQs of PFDS were used to estimate the mass eluted at this concentration, the theoretical mass eluted accounted for the original mass on the soil.

The other top ten highest concentration compounds (**Figure 4.4D-F**) showed greater differences in elution between the biologically active columns compared to the unaltered columns. All ten of these ECF-sulfonamide PFASs eluted at a higher fraction under both N_2-sparging and O_2-sparging compared to the unaltered, non-biologically active conditions. About 20% more of the initial FHxSA mass eluted from the sparged columns compared to the unaltered columns. This difference was even greater for the shorter-chained FASAs: ~8x more FPrSA, ~5x more FBSA, and ~5x more FPeSA. These differences may be indicative of biological transformation, as the soil contained many potential precursors to FASAs. Since the fractions eluted of all the aforementioned FASAs were greater than one, this further suggests that transformation of precursors (as opposed to enhanced desorption/elution) was at least partially responsible. An average of 235% of the original soil mass eluted for FPrSA, 163% for FBSA, 192% for FPeSA, and 158% for FHxSA. Many of the zwitterionic compounds in this soil could be precursors to FASAs based on their structures: for example, N-carboxyethyldimethyl ammoniopropyl-N-ethyl perfluoroalkane sulfonamide (CEtAmPr-N-EtFASA) and CMeAmPr-FASA.

The only compounds with less mass eluted from the biologically active columns compared with the unaltered columns were PFBA and FOSA. The large variability between the two PFBA values in the unaltered columns may be the reason for this discrepancy. For FOSA, over 80% of the mass eluted in the unaltered columns compared to <30% in the biologically active columns. It is unclear why a higher fraction eluted from the unaltered columns while the opposite was true for all other FASA homologs.

Despite the similarities seen in **Figure 4.4** between the O_2-sparged and N_2-sparged columns, there were specific PFASs for which higher cumulative masses eluted from the O_2-sparged columns than the N_2-sparged columns. The difference between the two sets of columns was greatest for zwitterionic PFASs AmPr-FHxSA, N-hydroxyethyldimethyl ammoniopropyl perfluorohexanesulfonamide (EtOH-AmPr-FHxSA), and TAmPr-FHxSA (**Figure 4.5**). The ratios of the average O_2-sparged masses eluted over the average N_2-sparged masses eluted are 2.0, 2.9, and 2.5 for the three PFASs, respectively, when data are limited to the shorter experimental duration of the N_2-sparged columns. Since the O_2-sparged columns ran longer than the N_2-sparged columns, even more mass eluted by the end of the experiment (up to 50% additional mass). These three zwitterions made up a small proportion of the overall mass (<10% of the C6 mass). When PFAS mass eluted was summed by class or chain length, no major differences were apparent between the O_2-sparged and N_2-sparged columns. The difference in redox conditions and microbial activity seem to affect specific PFASs, most prominently the zwitterionic ECF-sulfonamides. Different geochemical conditions resulting from the differences in redox may play a role in the additional release of these zwitterionic PFASs.

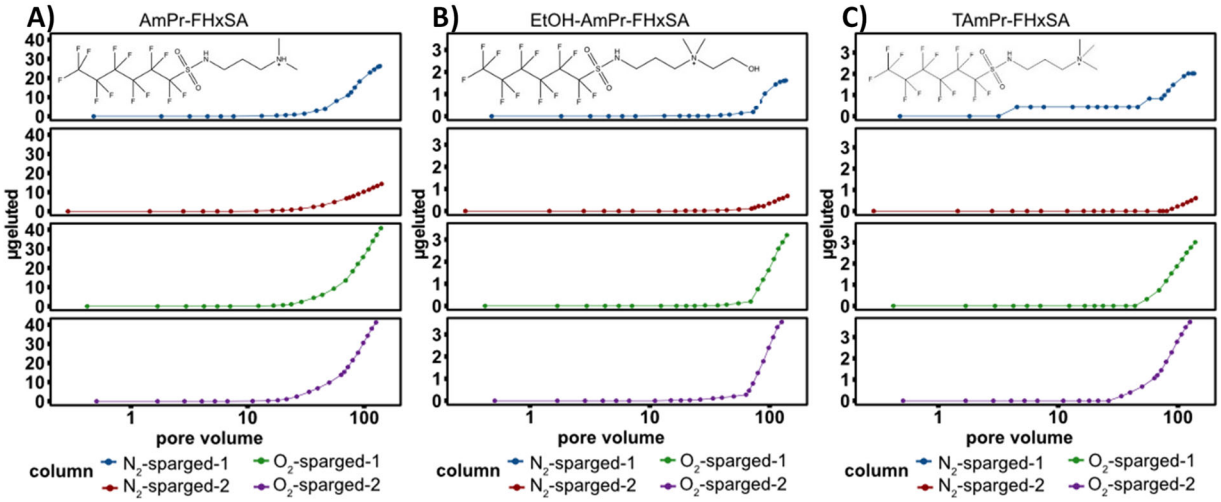

Figure 4.5 Cumulative mass eluted (µg) vs pore volume for three zwitterionic PFASs: A) AmPr-FHxSA, B) EtOH-AmPr-FHxSA, C) TAmPr-FHxSA. Data are only shown up to the pore volume at which the first column (N_2-sparged-1) clogged.

PFAS remaining on post-elution soils. Despite the long elution times, some PFAS mass remained on all column soils at the conclusion of the experiment. The PFAS concentrations on these post-elution soils were generally higher at the effluent end of the column than the influent end (**Figure 4.6**). This pattern was more consistent and prominent for the N_2-sparged columns. The ratios of total PFAA concentrations between the section closest to the effluent and the section closest to the influent were 2.0, 3.5, 2.1, and 1.4 for columns N_2-sparged-1, N_2-sparged-2, O_2-sparged-1, O_2-sparged-2, respectively. The concentrations remaining on the soil were also lower for the O_2-

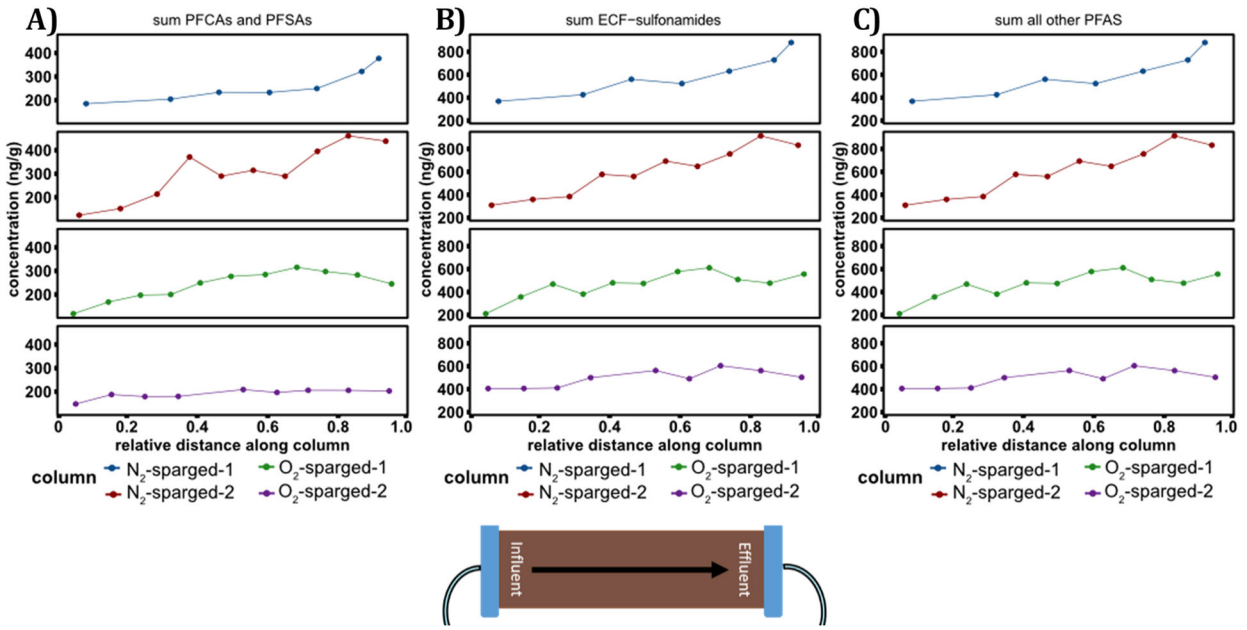

Figure 4.6 Concentration profiles (ng/g) along the soil columns analyzed post-elution: A) Sum of PFCAs and PFSAs, B) sum of all ECF-sulfonamides, C) sum of all other PFAS. Distance of 0 along the x-axis corresponds to the influent side of each column and distance of 1 corresponds to the effluent side of each column. Distances along x-axis are approximate based on the soil weight of each section.

sparged columns. The ratios of total ECF-sulfonamides between effluent and influent were 2.4, 2.7, 2.6, 1.2 and the ratios of total other PFASs were 2.3, 3.0, 2.5, and 1.3 for the two N_2 and two O_2-sparged columns, respectively. Column N_2-sparged-2 consistently had the highest concentration ratios and column O_2-sparged-2 generally had the lowest. Concentration differences were typically higher for longer-chain PFASs than shorter-chain PFASs. The greater concentration differences along the N_2-sparged columns may be due to preferential flow paths caused by clogged pores under reducing conditions. Altered flows due to clogged pores may decrease desorption and subsequent elution of PFASs from soils, particularly for the longer chain, stronger sorbing species. These heterogeneities are likely present under environmental subsurface conditions as well. The difference in experimental run times may also contribute to the lower concentrations remaining on O_2-sparged column soils.

PFAS mass balance. To assess transformation potential, mass balances were determined by comparing the sum of PFAS mass eluted in water and mass remaining on the post-elution soils to the PFAS mass initially present in each column. The results show that multiple PFAS classes have a large percentage of their mass unaccounted for and a few PFASs have additional mass produced. The major differences in mass eluted between the N_2-sparged and O_2-sparged columns were discussed previously; most inferred transformations discussed here were noted in both N_2-sparged and O_2-sparged columns. The mass balance for PFOA was 140-155% of the original soil mass across all columns, possibly due to transformation of precursors (discussed further below). The mass balance of PFOS was 58-66% of the original mass; the low recovery may be attributed to losses during sample preparation, since aliquots of the water samples were diluted directly from the original centrifuge tube to autosampler vials. The incomplete mass balance of PFOS may also be explained by the high concentrations (>5 times higher than all other PFASs) and subsequent

high dilution factors; any low bias in the PFOS analysis, such as losses during sample preparation, would therefore result in a large underestimation of PFAS mass recovered. The same effect likely affected other long chain PFSAs such as PFNS and PFDS, which are unlikely to transform but are more susceptible to losses during sample preparation due to their longer chain lengths.

More mass of all ≤C6 FASAs eluted in the water than was originally present in soil. The mass of perfluorohexane sulfonamide propionate (FHxSA-PrA) post-elution was also greater than the original mass by 144-181%. FHxSA-PrA is a structural isomer of N-methylperfluorohexane sulfonamido acetic acid (MeFHxSAA); insufficient fragmentation was obtained for a conclusive identification, but the observed fragments matched those reported in Liu et al. as "Compound #8".[51] Liu et al. reported this compound as a potential transformation product of a sulfonamido betaine structure. FHxSA-PrA and its homologs could be part of the same transformation pathways leading to FASA formation. Structures of these isomers, observed extracted ion chromatograms, and MS/MS fragmentation are shown in **Figure 4.7**. Further research will be needed to confirm whether these isomers are abundant at AFFF-impacted sites.

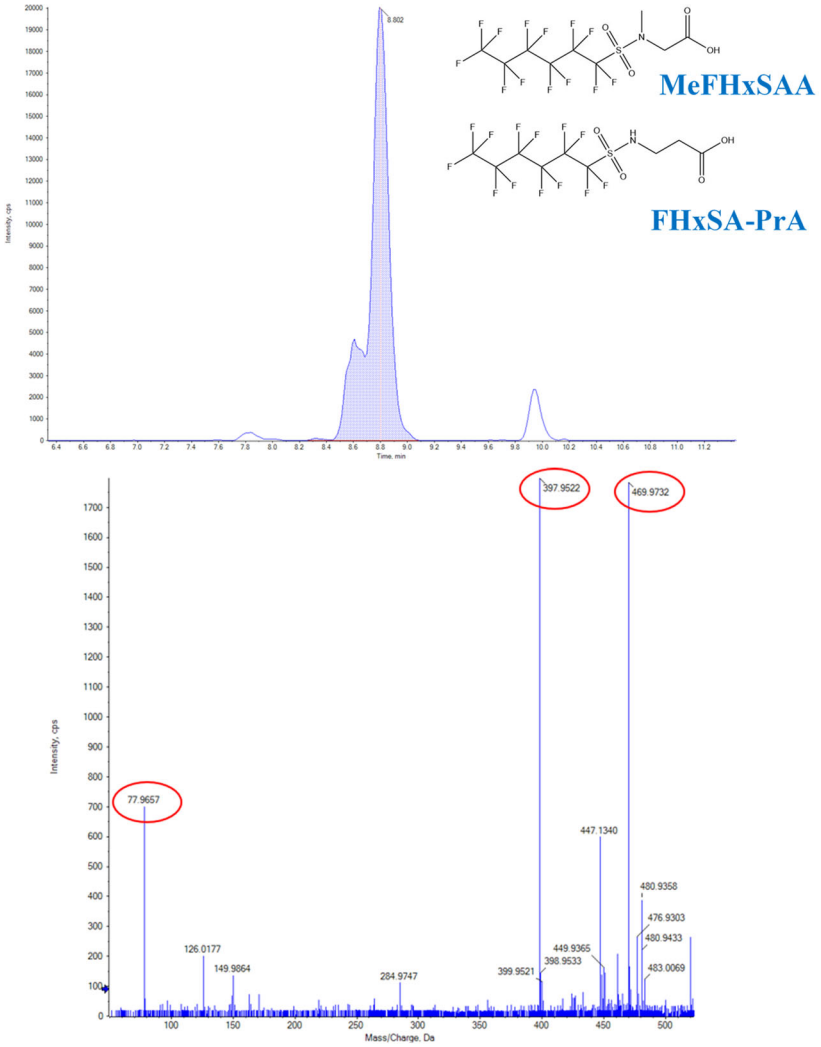

Figure 4.7 Chromatogram and MS/MS spectra of suspected FHxSA-PrA, with fragments matching those in Liu et al. circled in red. Similar fragmentation was observed for other chain lengths as well. Structures are shown for FHxSA-PrA and its isomer, MeFHxSAA.

N-sulfopropyl dimethylammoniopropyl perfluorohexanesulfonamide (SPrAmPr-FHxSA) had the highest over recovery of any zwitterion—135-166% of the original mass. Am-CPr-FPeSA had 118-147% of the original mass recovered, but the C6 homolog was around 100%. A compound with low recovery was 8:2 $FTSO_2PrAd$-DiMeEtS, (29-49% mass recovered) which is aerobically transformed by a pathway described in Weiner et al.[62] Based on the soil extraction recoveries in Nickerson et al.,[1] 8:2 $FTSO_2PrAd$-DiMeEtS could be produced during soil extraction from the degradation of 8:2 fluorotelomer thiapropanoamido dimethylethylsulfonate (8:2 FTTh-PrAd-DiMeEtS, aka 8:2 FtTAoS in Harding-Marjanovic et al. and 8:2 FTSAS in Weiner et al.)[54,62].

However, the consistent presence of 8:2 $FTSO_2PrAd$-DiMeEtS in effluents, which were analyzed without any extraction process, suggests that it is truly the oxygenated version that was originally present. Further, there were no detections of the precursor 8:2 FTTh-PrAd-DiMeEtS in water nor soil. As this surface soil experienced prolonged exposure to air in the field, the aerobic conversion of this precursor may have occurred prior to collection of the soil. Further biotransformation products of 8:2 $FTSO_2PrAd$-DiMeEtS include 8:2 FTS, shorter chain PFCAs, and potentially 8:2 unsaturated fluorotelomer carboxylic acid and 7:3 fluorotelomer carboxylic acid.[54,62] 6:2 $FTSO_2PrAd$-DiMeEtS was also detected in water at lower concentrations but not in soil. While there were many other instances of PFASs detected in water but not in the original soil, the high dilution factor of the soil samples precludes attributing these to transformation.

Mass balance calculations suggest that many zwitterionic PFASs were potentially transformed. The fractions of mass recovered for all detected C6 PFASs are shown in **Figure 4.8**. Low recoveries of multiple C6 zwitterionic PFASs were observed, of particular note CMeAmPr-FHxSA and N-carboxyethyldimethyl ammoniopropyl perfluorohexanesulfonamide (CEtAmPr-FHxSA) which together make up 42% of the total C6 concentration. The other homologs of CMeAmPr-FHxSA also had low recoveries: C4, C5, C7, and C8 homologs had recoveries of 67-72%, 54-73%, 16-32% and 33-53%, respectively. The C7 and C8 homologs were at the lowest concentrations in the original soil; therefore, their lower recoveries may also be due to dilution.

CEtAmPr-FASA and its isomer, AmPr-FASA-PrA, were both present in the original soil (**Figure 4.9**) but appear to have differing release and transformation. A fluorotelomer-derived isomer of these compounds is also possible but the presence of many odd numbered homologs indicated that these features were ECF-derived. Multiple chain lengths of AmPr-FASA-PrA were detected in water samples, whereas the CEtAmPr-FASA class was not detected in any water samples. Despite no elution, only 8-24% of the CEtAmPr-FASA mass remained on the soil at the end of the experiment. This suggests more extensive transformation of these isomers than the AmPr-FASA-PrA class despite their structural similarities. The placement of the propyl carboxylate group may have significant impacts on the reactivity: the isomer with the terminal amine appears less reactive than the isomer with the terminal carboxylate. Slow degradation of terminal amines among polyfluorinated substances has been noted in Mejia-Avendaño et al., where an amine intermediate was the rate-limiting step in the biotransformation of TAmPr-FOSA (aka PFOSAmS).[63]

The structural similarities between the classes with lower recoveries (CEtAmPr-N-EtFASA, CMeAmPr-FASA, EtOH-AmPr-FASA, and CEtAmPr-FASA) suggest that PFASs without terminal amines are more susceptible to transformation than comparable structures containing terminal amines (e.g. AmPr-FASA, AmPr-FASA-PrA). Mass balances of AmPr-FASA and AmPr-FASA-PrA were closer to 100%, with the lowest recovery for AmPr-FHxSA-PrA in N_2-sparged columns (63-69%; **Figure 4.8**). EtOH-AmPr-FHxSA, one of the zwitterions that had a higher mass eluted from the O_2-sparged columns than the N_2-sparged columns (**Figure 4.5**), had a mass balance of 66% in the N_2-sparged columns and 124% in the O_2-sparged columns (**Figure 4.8**). This difference may be due to transformation under anaerobic conditions, formation under aerobic conditions, or both.

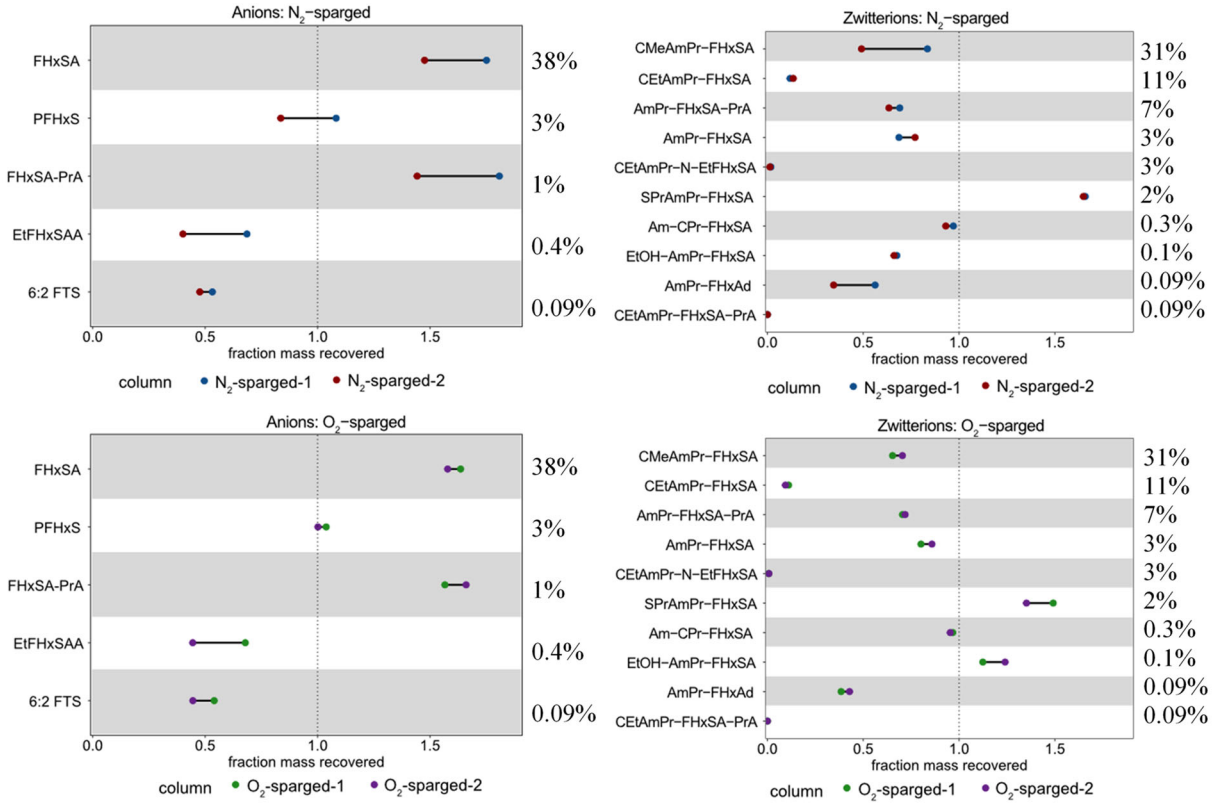

Figure 4.8 Fraction of mass recovered for all C6 anions and zwitterions. The percent concentration of each compound as a total of the C6 PFAS concentration in the original soil is listed alongside each pair of data points, and compounds are shown in order of decreasing contribution from top to bottom.

The substantial over-recoveries of most FASAs in the mass balance, along with the high number and concentrations of PFASs with complex ECF-sulfonamide structures, suggests FASAs may be among stable intermediate products of such transformations pathways. One of the few studies that attempted to quantify transformation rates of such ECF-sulfonamides was Mejia-Avendaño et al., but the very slow kinetics of TAmPr-FOSA transformation could not be determined during six month aerobic soil microcosms. While TAmPr-FOSA was very slowly transformed to PFOS (0.3 mol% of the initial mass by the end of six months), amide-based precursors were more readily transformed: by the end of 6 months, the concentration of PFOA increased to 30 mol % of the original PFOAAmS dosed.[63] N-dimethylammoniopropyl perfluoroalkane amide (AmPr-FAAd) is closely related to PFOAAmS and was present in this soil at low concentrations (e.g., 12.7 ng/g AmPr-FOAd). There was evidence of transformation of this precursor class in both sets of columns, with only 18-23% of AmPr-FOAd accounted for in the mass balance, as well as only 9-14% of AmPr-FHpAd and 35-56% of AmPr-FHxAd (**Figure 4.8**). Over-recovery of PFOA, a possible transformation product of AmPr-FOAd, was observed (140-155%); although transformation of AmPr-FOAd would not account for the entire mass of PFOA formed, it's possible there were other amide-based precursors in the soil that were not detected. Considering the high concentrations of PFSAs and low concentrations of PFCA precursors initially present in this soil, it is not surprising that large increases in PFSA or PFCA mass were not observed on the timescale of a few months. Therefore, these results cannot provide direct evidence for the

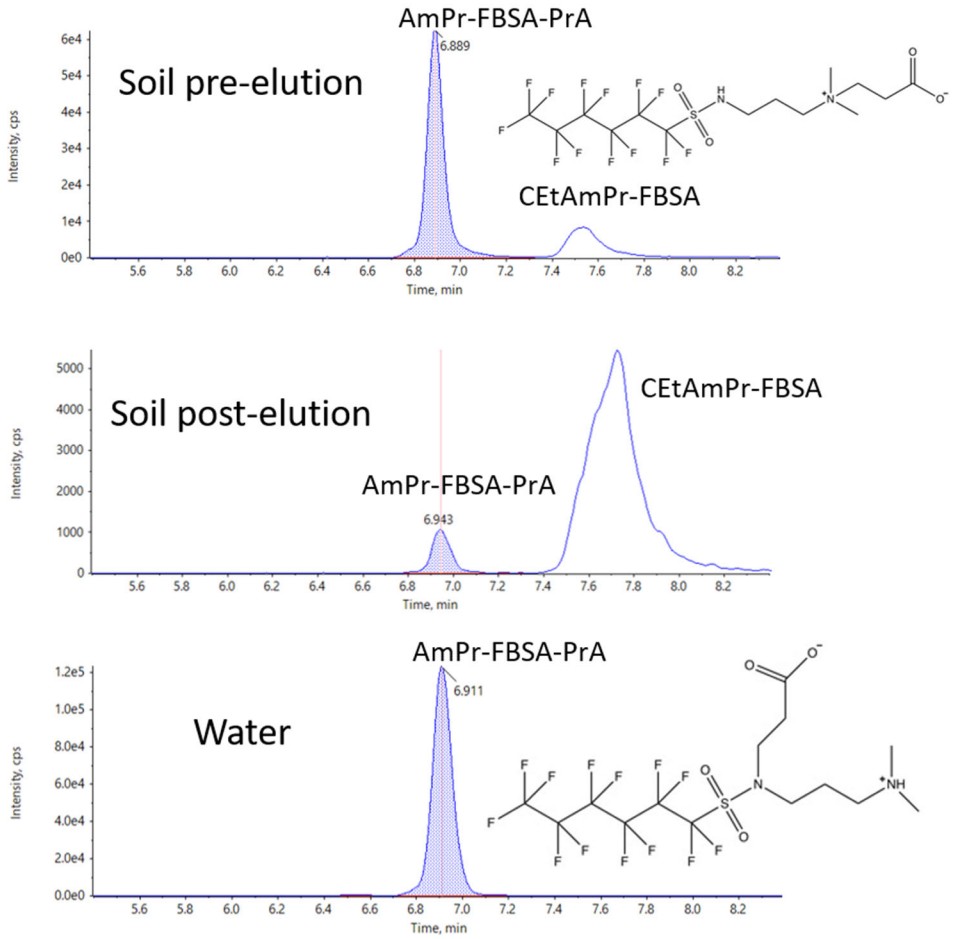

Figure 4.9 Extracted ion chromatograms of AmPr-FBSA-PrA and CEtAmPr-FBSA isomers. AmPr-FBSA-PrA was present in water effluents while CEtAmPr-FBSA was not. AmPr-FBSA-PrA identification was confirmed by MS/MS library matching.

hypothesis in McGuire et al. that conversion of ECF-derived precursors leads to substantial increases in PFSA mass.[64]

Task 4.2 *ISCO Experiments*

This subtask evaluated the effect of TCE *in-situ* chemical oxidation on the release of PFASs present in AFFF-impacted soils (**Figure 4.10**). Packed soil columns were prepared as for Tasks 1.2,1.4, and 4.1 column experiments: Kontes Chromaflex chromatography columns (4.8 x 15cm) were packed with Soil B that had previously been identified as containing anionic, zwitterionic and cationic PFASs.

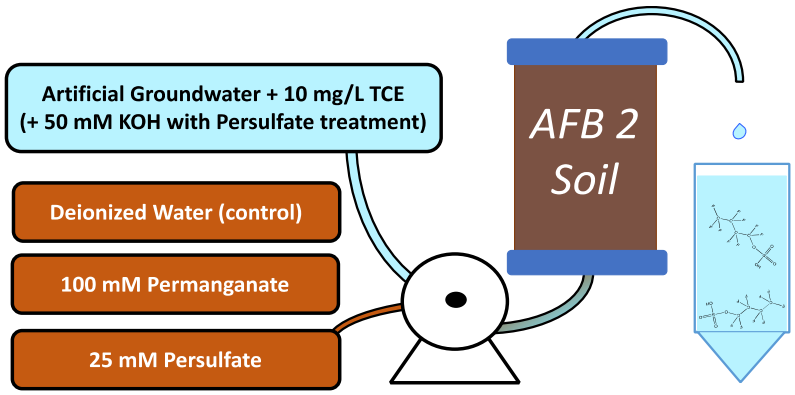

Figure 4.10 Schematic of Task 4.2 column experiments.

Control columns were exposed to pH 7 AGW and 10 mg/L TCE, which was pumped through the columns at ~ 2 pore volumes per day for 95 days. "Permanganate columns" were exposed to pH 7 AGW with 10 mg/L TCE for seven days, when 16 g / L potassium permanganate (~0.1 M $KMnO_4$) was added. The columns were run until they clogged 20 days later. Finally, "persulfate columns" were exposed to pH 7 AGW with 10 mg/L TCE for seven days, when 2.8 g/L potassium hydroxide (0.05 M) and 6.75 g/L potassium persulfate (~0.025 M) was also added. The column ran for an additional 60 days following the addition of basic potassium sulfate. The persulfate columns had initially been attempted with simulated ISCO derived from the addition of 20 g/L sodium hydroxide and 60 g/L potassium persulfate, however these columns clogged almost immediately. It was suspected that the high sodium concentrations caused the soils to swell, which increased the pressure inside the column until the pumps were unable to overcome the pressure. The persulfate columns were successfully restarted with lower concentrations of potassium persulfate and potassium hydroxide.

The column effluents were collected with a fraction collector for PFAS analysis by both ESI- and ESI+ QTOF-MS, as well as for TCE analysis by headspace GC-MS/MS. Persulfate and permanganate concentrations in the column effluents were determined by competitive titration of a ferrous ammonium sulfate solution with potassium permanganate. Finally, column effluent pH was monitored with an ion-selective electrode.

Results.

TCE concentrations were measured in the column effluents for the control columns and the columns treated with $KMnO_4$ (**Figure 4.11**). TCE was detected in control column effluents after 15 days but was never detected in the $KMnO_4$ column effluents. This indicates that TCE degradation is occurring in the $KMnO_4$–treated columns and that the experimental conditions are relevant to the environmental in-situ chemical oxidation of TCE by $KMnO_4$.

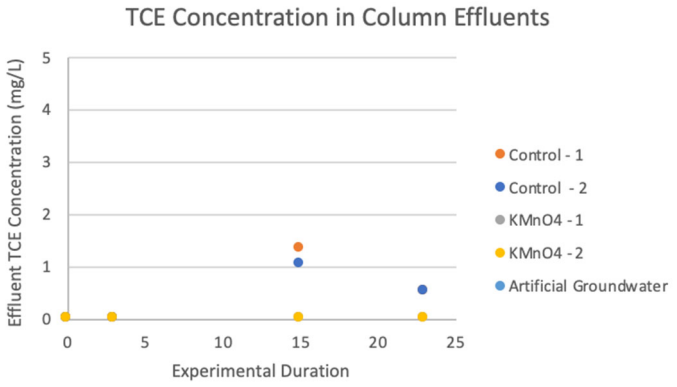

Figure 4.11 TCE effluent concentration in column effluents from duplicate control columns (Control – 1, -2) and columns treated with KMnO4 (KMnO4 -1, -2). The markers for control column effluent concentrations overlap for the sampling conducted at 23 d.

Effluent pHs were similar between replicate control, permanganate, and persulfate columns (**Figure 4.12**). This indicates similar temporal variation in column chemistry between replicate columns over the experimental durations. Effluent pHs of control columns and permanganate columns started near 5 and increased over the first 10 pore volumes until the effluent pH was ~8. For the permanganate columns, addition of permanganate occurred after 7 days and at this point in both permanganate columns there was a transient drop in pH. The persulfate columns appear similar in effluent pH to the control and permanganate columns for the first seven days, when the influent pH increased to 12.6 with potassium hydroxide and 6.75 g/L potassium persulfate addition. Following the addition of KOH and KS_2O_8, the effluent pH dropped to below 4 and then

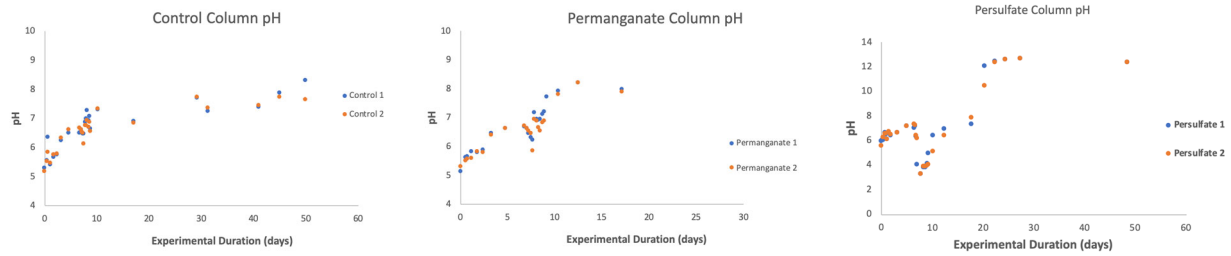

Figure 4.12 Column effluent pH over the experimental duration for control columns (left), permanganate columns (center) and persulfate columns (right), for the permanganate and persulfate columns, ISCO addition began at 7 d.

increased over 15 days to match the influent pH. A similar, sudden decrease in effluent pH was observed in experiments evaluating the influence of high ionic strength and pH on PFAS mobility.

The changes in effluent pH observed in the persulfate columns corresponded with changes in the effluent color (**Figure 4.13**). Initially, the persulfate column effluents were similar in color to the effluent from the control and permanganate columns. However, with the addition of KOH and KS_2O_8, the effluent initially became less yellow in color before slowly turning a very dark brown. This color progression could indicate a positive correlation between soil organic matter solubility and solution pH.

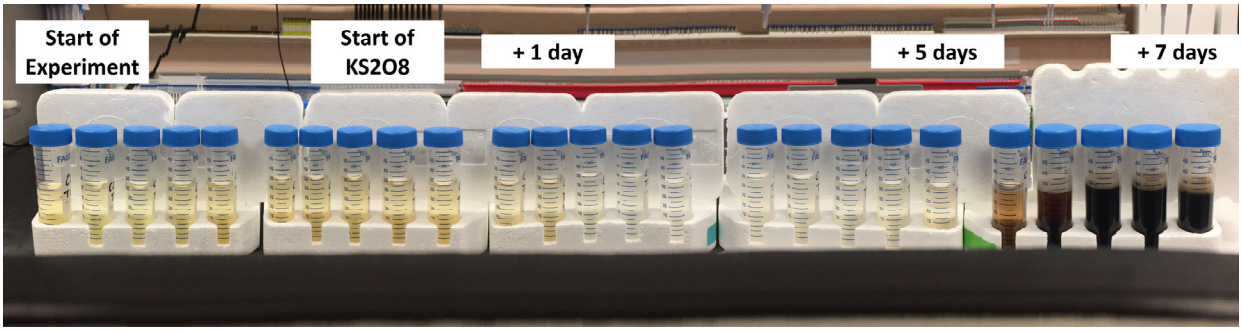

Figure 4.13 Effluent color progression for persulfate columns.

Effluent concentrations of PFAS, including PFHxA, PFOA, and PFHxS were measured with LC-QTOF-MS and varied between control, permanganate, and persulfate columns (**Figure 4.14**). Effluent concentrations similarly declined for all three displayed PFAS in all treatments. Following the addition of ISCO solutions at approximately 10 pore volumes, the effluent concentrations of all three PFAS increased in both the permanganate and persulfate-treated columns. All three example PFAS increased more rapidly and to higher concentrations in the permanganate-treated columns than the persulfate-treated columns; however, it is unclear if this difference is a function of the specific chemical oxidants or simply that they were added to the column at different concentrations (100 mM permanganate vs. 25 mM persulfate).

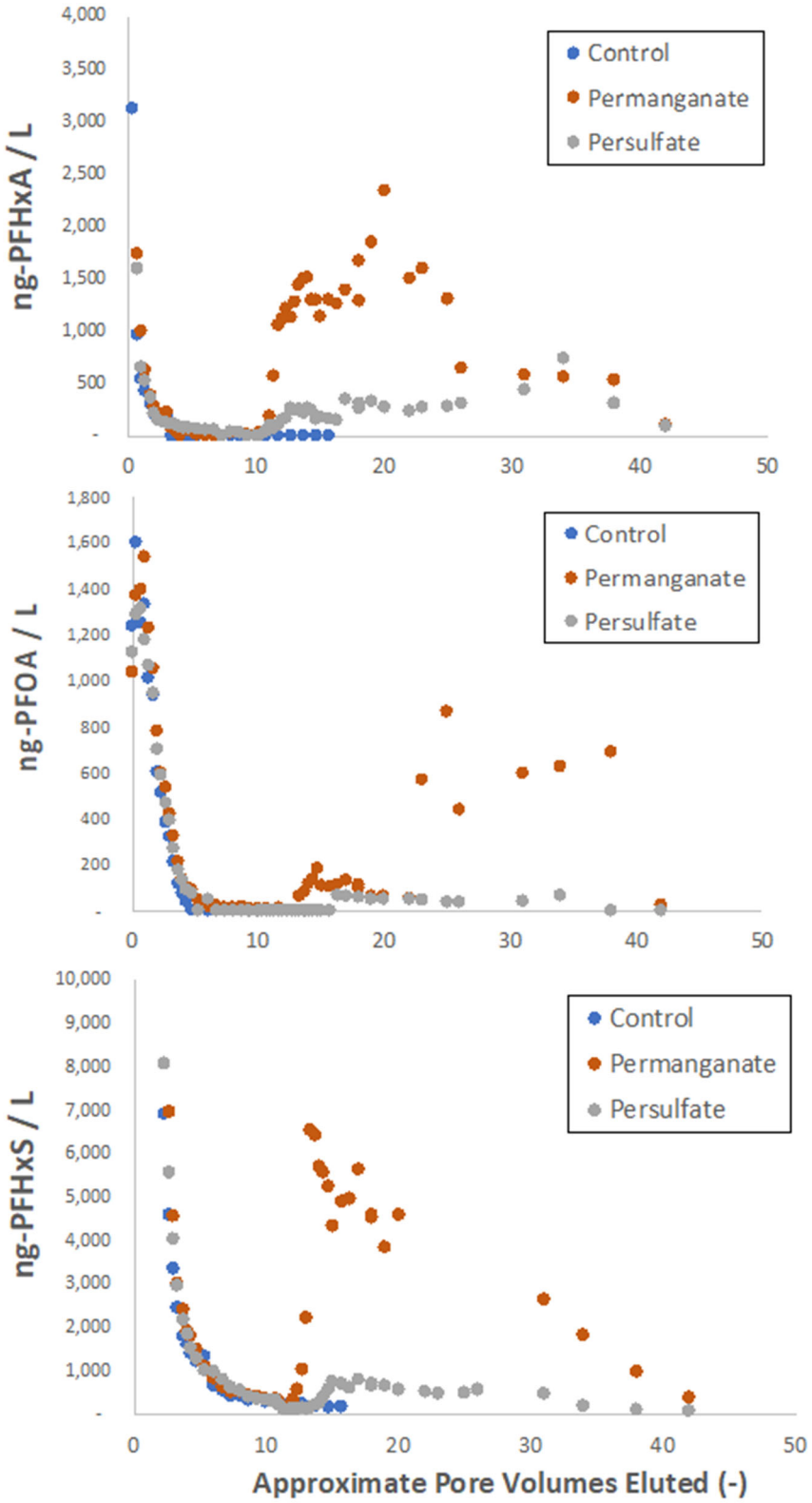

Figure 4.14 PFHxA (top), PFOA (middle) and PFHxS (bottom) concentrations in the effluent of example control, permanganate, and persulfate columns.

Conclusions

Task 1 of this project focused on the characterization and release of PFASs from AFFF-impacted soils and their interactions with interfaces. The two field-collected soils collected and used in this task were similar in terms of particle size, carbon content, and ion exchange capacity, but the PFAS concentrations and composition varied greatly for each soil. While Soil A showed a mix of PFCAs, PFSAs, and X:2 FTSs that indicated the presence of PFASs from a variety of AFFFs, Soil B was dominated by high concentrations of PFSAs and sulfonamide-based PFAA precursors that suggested 3M AFFF was the predominant PFAS source. However, when flushed with artificial groundwater under saturated conditions, the PFAS effluent concentration profiles, while varying with respect to overall concentration, were similar in that PFAS elution clearly varied in relation to both the head group as well as perfluorinated chain length. This has important implications for site monitoring and remediation, as some classes, including potential PFAA-precursors did not appear in the effluent until after the highly oxidized PFAAs were largely eluted.

In terms of interactions with non-soil phases, experiments evaluating PFAS interactions with Jet Fuel (and Jet Fuel-water interfaces) indicated that interfacial sorption coefficients (K_{nw}) for PFASs with chain lengths of less than 10 carbons were best fit to a linear model, where K_{nw} ranged from 0.06 – 0.26 cm (2-3 orders of magnitude higher than previously reported). PFCAs with 11 – 14 carbons were better fit to the Freundlich model and showed greater accumulation at the interface than shorter-chained compounds. Partitioning into bulk Jet Fuel A was not observed for PFASs below eight carbons. Single point K_n values decreased with increasing PFAS concentration indicating non-ideal partitioning for these PFASs and this relationship became more pronounced with increasing carbon chain length. Further, experiments to determine the CMCs for specific AFFF formulations indicated that the CMC was below the recommended 3% AFFF application rate, indicating that micelles are present when AFFFs are applied to fires. Reduced surface and interfacial tensions of AFFF-impacted waters after application can potentially increase soil wetting and infiltration. The presence of micelles also increases potential for NAPL and other co-contaminant transport.

Finally, experiments under **Task 1** aimed to examine the geochemical factors impacting the release of PFASs from AFFF-impacted soils indicated differences between the two field-collected soils. PFAS effluent concentration profiles from Soil A were similar regardless of initial AGW pH (5,7, or 9). Soil B showed greater differences in effluent concentration profiles with high pH (10) than low pH (3): the largest differences were observed for PFASs that took longer to elute from the soil, such as PFOS and FOSA. These compounds had higher effluent concentration maxima at pH 10 than at pH 7. High pH AGW also released more mass of these slowly eluting PFASs from the soil. Lower effluent concentration maxima were observed in the high sodium treatment compared to the high calcium treatment. Overall, results suggest that soil buffering capacity is highly relevant to PFAS transport and that remedial actions that produce large groundwater pH shifts may cause rapid release of PFASs that are typically less mobile.

In **Task 2** of this project, the diffusive transport of PFASs and the potential for abiotic reactions with clays were examined. In terms of diffusion, experimentally determined aqueous diffusivities were in good agreement with previously performed experiments that measured PFAA uptake into activated carbon. The Wilke-Chang model was not able to accurately predict the values nor

describe the trend for the range of PFAAs used in this study. The non-uniform trend in the PFAA diffusivities with respect to the molar volumes likely is reflective of unique molecular interactions associated with highly fluorinated compounds.

For the clay soil tube diffusion experiments, experimental results compared to numeric models showed that neglecting surface diffusion resulted in a severe underprediction (>10x for PFOS) of predicted aqueous concentrations. For the PFAAs and clay soil examined herein, surface diffusion contributions became important (>10% of the overall diffusion) at K_d values greater than approximately 0.5 L kg^{-1}.

With respect to abiotic reactions, the results of this study suggest that reactive iron induced reductive transformation of polyfluorinated PFAA precursors in AFFF is unlikely to be an important mechanism at most AFFF-impacted sites. However, ferrous iron minerals may play a small role in precursor transformation under oxic conditions due to generation of hydroxyl radicals. PFOSi was found to be very unstable under oxic conditions and rapidly oxidized to PFOS. This oxidative process may be important for AFFF-impacted sites where PFASs in anoxic source areas undergo transformation as the downgradient plume becomes aerobic.

The third task of this project, **Task 3**, focused on interactions with and transformations by microbial communities. The different AFFF formulations tested, a 3M formulation and a National Foam formulation, had different responses to aerobic transformation of non-fluorinated and fluorinated components of AFFF. While there were initial decreases in AmPr-FHxSA present in 3M in the live treatments, National Foam did not show a decoupling of the 6:2 FTSA-PrB between the live treatment and autoclaved control. However, microcosms with National Foam were able to biodegrade the non-fluorinated carbon (measured as TOC) from the system whereas the TOC in 3M stayed constant in the live treatment. Given that 3M AFFF completely inhibited BTEX biodegradation with the same soil inoculum, it is possible that the 3M AFFF is just more inhospitable to hydrocarbon biodegradation. Experiments with a specific sulfonamide precursor observed in 3M AFFF, AmPr-FHxSA, indicated that over the course of 70 days, it was transformed into FHxSA, and to a lesser extent PFHxS.

Our findings suggest that aerobic BTEX biodegradation can be impacted by the presence of ECF AFFF, in this case 3M California Guardian. A dilution of Peterson AFB AFFF inhibited BTEX biodegradation, but no inhibition was seen with AmPr-FHxSA alone. However, differences in extracellular and total metabolite abundances between AmPr-FHxSA, FHxSA, and PFHxS treatments compared to the PFAS-free control suggested AmPr-FHxSA (and perhaps other zwitterionic PFAS) may cause cell membrane leakage.

Anaerobic microorganisms (TCE coculture, anaerobic BTEX biodegradation) appear to be more tolerant of AFFF than aerobic systems. Treatments with spiked AmPr-FHxSA had slowed TCE dehalogenation rates with no lag phase, suggesting that microorganisms did not recover from the inhibition. Addition of DGBE individually or via AFFF resulted in stimulation of TCE dehalogenation, presumably because of glycol fermentation.

Task 4 of this project aimed to examine PFAS releases from field-collected soil under conditions meant to mimic in situ remedial activities. When aerobic microorganisms were specifically

stimulated to mimic biosparging, transformation of multiple ECF-sulfonamide precursors was suspected based on mass balance, despite the surface soil being exposed to air and water for years prior to collection: source zone soils likely still have potential for PFAS transformation years after AFFF release. The over recovery of ≤C6 FASAs in both sets of columns suggests this class is an important intermediate or terminal product of more complex structures' transformation pathways. O_2-sparging increased the release of particular PFASs such as AmPr-FHxSA compared to N_2-sparging, but no large differences were seen on a class basis. Both O_2-sparged and N_2-sparged columns released more fractional mass of ECF-sulfonamides than unaltered, non-biologically active columns (i.e., in comparison to Task 1). After 200+ pore volumes of flushing, detectable concentrations of many PFASs remained on the column soils, particularly for longer chain PFSAs and zwitterionic compounds.

In the experiments simulating in situ chemical oxidation, effluent concentrations of some PFASs (PFHxA, PFOA, and PFHxS) increased in both the permanganate and persulfate-treated columns following the addition of ISCO solutions at approximately 10 pore volumes. All three example PFASs increased more rapidly and to higher concentrations in the permanganate-treated columns than the persulfate-treated columns but it remains unclear whether this difference is attributed to the chemical oxidants themselves or the different concentrations of each oxidant.

In summary, this project confirmed that there are significant reservoirs of polyfluorinated substances still remaining on AFFF-impacted soils which can be very slowly released to groundwater. The release of these PFASs is dependent on both the perfluorinated tail length and the head group. Some of these PFASs (particularly those present in 3M AFFF) also inhibit microbial activity, with anaerobic communities appearing to be more tolerant to AFFF than aerobic microbial communities. Some ECF-derived polyfluorinated substances do appear to transform, albeit slowly, to PFAAs such as PFHxS, though perfluoroalkyl sulfonamide such as FHxSA may be semi-stable intermediates. Natural abiotic subsurface reactions with polyfluorinated substances are likely not significant with respect to PFAS transformations. Finally, data collected under this project indicate that alterations in subsurface biogeochemistry, whether through alterations in soil porewater pH or changing redox conditions due to biosparging or ISCO, can significantly impact the time and magnitude of the release of PFAS mass from AFFF-impacted soils.

References

(1) Nickerson, A.; Maizel, A. C.; Kulkarni, P. R.; Adamson, D. T.; Kornuc, J. J.; Higgins, C. P. Enhanced Extraction of AFFF-Associated PFASs from Source Zone Soils. *Environ. Sci. Technol.* **2020**, *54*, 4952–4962.

(2) Backe, W. J.; Day, T. C.; Field, J. A. Zwitterionic, Cationic, and Anionic Fluorinated Chemicals in Aqueous Film Forming Foam Formulations and Groundwater from U.S. Military Bases by Nonaqueous Large-Volume Injection HPLC-MS/MS. *Environ. Sci. Technol.* **2013**, *47* (10), 5226–5234.

(3) Barzen-Hanson, K. A.; Roberts, S. C.; Choyke, S.; Oetjen, K.; McAlees, A.; Riddell, N.; McCrindle, R.; Lee Ferguson, P.; Higgins, C. P.; Field, J. A. Discovery of 40 Classes of Per-and Polyfluoroalkyl Substances in Historical Aqueous Film-Forming Foams (AFFFs) and AFFF-Impacted Groundwater. *Environ. Sci. Technol.* **2017**, *51* (4), 2047–2057.

(4) D'Agostino, L. A.; Mabury, S. A. Identification of Novel Fluorinated Surfactants in Aqueous Film Forming Foams and Commercial Surfactant Concentrates. *Environ. Sci. Technol.* **2014**, *48* (1), 121–129.

(5) Pabon, M.; Corpart, J. M. Fluorinated Surfactants: Synthesis, Properties, Effluent Treatment. *J. Fluor. Chem.* **2002**, *114* (2), 149–156.

(6) Thomas, M. Fire-Fighting Foam Technology. In *Foam Engineering Fundamentals and Applications*; 2011; pp 411–454.

(7) NORMAN Suspect List Exchange. Network of Reference Laboratories Research Centres and Related Organisations for Monitoring of Emerging Environmental Substances. 2017.

(8) Stern, R. M.; Fan, W. Q. Aqueous Film-Forming Foam Compositions. US6,015,838, 2000.

(9) Hawrelak, M.; Bennett, E.; Metcalfe, C. The Environmental Fate of the Primary Degradation Products of Alkylphenol Ethoxylate Surfactants in Recycled Paper Sludge. *Chemosphere* **1999**, *39* (5), 745–752.

(10) Xiao, X.; Ulrich, B. A.; Chen, B.; Higgins, C. P. Sorption of Poly- and Perfluoroalkyl Substances (PFASs) Relevant to Aqueous Film-Forming Foam (AFFF)-Impacted Groundwater by Biochars and Activated Carbon. *Environ. Sci. Technol.* **2017**, *51* (11), 6342–6351.

(11) Schaefer, C. E.; DiCarlo, D. A.; Blunt, M. J. Experimental Measurement of Air-Water Interfacial Area during Gravity Drainage and Secondary Imbibition in Porous Media. *Water Resour. Res.* **2000**, *36* (4), 885–890.

(12) Brusseau, M. L. The Influence of Molecular Structure on the Adsorption of PFAS to Fluid-Fluid Interface: Using QSPR to Predict Interfacial Adsorption Coefficients. *Water Res.* **2019**, *152*, 148–158.

(13) Silva, J. A. K.; Martin, W. A.; Johnson, J. L.; McCray, J. E. Evaluating Air-Water and NAPL-Water Interfacial Adsorption and Retention of Perfluorocarboxylic Acids within the Vadose Zone. *J. Contam. Hydrol.* **2019**, *223*, 103472.

(14) Guelfo, J. L.; Higgins, C. P. Subsurface Transport Potential of Perfluoroalkyl Acids at Aqueous Film-Forming Foam (AFFF)-Impacted Sites. *Environ. Sci. Technol.* **2013**, *47* (9), 4164–4171.

(15) Schaefer, C. E.; Culina, V.; Nguyen, D.; Field, J. Uptake of Poly- And Perfluoroalkyl Substances at the Air-Water Interface. *Environ. Sci. Technol.* **2019**, *53* (21), 12442–12448.

(16) Cowell, M. A.; Kibbey, T. C. G.; Zimmerman, J. B.; Hayes, K. F. Partitioning of Ethoxylated Nonionic Surfactants in Water/NAPL Systems: Effects of Surfactant and

NAPL Properties. *Environ. Sci. Technol.* **2000**, *34* (8), 1583–1588.
(17) McKenzie, E. R.; Siegrist, R. L.; McCray, J. E.; Higgins, C. P. The Influence of a Non-Aqueous Phase Liquid (NAPL) and Chemical Oxidant Application on Perfluoroalkyl Acid (PFAA) Fate and Transport. *Water Res.* **2016**, *92*, 199–207.
(18) Belhaj, A. F.; Elraies, K. A.; Alnarabiji, M. S.; Shuhli, J. A. B. M.; Mahmood, S. M.; Ern, L. W. Experimental Investigation of Surfactant Partitioning in Pre-CMC and Post-CMC Regimes for Enhanced Oil Recovery Application. *Energies* **2019**, *12* (12).
(19) Sörengård, M.; Östblom, E.; Köhler, S.; Ahrens, L. Adsorption Behavior of Per- and Polyfluoralkyl Substances (PFASs) to 44 Inorganic and Organic Sorbents and Use of Dyes as Proxies for PFAS Sorption. *J. Environ. Chem. Eng.* **2020**, *8* (3), 103744.
(20) Handa, T.; Mukerjee, P. Surface Tensions of Nonideal Mixtures of Fluorocarbons and Hydrocarbons and Their Interfacial Tensions against Water. *J. Phys. Chem.* **1981**, *85* (25), 3916–3920.
(21) Kissa, E. *Fluorinated Surfactants: Synthesis, Properties, and Applications*; Dekker, M., Ed.; New York, 1994.
(22) Cussler, E. L. *Diffusion - Mass Transfer in Fluid Systems*; Cambridge University Press, 1994.
(23) Schaefer, C. E.; Choyke, S.; Ferguson, P. L.; Andaya, C.; Burant, A.; Maizel, A.; Strathmann, T. J.; Higgins, C. P. Electrochemical Transformations of Perfluoroalkyl Acid (PFAA) Precursors and PFAAs in Groundwater Impacted with Aqueous Film Forming Foams. *Environ. Sci. Technol.* **2018**, *52* (18), 10689–10697.
(24) Harada, K.; Xu, F.; Ono, K.; Iijima, T.; Koizumi, A. Effects of PFOS and PFOA on L-Type Ca2+ Currents in Guinea-Pig Ventricular Myocytes. *Biochem. Biophys. Res. Commun.* **2005**, *329* (2), 487–494.
(25) López-Fontán, J. L.; Sarmiento, F.; Schulz, P. C. The Aggregation of Sodium Perfluorooctanoate in Water. *Colloid Polym. Sci.* **2005**, *283* (8), 862–871.
(26) Nordstierna, L.; Furó, I.; Stilbs, P. Mixed Micelles of Fluorinated and Hydrogenated Surfactants. *J. Am. Chem. Soc.* **2006**, *128* (20), 6704–6712.
(27) Kim, J.; Izadyar, A.; Shen, M.; Ishimatsu, R.; Amemiya, S. Ion Permeability of the Nuclear Pore Complex and Ion-Induced Macromolecular Permeation as Studied by Scanning Electrochemical and Fluorescence Microscopy. *Anal. Chem.* **2014**, *86* (4), 2090–2098.
(28) Anderko, A.; Lencka, M. M. Modeling Self-Diffusion in Multicomponent Aqueous Electrolyte Systems in Wide Concentration Ranges. *Ind. Eng. Chem. Res.* **1998**, *37* (7), 2878–2888.
(29) Robel, A. E.; Marshall, K.; Dickinson, M.; Lunderberg, D.; Butt, C.; Peaslee, G.; Stapleton, H. M.; Field, J. A. Closing the Mass Balance on Fluorine on Papers and Textiles. *Environ. Sci. Technol.* **2017**, *51* (16), 9022–9032.
(30) Allred, B. M. K.; Lang, J. R.; Barlaz, M. A.; Field, J. A. Orthogonal Zirconium Diol/C18 Liquid Chromatography-Tandem Mass Spectrometry Analysis of Poly and Perfluoroalkyl Substances in Landfill Leachate. *J. Chromatogr. A* **2014**, *1359*, 202–211.
(31) Schotte, W. Prediction of the Molar Volume at the Normal Boiling Point. *Chem. Eng. J.* **1992**, *48* (3), 167–172.
(32) Goss, K.-U.; Bronner, G.; Harner, T.; Hertel, M.; Schmidt, T. C. The Partition Behavior of Fluorotelomer Alcohols and Olefins. *Environ. Sci. Technol.* **2006**, *40* (11), 3572–3577.
(33) Hayduk, W.; Laudie, H. Prediction of Diffusion Coefficients for Nonelectrolytes in Dilute Aqueous Solutions. *AlChE* **1974**, *20* (3), 611–615.

(34) Valderrama, C.; Gamisans, X.; de las Heras, X.; Farrán, A.; Cortina, J. L. Sorption Kinetics of Polycyclic Aromatic Hydrocarbons Removal Using Granular Activated Carbon: Intraparticle Diffusion Coefficients. *J. Hazard. Mater.* **2008**, *157* (2), 386–396.
(35) Wilke, C. R.; Chang, P. Correlation of Diffusion Coefficients in Dilute Solutions. *AlChE* **1955**, *1*, 264–270.
(36) Pereira, L. A. M.; Martins, L. F. G.; Ascenso, J. R.; Morgado, P.; Ramalho, J. P. P.; Filipe, E. J. M. Diffusion Coefficients of Fluorinated Surfactants in Water: Experimental Results and Prediction by Computer Simulation. *J. Chem. Eng. Data* **2014**, *59* (10), 3151–3159.
(37) Kim, M.; Li, L. Y.; Grace, J. R.; Yue, C. Selecting Reliable Physicochemical Properties of Perfluoroalkyl and Polyfluoroalkyl Substances (PFASs) Based on Molecular Descriptors. *Environ. Pollut.* **2015**, *196*, 462–472.
(38) Goss, K.-U.; Bronner, G. What Is So Special about the Sorption Behavior of Highly Fluorinated Compounds? *J. Phys. Chem. A* **2006**, *110* (30), 9518–9522.
(39) Schaefer, C. E.; Towne, R. M.; Lippincott, D. R.; Lacombe, P. J.; Bishop, M. E.; Dong, H. Abiotic Dechlorination in Rock Matrices Impacted by Long-Term Exposure to TCE. *Chemosphere* **2015**, *119*, 744–749.
(40) Hyun, S. P.; Hayes, K. F. Feasibility of Using in Situ FeS Precipitation for TCE Degradation. *J. Environ. Eng.* **2009**, *135* (10), 1009–1014.
(41) Crank, J. *The Mathematics of Diffusion*; Oxford University Press, 1995.
(42) Yoshida, H.; Maekawa, M.; Nango, M. Parallel Transport by Surface and Pore Diffusion in a Porous Membrane. *Chem. Engin. Sci.* **1991**, *46*, 429–438.
(43) Schaefer, C. E.; Kosson, D. S. Effects of a Trapped NAPL on the Diffusive Release of Organic Contaminants from Saturated Soils. *Environ. Engin. Sci* **2000**, *17*, 129–138.
(44) Gimmi, T.; Kosakowski, G. How Mobile Are Sorbed Cations in Clays and Clay Rocks? *Environ. Sci. Technol.* **2011**, *45*, 1443–1449.
(45) Schaefer, C. E.; Drennan, D. M.; Tran, D. N.; Garcia, R.; Christie, E.; Higgins, C. P.; Field, J. A. Measurement of Aqueous Diffusivities for Perfluoroalkyl Acids. *J. Environ, Engin.* **2019**, *145*, 1–4.
(46) Do, D. D.; Rice, R. G. On the Relative Importance of Pore and Surface Diffusion in Non-Equilibrium Adsorption Rate Processes. *Chem. Engin. Sci.* **1987**, *42*, 2269–2284.
(47) Miyabe, K.; Takeuchi, S. Estimation of Surface Diffusion Coefficient in Liquid Phase Adsorption. *Can. J. Chem. Engin.* **1998**, *76*, 887–892.
(48) Miyabe, K.; Guiochon, G. Analysis of Surface Diffusion Phenomena in Reversed-Phase Liquid Chromatography. *Anal. Chem* **1999**, *71*, 889–896.
(49) Bhatia, S. K.; Kalam, A.; Joglekar, H. S.; Joshi, J. B. Effective Diffusivity of Phenol in Activated Carbon. *Chem. Engin. Comm.* **1990**, *98*, 139–154.
(50) Ocampo-Perez, R.; Leyva-Ramos, R.; Sanchez-Polo, M.; Rivera-Utrilla, J. Role of Pore Volume and Surface Diffusion in the Adsorption of Aromatic Compounds on Activated Carbon. *Adsorption* **2013**, *19*, 945–957.
(51) Liu, M.; Munoz, G.; Duy, S. V.; Liu, J. Stability of Nitrogen-Containing Polyfluoroalkyl Substances in Aerobic Soils. *Environ. Sci. Technol.* **2021**, *55* (8), 4698–4708.
(52) Houtz, E. F.; Sedlak, D. L. Oxidative Conversion as a Means of Detecting Precursors to Perfluoroalkyl Acids in Urban Runoff. *Environ. Sci. Technol.* **2012**, *46* (17), 9342–9349.
(53) Chen, H.; Liu, M.; Munoz, G.; Duy, S. V.; Sauvé, S.; Yao, Y.; Sun, H.; Liu, J. Fast Generation of Perfluoroalkyl Acids from Polyfluoroalkyl Amine Oxides in Aerobic Soils. *Environ. Sci. Technol. Lett.* **2020**, *7* (10), 714–720.

(54) Harding-Marjanovic, K. C.; Houtz, E. F.; Yi, S.; Field, J. A.; Sedlak, D. L.; Alvarez-Cohen, L. Aerobic Biotransformation of Fluorotelomer Thioether Amido Sulfonate (Lodyne) in AFFF-Amended Microcosms. *Environ. Sci. Technol.* **2015**, *49* (13), 7666–7674.
(55) Weathers, T. S.; Higgins, C. P.; Sharp, J. O. Enhanced Biofilm Production by a Toluene-Degrading Rhodococcus Observed after Exposure to Perfluoroalkyl Acids. *Environ. Sci. Technol.* **2015**, *49* (9), 5458–5466.
(56) Clark, M. E.; Edelmann, R. E.; Duley, M. L.; Wall, J. D.; Fields, M. W. Biofilm Formation in Desulfovibrio Vulgaris Hildenborough Is Dependent upon Protein Filaments. *Environ. Microbiol.* **2007**, *9* (11), 2844–2854.
(57) Fiehn, O.; Wohlgemuth, G.; Scholz, M.; Kind, T.; Lee, D. Y.; Lu, Y.; Moon, S.; Nikolau, B. Quality Control for Plant Metabolomics: Reporting MSI-Compliant Studies. *Plant J.* **2008**, *53* (4), 691–704.
(58) Cao, L.; Jiang, H.; Yang, J.; Fan, L.; Li, F.; Huang, Q. Simultaneous Determination of Benzene and Toluene in Pesticide Emulsifiable Concentrate by Headspace GC-MS. *J. Anal. Methods Chem.* **2013**, *2013*, 1–6.
(59) Schieber, J. Iron Sulfide Formation. In *Encyclopedia of Geobiology*; Retiner, J., Thiel, V., Eds.; Springer Verlag, 2011; pp 486–502.
(60) Beller, H. R.; Grbic-Galic, D.; Reinhard, M. Microbial Degradation of Toluene under Sulfate-Reducing Conditions and the Influence of Iron on the Process. *Appl. Environ. Microbiol.* **1992**, *58* (3), 786–793.
(61) Noh, S.-L.; Choi, J.-M.; An, Y.-J.; Park, S.-S.; Cho, K.-S. Anaerobic Biodegradation of Toluene Coupled to Sulfate Reduction in Oil-Contaminated Soils: Optimum Environmental Conditions for Field Applications. *J. Environ. Sci. Heal. Part A* **2003**, *38* (6), 1087–1097.
(62) Weiner, B.; Yeung, L. W. Y.; Marchington, E. B.; D'agostino, L. A.; Mabury, S. A. Organic Fluorine Content in Aqueous Film Forming Foams (AFFFs) and Biodegradation of the Foam Component 6:2 Fluorotelomercaptoalkylamido Sulfonate (6:2 FTSAS). *Environ. Chem.* **2013**, *10*, 486–493.
(63) Mejia-Avendaño, S.; Duy, S. V.; Sauvé, S.; Liu, J. Generation of Perfluoroalkyl Acids from Aerobic Biotransformation of Quaternary Ammonium Polyfluoroalkyl Surfactants. *Environ. Sci. Technol.* **2016**, *50* (18), 9923–9932.
(64) McGuire, M. E.; Schaefer, C.; Richards, T.; Backe, W. J.; Field, J. A.; Houtz, E.; Sedlak, D. L.; Guelfo, J. L.; Wunsch, A.; Higgins, C. P. Evidence of Remediation-Induced Alteration of Subsurface Poly- and Perfluoroalkyl Substance Distribution at a Former Firefighter Training Area. *Environ. Sci. Technol.* **2014**, *48* (12), 6644–6652.

Appendix: Reporting and Dissemination

Reporting

The final task for this project included project reporting and dissemination of the results. Monthly financial reporting and quarterly progress reports were filed as required by SERDP. In progress review presentations were given as scheduled on an approximate annual basis. In addition, the results of this project were disseminated through oral and poster presentations, journal manuscripts, and webinars.

Dissemination

The results of this project resulted in 24 presentations and 3 webinars:

Presentations:

1. Higgins, C.P. The Coming Challenges of PFASs in Water and Soil: Implications for Human Exposure. University of Wisconsin, Madison Departmental Seminar Series. 13 November, 2020.
2. Higgins, C.P. Fate, Transport, and Bioaccumulation of Poly-and Perfluoroalkyl Substances (PFASs). University of Maryland Center for Environmental Science PFAS Roundtable. 5 October, 2020.
3. Higgins, C.P. PFAS and HRMS: What Will You Miss With Conventional LC-MS/MS? National Environmental Monitoring Conference, 9-12 August, 2020.
4. Higgins, C.P. Poly- and Perfluoroalkyl Substance Challenges: a U.S. Perspective. University of Queensland, Queensland Alliance for Environmental Health Sciences, Brisbane, Queensland, Australia. 28 February, 2020.
5. Higgins, C.P. Poly-and Perfluoroalkyl Substances (PFASs): What's the Fuss? Presentation to National Academy of Engineering, Civil Section Meeting. Washington, DC. 7 October, 2019.
6. Higgins, C.P. Poly- and Perfluoroalkyl Substances (PFASs) in at Aqueous Film Forming Foam (AFFF)-Impacted Sites: Going Beyond EPA Method 537. PFAS 2019: The 2nd National Conference on Per- and Polyfluoroalkyl Substances. Boston, Massachusetts 10 June, 2019.
7. Higgins, C.P. The Coming Challenges of PFASs in Water and Soil: Implications for Human Exposure. Arizona State University, School of Sustainable Engineering and the Built Environment, Tempe, Arizona. 23 April, 2019.
8. Higgins, C.P. The Coming Challenges of PFASs in Water and Soil: Implications for Human Exposure. Massachusetts Institute of Technology, Department of Civil and Environmental Engineering. Cambridge, Massachusetts. 19 April, 2019.
9. Higgins, C.P. The Challenges of Poly- and Perfluoroalkyl Substances (PFASs) in Soils. University of New South Wales, Sydney, Australia. 5 March, 2019.
10. Higgins, C.P. Poly- and Perfluoroalkyl Substances (PFASs) in Soils - Assessment and Fate. RemTec Summit. Denver, Colorado. 26 February, 2019.
11. Higgins, C.P. Poly- and Perfluoroalkyl Substances (PFASs) in Soils - Assessment and Fate. PFAS in soils workshop – behaviour, fate, risks and remediation. Canberra, Australia. 21 November, 2018.

12. Higgins, C.P. “Review on Managing Poly- and Perfluoroalkyl Substances (PFASs) in Contaminated Soils.” National Soils Conference 2018. Canberra, Australia. 20 November, 2018
13. Higgins, C.P. “The Many Challenges of Poly- and Perfluoroalkyl Substances (PFASs).” University of Queensland, Queensland Alliance for Environmental Health Sciences. Brisbane, Australia. 14 November, 2018
14. Higgins, CP. “The Importance of Polyfluorinated Substances.” Harvard University, John A. Paulson School of Engineering and Applied Sciences. Cambridge, Massachusetts. 27 August, 2018
15. Higgins, C.P. Poly-and Perfluoroalkyl Substances (PFASs) as Environmental Contaminants: Current State of Knowledge. Colorado Environmental Management Society. Denver, Colorado. 14 August, 2018.
16. Maizel, A. and Higgins, C. P. Combined Analytical Approaches to Assess Poly- and Perfluoroalkyl Substances in the Environment. Gordon Research Seminar on Environmental Sciences: Water. 23-24 June, 2018. Plymouth, New Hampshire.
17. Maizel, A. and Higgins, C. P. Semi-quantitative Suspect Screening of PFAS in AFFF-impacted Soils. Gordon Research Conference on Environmental Sciences: Water. 24-29 June, 2018. Plymouth, New Hampshire.
18. Higgins, C.P. Poly-and PerfluoroalkylSubstances (PFASs) as Environmental Contaminants: Current State of Knowledge. ExxonMobil Biomedical Sciences, Inc.(EMBSI). Clinton, New Jersey. 3 May, 2018.
19. Higgins, C.P. The Importance of Polyfluorinated Substances as Groundwater Contaminants. New Jersey Department of Environmental Protection. Trenton, New Jersey. 2 May, 2018.
20. Higgins, C.P. Remediation Challenges and Opportunities for AFFF-impacted Sites. Toxicology and Risk Assessment Conference, Cincinnati, Ohio. 25 April, 2018.
21. Higgins, C.P. Remediation Challenges and Opportunities for AFFF-impacted Sites. Emerging Contaminants Summit. Westminster, Colorado. 7 March, 2018.
22. Higgins, C.P. Remediation Challenges and Opportunities for AFFF-impacted Sites. Federal Information Exchange on PFAS. Bethesda, Maryland. 6 February, 2018.
23. Higgins, C.P. Environmental Fate and Transport of Poly- and Perfluoroalkyl Substances at Aqueous Film-Forming Foam Impacted Sites. American Geophysical Union Fall Meeting. New Orleans, Louisiana. 14 December, 2017.
24. Higgins, C.P. Fate and Transport of PFASs at AFFF-impacted Sites: The Current State of Knowledge. Strategic Environmental Research and Development Program Annual Symposium. Washington, District of Columbia. 28 November, 2017.

Webinars:

1. Higgins, C.P. Poly-and Perfluoroalkyl Substances (PFAS) Released from Aqueous Film Forming Foam (AFFF) Source Zones. Interstate Technology and Regulatory Council (ITRC) PFAS Team Teleconference. 17 November, 2020. (Virtual Meeting)
2. Higgins, C.P. The Challenges of Poly-and Perfluoroalkyl Substances (PFASs) in Water. American Chemical Society, Environmental Chemistry Division Webinar Series, 7 November, 2019.
3. Higgins, C.P. Application of High-resolution Mass Spectrometry to Environmental Analysis of Poly- and Perfluoroalkyl Substances (PFASs). SCIEX Webinar. 28 May, 2019

Peer-reviewed Publications (to date):

1. Schaefer, C.E., Drennan, D., Nickerson, A., Maizel, A., and C.P. Higgins. 2021. Diffusion of Perfluoroalkyl Acids through Clay-Rich Soil. *Journal of Contaminant Hydrology.* 241: 103814. DOI: doi.org/10.1016/j.jconhyd.2021.103814
2. Nickerson, A., Maizel, A., Kulkarni, P., Adamson, D.T., Kornuc, J. and C.P. Higgins. 2020. Enhanced extraction of AFFF-associated PFASs from source zone soils. *Environmental Science and Technology.* 54 (8): 4952–4962. DOI: doi/10.1021/acs.est.0c00792
3. Garcia, R., Chiaia-Hernández, A., Lara-Martín, P.A., Loos, M., Hollender, J., Oetjen, K., Higgins, C.P., and J.A. Field. 2019. Suspect Screening of Hydrocarbon Surfactants in AFFFs and AFFF-Contaminated Groundwater by High Resolution Mass Spectrometry. *Environmental Science and Technology,* 53:8068−8077. DOI: doi/10.1021/acs.est.9b01895
4. Schaefer, C.E., Drennan, D.M., Tran, D.N., Garcia, R., Christie, E., Higgins, C.P., and J.A. Field. 2019. Measurement of Aqueous Diffusivities for Perfluoroalkyl Acids *Journal of Environmental Engineering,* 145(11):06019006. DOI: 10.1061/(ASCE)EE.1943-7870.0001585.

Manuscripts in Progress:

1. Maizel, A.C., Shea, S., Nickerson, A., Schaefer, C.E., and C.P. Higgins. Release of Per- and Polyfluoroalkyl Substances from Aqueous Film-Forming Foam Impacted Soils. *In Review.*
2. Nickerson, A., Maizel, A.C., Olivares, C.I., Schaefer, C.E. and C. P. Higgins. Simulating Impacts of Biosparging on Release and Transformation of Per- and Polyfluoroalkyl Substances from Aqueous Film-Forming Foam Impacted Soil. *In Review*
3. Olivares, C.I., Yi, S., Cook, E.K., Choi, Y.J., Montagnolli, R., Byrne, A., Higgins, C.P., Sedlak, D.L. and L. Alvarez-Cohen. Cometabolism with BTEX degradation Increases Yield of Perfluoroalkyl Carboxylic Acids from Aerobic 6:2 FtTAoS Biotransformation, *In Preparation.*
4. Nickerson, A., Maizel, A.C., Schaefer, C.E. and C. P. Higgins. Solution Chemistry Impacts on the Release of Poly- and Perfluoroalkyl Substances from Aqueous Film-Forming Foam Impacted Soils. *In Preparation.*
5. Nickerson, A., Maizel, A.C., Schaefer, C.E. and C. P. Higgins. Simulating Impacts of In situ Chemical Oxidation for TCE on the Release and Transformation of Per- and Polyfluoroalkyl Substances from Aqueous Film-Forming Foam Impacted Soil. *In Preparation.*

Awards and Other Impacts:

This project was selected by SERDP as the 2020 Environmental Restoration Project of the Year. In addition, both C.P. Higgins and J.A. Field have actively participated in the ITRC PFAS team, ensuring that the most up-to-date information is included in trainings. The techniques and approaches to PFAS analysis and interpretation has been disseminated to many other SERDP and ESTCP projects. Multiple graduate students and postdoctoral fellows received training under this project. Many of these individuals have transitioned to positions at academic universities, government laboratories (i.e., NIST), and even contract laboratories, further ensuring dissemination of the knowledge collected as part of this work.